STATISTICAL LEARNING AND OPTIMIZATION METHODS FOR IMPROVING THE EFFICIENCY IN LANDSCAPE IMAGE CLUSTERING AND CLASSIFICATION PROBLEMS

SELİME GÜROL

SEPTEMBER 2005

STATISTICAL LEARNING AND OPTIMIZATION METHODS FOR IMPROVING THE EFFICIENCY IN LANDSCAPE IMAGE CLUSTERING AND CLASSIFICATION PROBLEMS

A THESIS SUBMITTED TO
THE GRADUATE SCHOOL OF APPLIED MATHEMATICS
OF
THE MIDDLE EAST TECHNICAL UNIVERSITY

BY

SELİME GÜROL

IN PARTIAL FULFILLMENT OF THE REQUIREMENTS FOR THE DEGREE OF
MASTER OF SCIENCE
IN
THE DEPARTMENT OF SCIENTIFIC COMPUTING

SEPTEMBER 2005

Approval of the Graduate School of Applied Mathematics

Prof.Dr. Ersan AKYILDIZ
Director

I certify that this thesis satisfies all the requirements as a thesis for the degree of Master of Science.

Prof. Dr. Bülent KARASÖZEN
Head of Department

This is to certify that we have read this thesis and that in our opinion it is fully adequate, in scope and quality, as a thesis for the degree of Master of Science.

Assist. Prof. Dr. Hakan Öktem
Supervisor

Examining Committee Members

Prof. Dr. Bülent Karasözen _____

Assoc. Prof. Dr. Tanıl Ergenç _____

Assist. Prof. Dr. A. Özgür Kişisel _____

Assist. Prof. Dr. Hakan Öktem _____

Dr. Tamer Özalp _____

I hereby declare that all information in this document has been obtained and presented in accordance with academic rules and ethical conduct. I also declare that, as required by these rules and conduct, I have fully cited and referenced all material and results that are not original to this work.

Name, Last name: Selime Gürol

Signature:

ABSTRACT

STATISTICAL LEARNING AND OPTIMIZATION METHODS FOR IMPROVING THE EFFICIENCY IN LANDSCAPE IMAGE CLUSTERING AND CLASSIFICATION PROBLEMS

Selime Gürol
M.Sc., Department of Scientific Computing
Supervisor: Assist. Prof. Dr. Hakan Öktem
Co-Supervisor: Prof. Dr. Bülent Karasözen
September 2005, 110 pages

Remote sensing techniques are vital for early detection of several problems such as natural disasters, ecological problems and collecting information necessary for finding optimum solutions to those problems. Remotely sensed information has also important uses in predicting the future risks, urban planning, communication. Recent developments in remote sensing instrumentation offered a challenge to the mathematical and statistical methods to process the acquired information.

Classification of satellite images in the context of land cover classification is the main concern of this study. Land cover classification can be performed by statistical learning methods like additive models, decision trees, neural networks, k-means methods which are already popular in unsupervised classification and clustering of image scene inverse problems.

Due to the degradation and corruption of satellite images, the classification performance is limited both by the accuracy of clustering and by the extent of the classification. In this study, we are concerned with understanding the performance of the available unsupervised methods with k-means, supervised methods with Gaussian maximum likelihood which are very popular methods in land cover classification. A broader approach to the classification problem based on finding the optimal dis-

criminants from a larger range of functions is considered also in this work. A novel method based on threshold decomposition and Boolean discriminant functions is developed as an implementable application of this approach. All methods are applied to BILSAT and Landsat satellite images using MATLAB software.

Keywords: Remote Sensing, Land Cover Classification, Classification Techniques, Discriminant Function, Optimization, Statistical Learning, BILSAT

ÖZ

GÖRÜNTÜ KÜMELENDİRME VE SINIFLANDIRMA ALGORİTMALARININ PERFORMANSINI ARTTIRMAK İÇİN İSTATİSTİKSEL ÖĞRENME VE OPTİMİZASYON METODLARININ KULLANIMI

Selime Gürol
Yüksek Lisans, Bilimsel Hesaplama Bölümü
Tez Yöneticisi: Assist. Prof. Dr. Hakan Öktem
Ortak Tez Yöneticisi: Prof. Dr. Bülent Karasözen

Eylül 2005, 110 sayfa

Uzaktan algılama teknikleri; doğal afetler, ekolojik problemler gibi çeşitli problemlerin erken farkedilmesinde ve bu problemlere optimum sonuçların bulunması için gerekli bilginin elde edilmesinde hayati önem taşımaktadır. Uzaktan algılanan bilginin aynı zamanda risk tahmini, kent planlaması ve haberleşme gibi alanlarda da önemli bir kullanımı vardır. Uzaktan algılama enstrümantasyonundaki son gelişmeler elde edilen bilgileri anlamlı hale getirecek olan matematiksel ve istatistiksel metodların önemini artırmıştır.

Bu çalışma genel olarak uydu görüntülerinin arazi örtüsü sınıflandırmasını içermektedir. Arazi örtüsü sınıflandırılması, halen görüntülerin kümelenmesi ve sınıflandırılması için kullanılan toplamsal metodlar, karar verici ağaçlar, yapay sinir ağları, k-ortalama metodları gibi popüler istatistiksel metodlarla gerçekleştirilebilir.

Görüntünün bozulması ve gürültü gibi etkenler nedeniyle görüntü kümelendirme ve sınıflandırma algoritmaları hem performans açısından hem de yapılabilir sınıflandırmanın detayı açısından sınırlıdır. Bu çalışmada arazi örtüsü sınıflandırmasında kullanılan popüler metodların performansını anlamak için eğitimsiz sınıflandırmada k-ortalama yöntemi ve eğitimli sınıflandırmada da Gauss maksimum olabilirlik yönte-

mi kullanılmıştır. Sınıflandırma probleminin çözümü için bu metodlara alternatif olarak, daha geniş bir fonksiyon kümesinden optimum ayırt edici fonksiyonu bulmaya dayalı bir yaklaşım düşünülmüştür. Bu yaklaşımın uygulanabilmesi için eşik ayrıştırma ve Boolean ayırt edici fonksiyonlarına dayanan özgün bir yöntem geliştirilmiştir. Bütün yöntemler BILSAT ve Landsat uydu görüntüleri kullanılarak MATLAB yazılımında test edilmiştir.

Anahtar Kelimeler: Uzaktan Algılama, Arazi Örtüsü Sınıflandırması, Sınıflandırma Teknikleri, Ayırt Edici Fonksiyon, Optimizasyon, İstatistiksel Öğrenme, BILSAT

To my family

ACKNOWLEDGMENT

I would like to express my gratitude to my advisor, Assist Prof. Dr. Hakan Öktem, for his friendship, exemplary effort and support during this study.

I would like to thank Prof. Dr. Bülent Karasözen for his valuable contribution to this study. I also thank Prof. Dr. Gerhard Wilhelm Weber for his friendship and support.

My sincere thanks go to Dr. Tamer Özalp whose guidance, support and advice began before this study encouraged me to concern over remote sensing area. Special thanks to European Space Agency and International Space University for their contribution during this study. This contribution has broadened my perspective on remote sensing.

Sincere thanks to Micheline Tabache, member of ESA International Relations Department, for her support and valuable contribution during this study.

I am grateful to my friend Didem for her sharing this hard period with me, encouragement, understanding, patience and guidance throughout this study. I am thankful to my friend Aslı and my homemate Bilge for not feeling myself alone and motivating me.

I would like thank to my aunt Zeynep Akçay for her encouragement, advice and support during my study.

It is very important for the continuation of the study to be in a peaceful place which is supported during all my study from my institute. So, thanks each of IAM (Institute of Applied Mathematics) members to feel myself in comfort.

This work was supported by The Scientific and Technical Research Council of Turkey MSc. Scholarship Program (TUBITAK Yurt İçi Yüksek Lisans Burs Programı).

Special thanks to BILTEN (Information Technologies and Electronics Research Institute) and IKONOS Space Imaging for supplying the data which is very critical for this study.

None of my study would have been possible without the support of my family. Thanks each of them for their continuous support and endless patience.

TABLE OF CONTENTS

APPENDICES

LIST OF TABLES

LIST OF FIGURES

LIST OF ABBREVIATIONS AND ACRONYMS

AIAA	American Institute of Aeronautics and Astronautics
ARTMAP	Adaptive Resonance Theory
ANN	Artificial Neural Network
BILTEN	Information Technologies and Electronics Research Institute
BILSAT-1	BILTEN Satellite-1
DN	Digital Number
DTC-LSMA	Decision Tree Classification based on Linear Spectral Mixture Analysis
ECHO	Extraction and Classification of Homogeneous Objects
EOSAT	Earth Observation Satellite
ERDAS	Earth Resources Data Analysis System (Commercial software)
ERTS-1	Earth Resources Technology Satellite-1
ESA	European Space Agency
ETM+	Enhanced Thematic Mapper Plus
GIS	Geographic Information System
IFOV	Instantaneous Field Of View
ISU	International Space University
KHTT	Know-How Transfer and Training
Landsat-1	Land Satellite-1
MATLAB	Matrix Laboratory(A commercial software by MATHworks Inc.)
METU	Middle East Technical University
MLC	Maximum Likelihood Classifier
NASA	National Aeronautics and Space Administration
PSF	Point Spread Function
RGB	Red Green Blue
SNR	Signal-to-Noise Ratio
SOM	Self Organized feature Map
SPOT-1	Satellite Pour l'Observation de la Terre-1
SSTL	Surrey Satellite Technology Limited
TUBITAK	The Scientific and Technical Research Council of Turkey

CHAPTER 1

INTRODUCTION

The impacts of real world problems such as natural disasters, global warming, limited water resources are increasing day by day together with the complexity of handling these impacts on humanity and nature. As a result, effective and sustainable future management of earth requires continuous monitoring of our planet.

A lot of scientific and socio-economic research is being held to understand those problems. *Remote sensing* is the quickest method to detect the above mentioned problems as early as possible or predict the future risks as accurate as possible with an optimum cost. In [21, 34], remote sensing is defined as the science, art and technology of obtaining reliable information about an object, area, or phenomenon through the analysis of data acquired by a device that is not in contact with the object, area, or phenomenon. This remotely acquired information has also the potential to be used in finding out global solutions to those problems.

The first use of the term remote sensing is in the 1960's. NASA established a research program in remote sensing in the 1960's. In the 1970's remote sensing is also started to be used in civil applications after launching of Landsat-1. Remote sensing started to play a very important role in technology, and other countries launched their own earth observation satellites in following years. In Turkey, remote sensing studies were started in the 1980's. Turkey had its first earth observation satellite BILSAT-1 in September 2003.

Remote sensing has lots of application areas including meteorology, climatology, geology, archeology, military, land cover/land use, planetary studies, etc.. In this study, land cover classification is the main concern.

During the development of remote sensing, considerable research has been devoted to image classification for obtaining high quality of thematic-maps which are the important outputs of remote sensing system.

In the system of remote sensing, there are many error sources which affect the accuracy of the classified image according to the ground truth data. These errors can occur in acquisition, data processing, data analysis, data conversion, and in decision making phases. In this study, the errors originated from data classification phase are concerned.

The classification of pixels of an image is performed by employing a difference metric or a classifier function. Most of the conventional methods in literature are based on a predetermined classifier like Euclidian distance from the class mean, k-nearest neighbor algorithm, minimum distance classifier, Gaussian maximum likelihood, etc.. However, due to the several reasons including noise in the images, non-unique distribution of the data into classes, existence of texture type of features, dependence of the brightness values to the angle of the projection, etc., the performance of those conventional algorithms are around 65 % which is not sufficient for many applications. A broader approach to this problem is finding the optimal discriminants from a larger range of functions. An implementable application of this approach can be using threshold decomposition and Boolean discriminant functions to partition the feature space into subspaces each corresponding to a class.

1.1 Purpose and Scope

In this study remote sensing especially for land cover classification was investigated by using satellite data. The study was mainly focused on the concept of classification methods. Basically, unsupervised and supervised learning techniques were applied to better understanding land cover classification of the study area. These are statistical and distribution free methods. Secondly the study was directed to develop an algorithm for each method in MATLAB. After that the methods were implemented and compared to get better performance of the used algorithms. Finally, the research was designed to show different perspectives for the investigated problem.

1.2 Study Area

Middle East Technical University (METU) settlement was chosen to implement the classification methods and to test the performance of each classifier. The reason for studying this location is its covering various landscape features in a distance that we can make a field study easily. METU campus is located on the Ankara-Eskişehir highway about 20 kilometers from the centrum of Ankara (see Figure 1.1 and 1.2). The campus area is 4500 hectares and the forest area is 3043 hectares, including Lake Eymir [72]. Since the early 1960's the area has been forested by voluntary university employees and students. Originally the area is almost bare soil, which is typical for Central Anatolia [56].

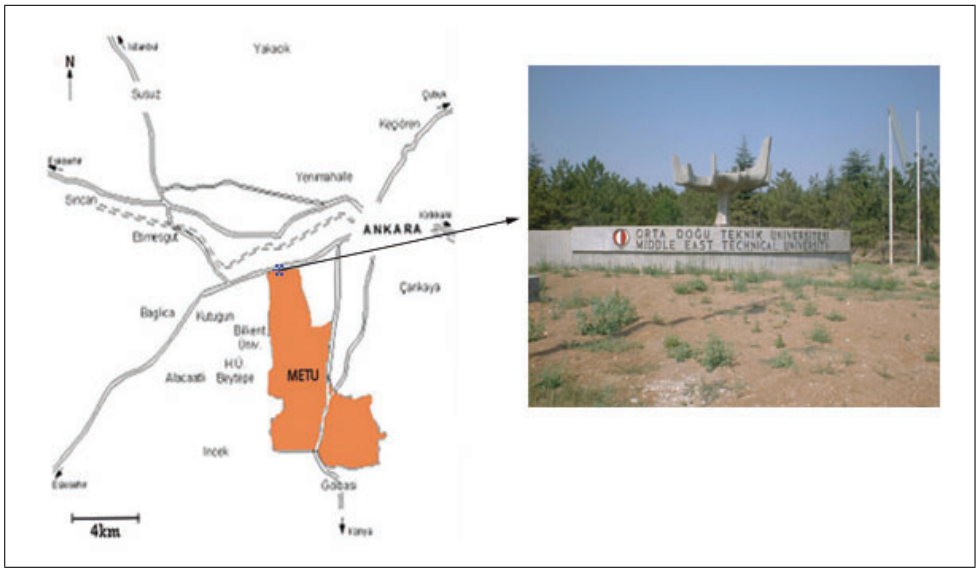

Figure 1.1: Location map of study area (METU) [56].

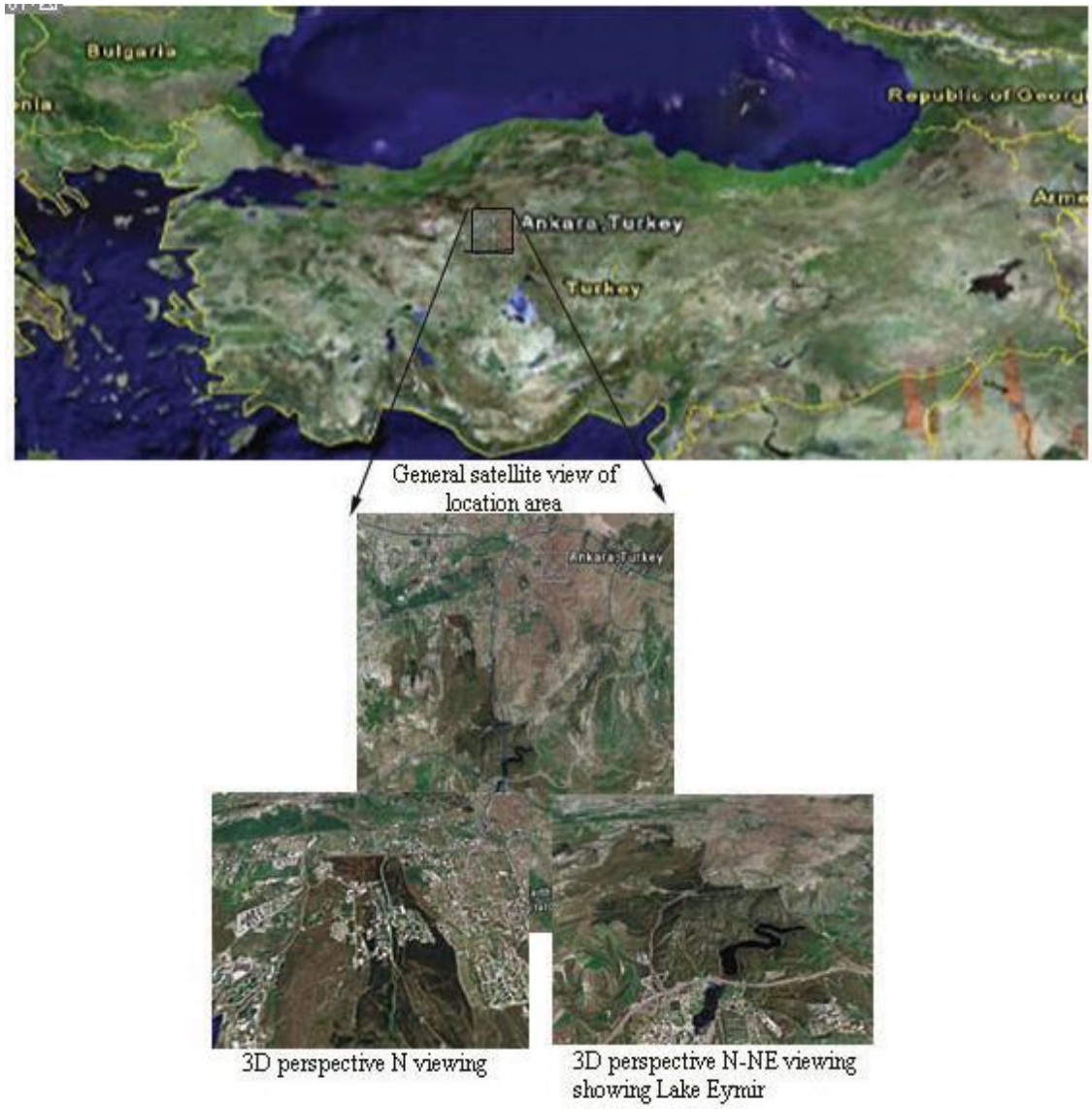

Figure 1.2: Different views from satellite RGB images of the study area acquired from reference [69].

1.3 Background

The first application in aerial remote sensing was started by using the balloons in the late 1700's. Balloons, kites, and pigeons were used for obtaining the comprehensive view of the earth. During the first and second world war there were so many improvements in the area of military and civil remote sensing. The modern era of remote sensing began with the first dedicated civil remote sensing satellite, NASA Earth Resources Technology Satellite (ERTS-1). It was conceived in 1965 and launched on July 23, 1972 with the name of Landsat-1. Then, the system was commercialized by transferring the system to the Earth Observation Satellite Cooperation. After that France joined this commercial remote sensing market by launching SPOT-1 in 1986. Many operational civil remote sensing satellites have been launched by several international and national organizations like ESA, Canada, Japan, Russia, India and Turkey for twenty years [21, 53].

The critical point of remote sensing from its definition is acquiring information by measuring at a distance, rather than in situ. This appears as an advantage of receiving a repetitive and coherent view of earth in small periods of time with a wide range of landscape.

The remotely collected data can be of many forms including variations in force distributions, acoustic wave distributions, or electromagnetic energy distributions [34]. Most of the application areas in remote sensing require data obtained from electromagnetic waves. Sensors placed on a satellite or aircraft records electromagnetic waves (see Figure 1.3) from different spectral bands to meet the need of different data users (see Table 1.1). Therefore, the system map, monitor earth resources and provide useful information for scientific, commercial or public service activities.

A typical remote sensing system consists of subsystems (see Figure 1.4). It requires two complex processing units which are data acquisition and data analysis to obtain information about phenomena under investigation. The steps followed in Figure 1.4 are:

(1) Energy Source: Remote sensing sytem's fundamental expose is the energy source. The system takes an action with this source which exposes electromagnetic

Table 1.1: Spectral Bands Characteristics [57].

Spectral Bands	Uses
Blue 0.450-0.515	Good for water penetration; strong vegetation absorbance Good for differentiating soil from vegetation
Green 0.525-0.605	Good for measure visible green reflectance peak of vegetation Useful for sediment concentrations in turbid water.
Red 0.630-0.690	Strongly absorbed by chlorophyll; important for vegetation discrimination
NIR 0.750-0.900	Very strong vegetation reflectance; Useful for determining biomass.Complete absorbtion of water
Mid-Infrared 1.55-1.75	Moisture sensitive
Thermal 10.40-12.50	Soil moisture discrimination and thermal mapping
Far-Infrared 2.09-2.35	Good for discriminating rock types

energy to the target of interest. Source of the system is divided into two as a passive or active imaging system [21]. If the source is the sun then the system is called a *passive imaging system*. If the system records the electromagnetic energy that is sent from itself or in other words if the system uses its own artificial radiation then it is called an *active imaging system*. In this study, images from passive imaging system is investigated.

(2) Radiation and the Atmosphere: The electromagnetic waves in different wavelengths coming from the satellite or sun first interacts with the atmosphere (see Figure 1.5). Some of the electromagnetic radiation is absorbed by the atmosphere because the gases in the atmosphere form important barriers to transmission of electromagnetic radiation through the atmosphere. The interaction of waves and the atmopshere is determined by surface reflectance, emission and topography [53]. Therefore, atmospheric effects may have substantial impact upon the quality of images and data generated by the sensor [7] by blurring it and reducing its contrast [2].

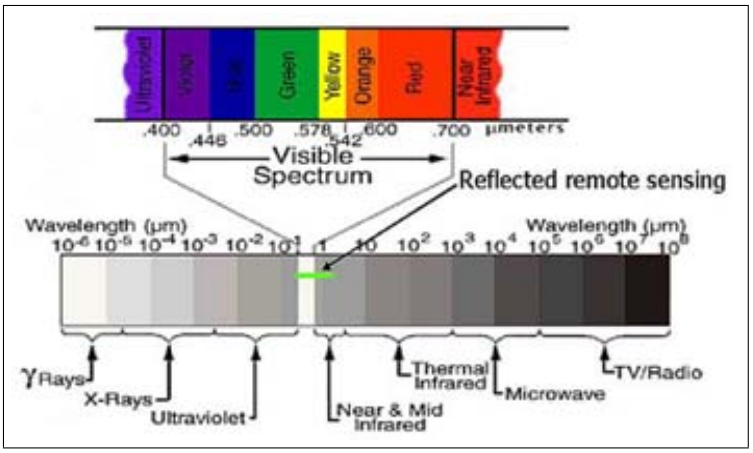

Figure 1.3: Electromagnetic Spectrum [70].

When the energy interacts with the Earth surface, some is scattered, some is absorbed by the target and some is reflected (see Figure 1.6). Reflection, absorbtion and transmission rates of the radiation depends on the nature of the surface, the wavelength of energy and the incident angle. While the energy go back through the direction of satellite, it is again absorbed by the atmosphere. The sensor records this remaining energy for an input to obtain the raw data of the interested area [68, 7].

(3) Sensor: There should be an electromagnetic sensor to collect and record the total electromagnetic radiation in various wavelength regions known as spectral bands which is reflected from the earth surface. The sensor records energy in different bands because measurements over several spectral bands make up a "spectral response pattern", or "signature" which is unique to an object at a specific temperature [21].

Sensor characteristics are determined by spatial resolution (size of the picture element), radiometric resolution (smallest detected and quantified increment of exposure), spectral resolution (wavelength bandwidths and number of bands) and temporal resolution (frequency of covering the same area by the same instrument) which directly affect the data quality and assist in choosing the right data for various applications [30].

Some types of sensors according to the aim of the investigation are atmospheric

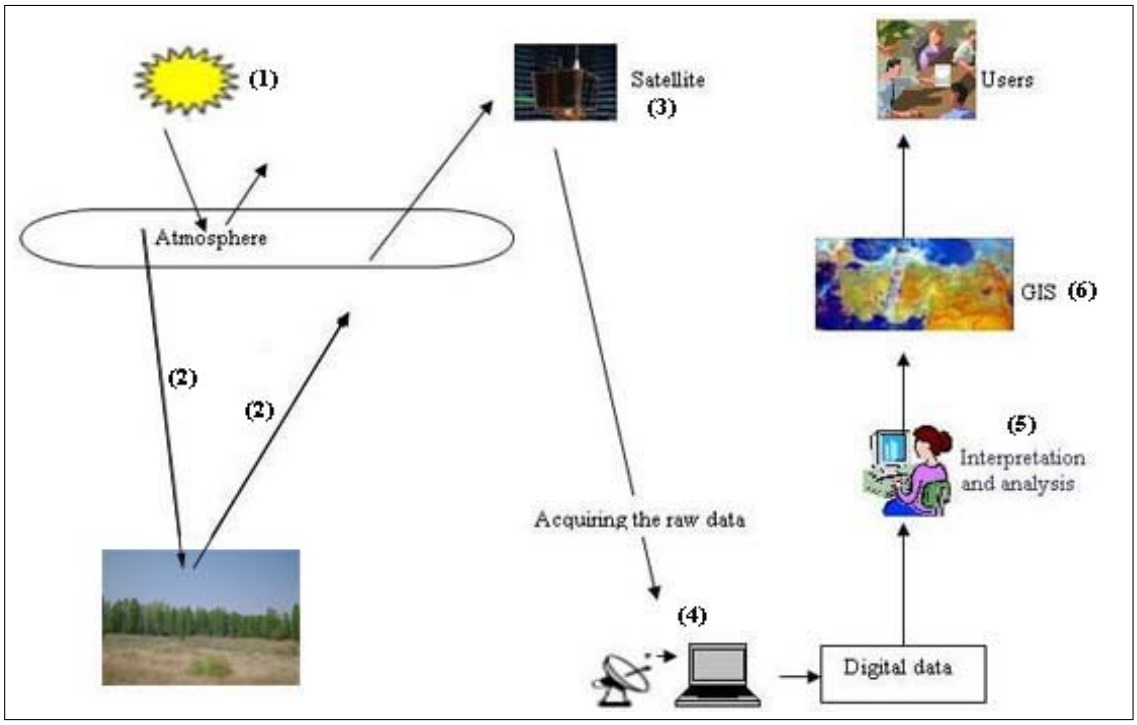

Figure 1.4: A Typical Satellite Based Remote Sensing System.

chemistry instruments, cloud profile and rain radars, earth radiation budget radiometers, high resolution optical imagers, imaging microwave radars, Lidars, Ocean colour instruments, radar altimeters, scatterometers [8].

(4) Transmission, Reception, and Processing: In electro-optical remote sensing, the recording elements produce an electrical signal, and this signal is recorded in a digital form [21]. This digitized image can then be processed by computer [24].

The electronic signal formulation can be given as:

$$e_b(x,y) = \int_{\alpha_{\min}}^{\alpha_{\max}} \int_{\beta_{\min}}^{\beta_{\max}} s_b(\alpha,\beta) PSF_{net}(x-\alpha, y-\beta) d\alpha d\beta,$$

where e_b is the electronic signal in band b, s_b is the signal measured by the sensor, PSF_{net} is the *Point Spread Function* (PSF) which is a weightening function for a spatial convolution, (x, y) represent the coordinates and the limits of the integral

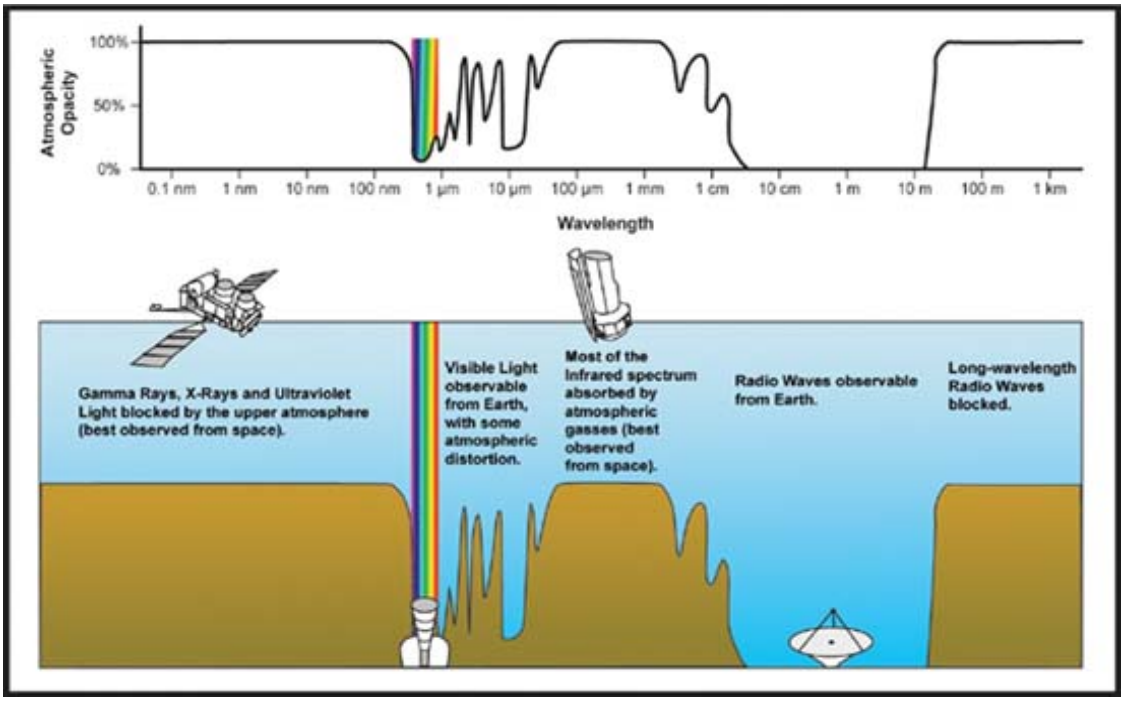

Figure 1.5: Atmospheric electromagnetic transmittance [67].

(α, β) define the spatial extent of the PSF about the coordinate (x, y) [53]. Then, this electronic signal is amplified electronically and filtered by the electronics PSF. The amplification stage is designed to provide sufficient signal level to A/D for quantization, without incurring saturation.

The data is sampled as

$$a_b(i, j) = a_b(i\triangle x, j\triangle y),$$

where $\triangle x$ and $\triangle y$ are the sampling periods.

For quantization the amplified signal, a_b, is sampled and each sample is quantized into digital numbers (DN) using a finite number of bits [24]. The final DN at pixel p and band b is,

$$DN_{pb} = int[a_b],$$

where $int[\ ]$ operator converts the output of the signal amplifier to the nearest

Figure 1.6: Electromagnetic waves interaction with the target. (A:Absorption, T: Transmission, R: Reflection, I: Incidence) [68].

integer value (see Figure 1.7) [53]. In Figure 1.7, Q (the number of bits/pixel) defines the radiometric resolution of the system [53]. The number of discrete DNs are determined by Q.

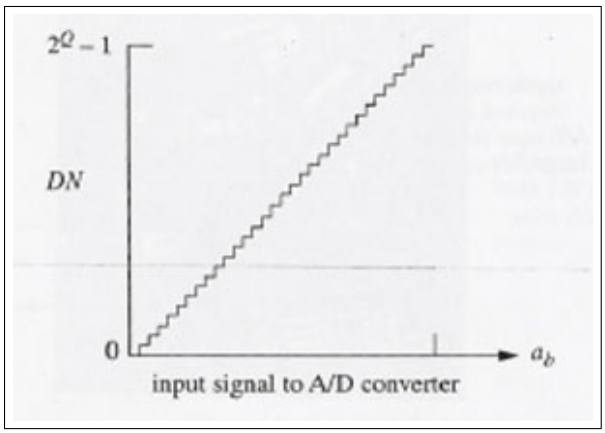

Figure 1.7: Relation between a_b and DN output [53].

As a summary, the instrument receives all the radiation from a certain area on the ground (IFOV) and generates a response. The signal of interest is degraded by the sensor during this transformation. Therefore, it is important a deep understanding of this degradation for designing the algorithms of image processing [53].

The signal attributed to any given pixel arises as a result of contributions not only from the field of view corresponding to that pixel but also includes contributions that properly belong to neighboring pixels. The pixel intensities are not independent but there is an autocorrelation among them [12]. While designing the classification algorithm, it is important to take into consideration of the neighbouring pixels.

(5) Interpretation and Analysis: Until now data acquisition process is explained. After this process the raw data is obtained and ready for data analysis. The remotely sensed data analysis consists of two elements, digital processing and visual interpretation.Visual interpretation and digital image processing should allow the analyst to perform scientific visualization, defined as "visually exploring data and information in such a way as to gain understanding and insight into the data" [26].

For processing the digital data some preprocessing operations including geometric correction, radiometric correction, noise removal, masking should be done to correct the distorted or degraded image data. These procedures are also important in the comparison of the two images obtained from different sensors. After preprocessing is complete, the analyst may use feature extraction to reduce the dimensionality of the data or change the dimensions according to the desired solutions. Therefore, the physical feature on the Earth's surface is converted to a useful information in the data, known as feature with a transformation function.

The analyst chooses one of the classification techniques according to the purpose of the study and data set to assign each pixel to a specific class using their spectral characteristics. The feature space is used as an input to the classification procedure. So, individual pixels are grouped according to their similarities determined by the analyst. These groups could be specific regions which have common geologic properties which make it possible to derive information about land use, vegetation type etc. After classification is completed, accuracy assessment should be done to have the knowledge of what is the performance of the analyst's results.

The output of the analysis could be maps, data and a report. These three elements of results give the user information about the data source, the method of analysis, the outcome and its reliability [7].

(6) Application: The final data of the remote sensing is integrated with the other outputs to better understand the target information, reveal some new information and help to solve complex problems. The integration of classified remotely sensed data types requires accurate registration of various data layers, spatial data infrastructure and standards, classification schemes, accuracy of each data layer, use of positioning systems, data compability, and selection of appropriate spatial mod-

elling techniques [21]. This system, a computerized system, designed to enter, store, manipulate,analyze and display the spatial data is called Geographic Information System (GIS).

Until this part, overview of remote sensing field is pointed out. Like other fields, lots of data are generated in remote sensing. In this study, the aim is to extract important patterns and trends, and learn necessary information from the data [19]. The learning problems can be grouped as supervised and unsupervised. In unsupervised learning or clustering, tha aim is to group a given collection of unlabeled patterns into meaningful clusters [25]. In supervised learning, the goal is to predict the outputs according to the priori knowledge about the data. In this study, unsupervised and supervised learning concepts are handled for the satellite image classification purpose.

1.4 Literature Survey

The expected global changes to the earth system make the information about our environment vital for the effective and sustainable future management [8]. Since the 1970's, scientists have been developing the field of remote sensing for this purpose. One of the most important applications in remote sensing is land cover classification which is pointed out in this study.

Classification is the process of the assignment of a phenomena to a predefined category. As a result of the development in digital computing, classification techniques were developed by many disciplines, including statistics, communication theory, biology, psychology, linguistics, and computer science besides remote sensing [64]. Classification techniques were improved generally through the main techniques including unsupervised and supervised classification techniques. There are different criteria for optimal classification that include minimizing the probability of error [15] and minimizing the average cost of a decision [64].

In the context of remote sensing, classification takes into account the reflectance spectrum of land covers additionally in some cases spatial context information such as slope and texture. Since remote sensing has become very popular for 20 years, there are lots of studies related with this research area. The majority of articles stud-

ied in this work are concerned with land cover mapping by using the multispectral data obtained from the passive remote sensing system.

In general, we can classify the studies related with classification into two according to their aim. One group is focused on the improvement of the classification process, others on the use of well-known classification methods through the types of remote sensing applications [29, 31, 37, 61, 60]. The classificaton process can be generalized with the following diagram [60].

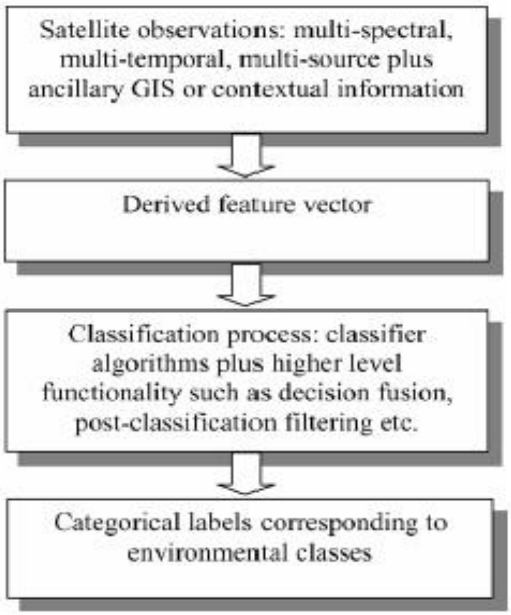

Schematic of classification process.

During the 15 years period, the improvements in classification take place in three directions:

1. The development of classification algorithm including training strategy and approaches to seperate feature space into classes based on statistical or distribution-free methods [60].

2. The development of novel-systems level approaches that augment the underlying classifier algorithms, e.g. fuzzy classifiers [60].

3. The exploitation of multiple types of data or ancillary information, both numerical or categorical, in a classification process [60].

Beginning with the simplest approach to classification, *unsupervised classification* has the advantages over others when there is no priori information about area under consideration. *Kartikeyan et al.* [28] discussed unsupervised classification problems and propose a new technique for the segmentation of multispectral remote sensing imagery. Also *Jain et al.* [25] gave a review about data clustering.

When sufficient information about the imagery to be classified is obtained, one of the most common and widespread supervised method is *Gaussian maximum likelihood classification method* [13]. *Jackson and Langrebe* [23] contributed to the development of the supervised maximum likelihood method which is based on the statistical assumptions.

Distribution free methods such as *neural networks* [59], and *decision trees* [45] are developed as an alternative to the methods that require statistical frequency distribution. *Yoshida and Omatu* [62] developed a decision tree classifier based on linear spectral mixture and state that it has good performance to address the land-cover heterogeneity.

The reason for the *decision tree methods* to become popular in classification can be ordered as [18, 45]: its ability to handle data measured on different scales, lack of any assumptions concerning the distributions of the data in each of the classes, flexibility and ability to handle non-linear relationships between features and classes.

Neural networks have been developed for ten years and majority find that this method produce similar or superior performance with respect to the *maximum likelihood classifier* (MLC) [6, 20, 36, 46]. The most popular neural network technique is back propagating multi layer perceptron neural network [20, 45, 46]. The others can be ordered as binary diamond neural networks [51], delta rule and generalized delta rule [5]. Also, *Porter et al.* [49] proposed a new network architecture. The main disadvantage of this method is the fact that it is not computationally efficient as the others.

There are so many articles comparing these methods. *Benediktsson et al., Paola and Schowengerdt* [5, 46] compared neural networks and statistical methods. *Pal and Paul* [45] made a comparision between decision tree, MLC and neural networks.

Another approach is combining different classifiers in one classifier, named as *hybrid classifier* in the literature, e.g. a hybrid classifer approach using Decision

Tree and ARTMAP (Adaptive Resonance Theory) neural network [35], MLC and decision tree [38]. Also, Extraction and Classification of Homogeneous Objects (ECHO) classifier which is part of the MultiSpec software package that has been developed at Purdue University and funded by NASA can be given as an example to hybrid classifiers. ECHO is a multistage spectral-spatial classifier that combines spectral and spatial/textural features; hence it is hybrid in character [37, 62]. *Kelly et al.* [29] compared hybrid systems with the usual classification methods. *McCauley and Engel* [41] compared ECHO and MLC.

Recently, there are new developments on the *optimization* of the classifiers through various classifiers. Multiple classifier systems have proved to be a valuable approach for combining classifiers [54]. Also discriminant analysis, quadratic discriminat functions [10], genetic algorithms [50] are discussed in the context of classification process.

The application of the spatial knowledge is highly effective in improving the accuracy of results obtained by means of parametric classification [5, 18]. *Schackelford and Davis* [52] verified that classification accuracies increase and more accurate land cover maps are obtained when spatial information, e.g. entropy, data range, skewness and spectral information were combined for the classification process. *Myint et al., Orun, Zhu and Yang* [43, 44, 65] demonstrated that textures provide important characteristics for the analysis of many types of images. *Zhu and Yang* [65] used wavelet transforms in texture analysis which can be an input for the classification. *Walter* [58] proposed the usage of laser data for extracting information about slope, average object height, etc..

In general, different classifiers have their own advantages and disadvantages. For a given problem, which classifier is more appropriate depends on a variety of factors. The analyst's experience and the complexity of a study area should be an important factor in selecting which algorithm to use [37]. The quality of training datasets required abundant and accurate field measurements from all classes of interest [37], the choice of the sensor, the number of spectral bands and the quality measure of a signal in terms of noise, Signal-to-Noise ratio (SNR), can significantly influence the accuracy of the classification [48].

Wilkinson [60] examined the articles related with the classification of remotely

sensed images from Photogrammetric Engineering and Remote Sensing from January 1989 until December 2003. Recently, multisource image is also considered for improvement of image classification. New and efficient ideas for this research area can be expected to contribute more in future.

1.5 Field Survey

Field study was made on June, 2005. Some pictures and samples were taken from various part of the study area. Throughout the field study, IKONOS image and air photo with 0.50 m resolution taken on 1999, five main classes were determined to be classified in the study area by taking the reference of Anderson's land cover classification system [1]. They are built-up land, agricultural land, forest land, water and mixed barren land containing soil and rocky terrain. These classes are described as follows.

Built-up Land: Built-up land is comprised of areas of intensive use with much of the land covered by structures [1]. In METU area, the dormitories, houses and buildings in the campus area was included this class (see Figure 1.8 and 1.9).

Figure 1.8: Built-up Land.

Figure 1.9: Builtup view from airphoto.

Agricultural Land: Agricultural land may be defined broadly as land used primarily for production of food and fiber [1]. In field studies, we realized that most of the agricultural land in METU settlement is wheat (see Figure 1.10 and 1.11).

Figure 1.10: Agricultural Land.

Figure 1.11: Agricultural Land view from airphoto.

Forest Land: Forest lands have a tree-crown areal density (crown closure percentage) of 10 percent or more, are stocked with trees capable of producing timber or other wood products, and exert an influence on the climate or water regime [1]. In METU area, the forest land is a mixture of poplar and various types of pine (see Figure 1.12 and 1.13). Some regions, trees are widely spaced whereas in some places they are very close to each other. Because of the poor composition of the soil for vegetation and lack of good care, some forest area is being lost.

Figure 1.12: Forest Land.

Figure 1.13: Forest Land view from airphoto.

Water: Eymir Lake is in this category (see Figure 1.14 and 1.15). Lake is in the 'S' shape which is seen from the satellite images very clearly. Lake Eymir is an alluvial dam lake that was formed by the damming of the İmrahor River valley at the beginning of this century. Lake Eymir is a shallow lake. Due to feeding of the dominant fish tench (Tinca tinca) and carp (Cyprinus carpio) of the lake by stirring up the sediment, perviousness of the radiance is low from the lake [4].

Figure 1.14: Lake Eymir.

Figure 1.15: Lake Eymir view from airphoto.

Barren Land: Barren land is a region of limited ability to support life and in which less than one-third of the area has vegetation or other cover [1]. In METU, it is composed of soil and rocks. Also vegetation is widely spaced in this area (see Figure 1.16 and 1.17). In the classification, first barren land was classified in two categories as soil and rocky terrain, and then combined in one class as a *mixture barren land.*

Figure 1.16: Mixed Barren Land.

Figure 1.17: Barren Land view from airphoto.

1.6 Data Characteristics Used in the Study

Like in the majority of the research areas, the most important input to the remote sensing system for the aim of classification is the data. In this study, three kinds of data were used for the assessment of the classification procedure. Multispectral images from BILSAT, Landsat-7 and IKONOS were acquired for the research purposes. BILSAT and Landsat-7 images (see Appendix B and Appendix C) were used as an input data to the classification. IKONOS image was used as a reference data in this study. Using different data advance to compare the performance of classification algorithms and analyze the results in a more realistic way.

1.6.1 BILSAT-1 Data

BILSAT-1 is an enhanced micro satellite designed and manufactured in the framework of a KHTT programme between SSTL (UK) and TUBITAK-BILTEN (Turkey). It was launched by a COSMOS 3M launch vehicle from the Plesetsk Cosmodrome in Russia on September 27, 2003 [63]. It is Turkey's first source of multispectral imagery. BILSAT-1 multi-spectral imaging system records in red, green, blue and near infrared channels (see Table 1.2). BILSAT-1 image was obtained from TUBITAK-BILTEN which was acquired on summer of 2004. This image is geometrically corrected according to reference red channel [63]. It is not corrected radiometrically.

Table 1.2: BILSAT imagery characteristics.

Band numbers	Spectral Bands(microns)	Spatial Resolution(m)
1 Blue	0.448-0.516	27
2 Green	0.523-0.605	27
3 Red	0.629-0.690	27
4 NIR	0.774-0.900	27
Panchromatic	0.520-0.900	12

1.6.2 Landsat-7 Data

Since the early 1970's, USA Landsat satellites have been supplying multispectral images of the Earth continuously for an input to different applications. These images have taken critical role in the development of remote sensing system. Landsat-7 is the latest satellite in these series. It was successfully launched from Vandenburg Air Force Base on April 15, 1999. Its payload is a single nadir-pointing instrument, called as Enhanced Thematic Mapper Plus (ETM+). Landsat-7 ETM+ records in 7 bands ranging from blue to thermal in spectral range [71] (see Table 1.3).

Landsat ETM+ image (path 177, row 32) used in this study for classification process was acquired on June 30, 2001 containing Middle East Technical University (METU) settlement. Data was obtained from INTA Space Imaging including all bands that were radiometrically and geometrically corrected. Geometric correction is done with image to map registration method. Data is a Fast L-7A Format. It is a derivative of the fast format originally developed by EOSAT as a means for quickly accessing Landsat 4 and 5 image data [71].

Table 1.3: Landsat 7 ETM+ imagery characteristics.

Band Numbers	Spectral Bands(microns)	Spatial Resolution(m)
1 Blue	0.450-0.515	30
2 Green	0.525-0.605	30
3 Red	0.630-0.690	30
4 NIR	0.750-0.900	30
5 Mid-Infrared	1.55-1.75	30
6 Thermal	10.40-12.50	60
7 Far-Infrared	2.09-2.35	30
Panchromatic	0.52-0.90	15

1.6.3 IKONOS Data

IKONOS which is USA's high resolution satellite imagery, launched from Vandenberg Air Force Base, California on 24 September 1999 [22]. It is the first commercially available high resolution data. IKONOS data containing part of METU settlement was acquired from INTA Space Imaging for research purpose. IKONOS imaging system records in red, green, blue and near infrared channels (see Table 1.4). The data is represented (quantized) by 11 bits per pixel. Its format is Geotiff [22]. Data is radiometrically and geometrically corrected. Data type is PAN/MSI which means RGB bands' spatial resolution was decreased from 4m to 1m taking reference as a pancromatic band having a 1m resolution. PAN data is not useful for classification process. These data were used in determining the training areas, taking the advantage of high resolution.

Table 1.4: IKONOS imagery characteristics.

Band numbers	Spectral Bands(microns)	Spatial Resolution(m)
1 Blue	0.450-0.515	4
2 Green	0.525-0.605	4
3 Red	0.630-0.690	4
4 NIR	0.750-0.900	4
Panchromatic	0.526-0.929	1

CHAPTER 2

DATA ANALYSIS

Data analysis is the product step of the system where the remotely sensed data are examined, displayed and analyzed. Two different kinds of analyses can be done in this step. The first one is the visual interpretation, and the other one is digital image processing. After developments in the remote sensing systems, analysts realized that visual interpretation would not give enough information that they had expected. In time, the quality (e.g. resolution) of the remotely acquired data increased to allow extraction of more information by digital image processing methods with respect to visual interpretation. Presently, digital processing with the aid of computers is one of milestones of remote sensing. The *advantages* of digital processing can be ordered as follows [7, 21, 53]:

1. Computers can go beyond the human eyes which are sensitive to only 32 gray levels. Computers mostly use 256 levels which aids to do more detail processing.

2. The repeatability of using complex algorithms and obtain same results with the same inputs and algorithms.

3. The memory capacity.

4. The capability to store all inputs, outputs make it possible to solve complex problems by combining the different informations of the same area under investigation.

Usually, the input data for the analysis is the digital data which is obtained from the radiation coming from the target and recorded by the sensor (see Section 1.3). First of all, the digital data pass through some processing to make the data

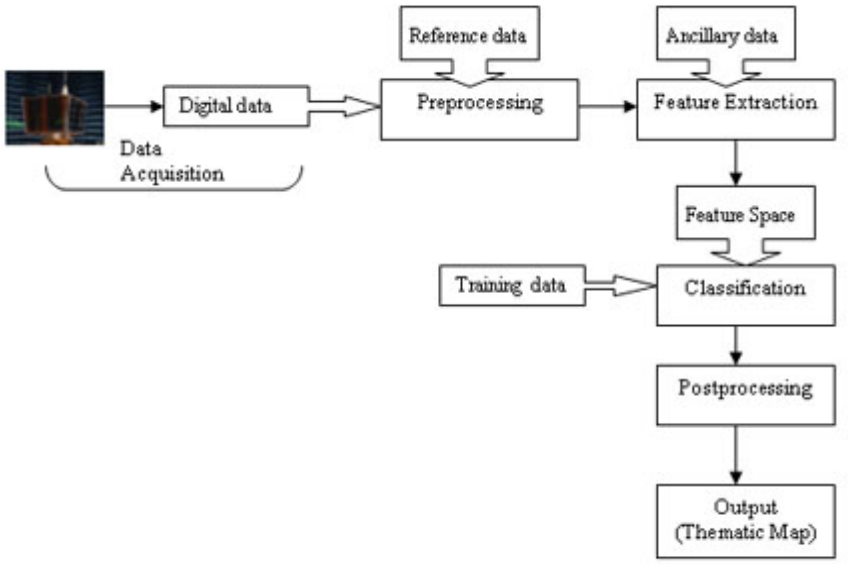

Figure 2.1: Data Analysis Flow.

ready for the classification process which could be *geometric correction, radiometric correction, denoising* known as preprocessing. After preprocessing methods, image classification is performed according to the problem under investigation to extract the information. The aim of the *image classification* in the context of remote sensing is to assign each pixel in the digital data to a specified cluster. In this study, land cover classification is under consideration which is the main step in the analysis of any remotely sensed satellite imagery for most applications. Details will be discussed in the following chapter.

The classified image can be processed again for the visual analysis if necessary. When classification is completed, accuracy assessment should be performed for quantifying the reliability of the classified image. Classified image (thematic map) is ready for the end users such as farmers, researchers, etc., after accuracy assessment. This data also can be used as an input to GIS for extracting different informations from the same area.

Data analysis flow can be summarized in Figure 2.1.

2.1 Image Rectification and Restoration

2.1.1 Geometric Correction

The sources of geometric distortions are originated from variations in the altitude, attitude, velocity of the sensor platform, panoramic distortion, earth curvature, atmospheric refraction, relief displacement and nonlinearities in the sweep of a sensor's IFOV [34].

Geometric correction can be given by the following formula [34]:

$$x = f_1(X, Y) \text{ and } y = f_2(X, Y),$$

where (x, y) denote distorted–image coordinates (column, row), (X, Y) denote correct map coordinates, and f_1, f_2 are the transformation functions.

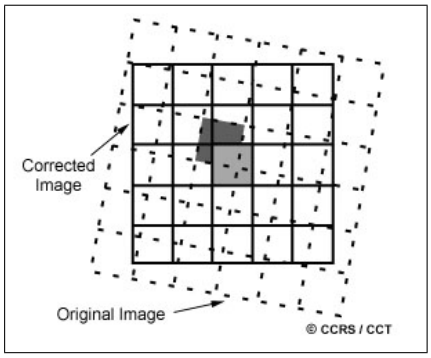

Figure 2.2: Example to the geometric correction by nearest neighbor method.

Most common techniques for geometric correction are *image to map* rectification and *image to image* registration through the selection of a large number of ground control prints [30]. In order to geometrically correct the original distorted image, *resampling* is used to determine the new digital values for the new pixel locations. In the resampling process, the new pixel values are calculated from the original digital pixel values in the uncorrected image. Nearest neighbour, bilinear interpolation and cubic convolution are the methods for resampling [68] (for details See [26, 34]). Figure 2.2 is an example for the nearest neighbour method which assigns the new pixel values according to the closest distance in the original image.

Geometric corrections are important in assessing the accuracy with the reference data and also in GIS applications. Landsat-7, BILSAT and IKONOS data were acquired in a geometrically corrected form. For Landsat-7 data, the correction was made geometrically by the image to map registration method. BILSAT data was corrected geometrically by the image to image registration method according to the red channel reference data. This data was also corrected geometrically according to the Landsat image using ERDAS software.

2.1.2 Radiometric Correction

The radiometric distortions are originated from the changes in scene illumination, atmospheric conditions, viewing geometry and instrument response characteristics [34]. Distortion caused by viewing geometry mostly occurs in the case of airborne data collection.

In the case of satellite data collection, mosaics of image can be generated by collecting data of the same area in different times and different bands [34]. When images are taken in different times, the sun elevation and the earth-sun distance are different. Both of these two factors can cause mistakes in the interpretation of the images. So, there is a need to overcome these problems by applying sun elevation correction and earth-sun distance correction.

The sun elevation correction is the seasonal position of the sun relative to the earth [34]. Image data acquired under different solar illumination angles are normalized by calculating pixel brightness values. Here, it is assumed that the sun was at the zenith on each date of sensing. The image is usually corrected by dividing each pixel value in a scene by the sine of the solar elevation angle for the particular time and location of imaging. The earth-sun distance correction is done by normalizing for the seasonal changes in the distance between in earth and the sun [34].

The combined influence of solar zenith angle and earth-sun distance on the irradiance incident on the earth's surface ignoring atmospheric effects can be given as [34],

$$E = \frac{E_0 \cos\theta_0}{d^2}$$

where E denotes the normalized solar irradiance, E_0 is the solar irradiance at mean earth-sun distance, θ_0 denotes sun's angle from the zenith, and d is the earth-sun distance, in astronomical units [34].

Since the remotely acquired data generally are brightness values in different regions of electromagnetic spectrum, radiometric distortions affect directly the classification results.

2.1.3 Noise Removal

Noise can either degrade or totally mask the radiometric information content of a digital image. Any unwanted disturbance in the image can be originated from

1. limitations in the sensing signal digitization,
2. data recording process,
3. background radiation,
4. thermal noise on the sensors,
5. sampling and quantization losses,
6. noise of the electronic circuits,
7. atmospheric affects,
8. scattering.

It should be known how much of the recorded signal that in average is usable information and how much is unwanted distortion or noise [66] which determines the quality measure of a signal in terms of noise, known as the *signal to noise ratio* (SNR). It is a measure of signal strength relative to background noise.

Noise removal includes any subsequent enhancement or classification of the image data. The objective is to restore an image to as close as approximation of the original scene as possible [34].

2.2 Image Enhancement

The objective is to create "new" images from the original image data in order to improve the visual interpretation and display of the data for extracting the features of interest (see Figure 2.3). Contrast manipulation (e.g. gray-level thresholding, level slicing), spatial feature manipulation (e.g. spatial filtering, Fourier analysis) and multi-image manipulation (e.g. principal components, vegetation components) are the techniques of image enhancement [30, 34].

Image enhancement algorithms are mostly application dependent and subjective [17]. For example, the Laplacian operator can be used to highlight details, gradient to enhance edges, grey-level transformation to increase dynamic range. For classification process image enhanced data was not used commonly because of the loss of information during the processing. This process is useful after classification for visual interpretation.

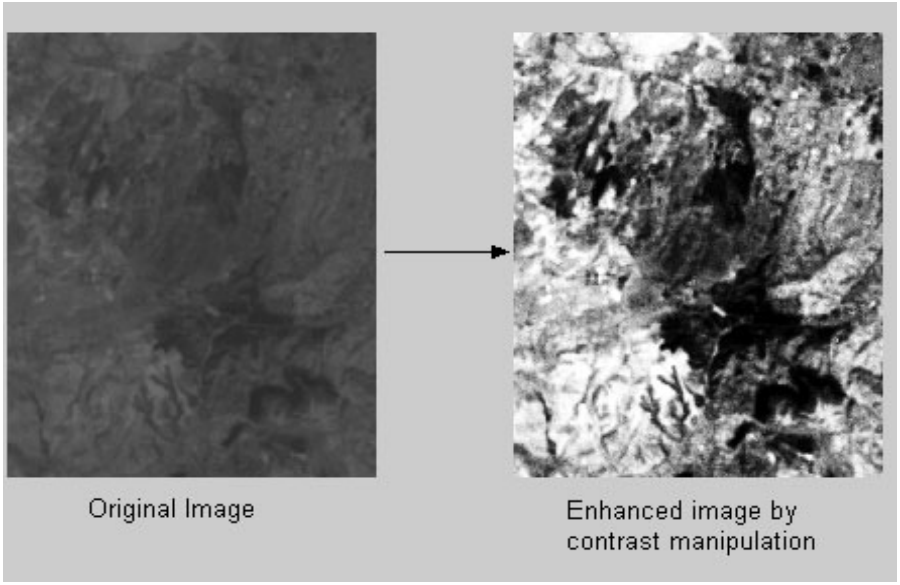

Figure 2.3: Image enhancement of image includes METU settlement from BILSAT red channel.

CHAPTER 3

IMAGE CLASSIFICATION

According to development in the space technology, remote sensing has become important in pattern classification from viewpoint of global environmental problems [62]. Classification is regarded as a fundamental process in remote sensing, which lies at the heart of transformation from satellite image to usable geographic product [60]. The goal of the classification is to assign each pixel to one of the user defined clusters by using their spectral reflectance in various bands (additional characteristic properties can also be added).

In the literature, there are so many classification techniques and their number increase day by day. They all give different results with the different training sets which consist of pixels with their spectra and ground truth values [51]. Both selecting the training data and choosing the optimal classification algorithm is very important in the classification process. It directly affects the classification performance. Determining the classification technique used for the study is dependent on the purpose of the study and data characteristics that will be used for the classification process. The data characteristic considerations involve the selection of the data of proper spectral resolution, spatial resolution, radiometric resolution, temporal resolution, data formats, data availability, cost, and the data quality [30]. Therefore, it can be concluded that classification system is a complex system with all these parameters.

3.1 Problem Statement

In image classification, as it is mentioned before, the input image should be a digital data for digitally processing the remotely sensed data. *Digital data* can be obtained from instruments that calibrated onto the satellite or airplane by recording the reflected or emitted radiation from individual patches of ground, known as *pixels*. Digital data is composed of these pixels which are recorded digitally by numeric values. Discrete digital values for each pixel are recorded in a form suitable for analysis by digital computers [7]. These values are popularly known as *digital numbers* (DN) or brightness values and these values do not represent the true radiometric values because of the radiometric distortions (see Subsection 2.1.2).

The number of the brightness values within a digital image is determined by the number of the bits available. The 8-bit permits a maximum range of 256 possible values (0 to 255) for each pixel. However, 6 bits would decrease the range of brightness values to 64 (0 to 63). So; it is clear that the number of bits determine the radiometric resolution.

The digital data can be expressed as:

$I = y(i, j)$, where $y(i, j) = (y_1(i, j), y_2(i, j), ..., y_n(i, j))$ is a vector representing the features of the pixel with a location (i, j).

Here, $y_1(i, j), y_2(i, j), ..., y_n(i, j)$ represents the features describing the object which may be spectral reflectance or emittance values form optical or infrared imagery, radar backscatter values, secondary measurements derived from the image (such as texture), or geographical features such as terrain elevation, slope and aspect [55]. This set of of gray-scale values for a single pixel known as a pattern. Thus, a pattern is a set of measurements on the chosen features for the individual that is to be classified [39].

For example,

$y_1(i, j) = 49$ can denote the digital number which represents the intensity of the red light reflected from pixel (i, j);

$y_2(i, j) = 53$ can denote the digital number which represents the intensity of the green light reflected from pixel (i, j);

$y_3(i, j) = 70$ can denote denote the digital number which represents the intensity

of the blue light reflected from pixel (i, j).

Let $y(i, j) = (y_1(i, j), y_2(i, j), y_3(i, j))$ denote the pattern vector of pixel of a multispectral image.

Thus, each pixel is represented as a pattern vector composed of the features. To do geometric calculations, each feature is thought to be an axis of multidimensional space. Then, a pixel can be represented as a point in that space. This space that represents all the possible values of a pixel is called the *state space* (see Figure 3.1). The values of neighbouring samples form spatial patterns. The space representing all possible patterns of neighbouring pixels is called the *function space.*

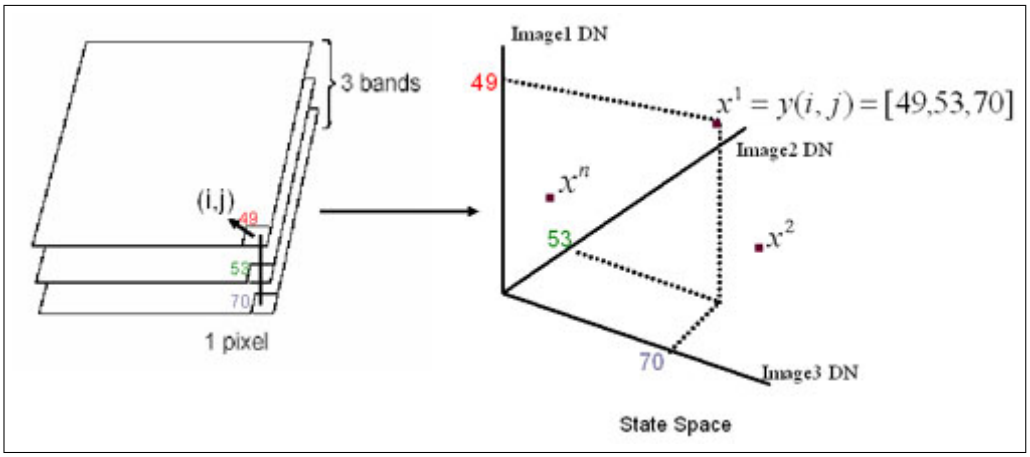

Figure 3.1: State Space Representation.

The computational requirements of classification are generally positively correlated with the number of features used as input to the classification algorithm. Thus, in order to facilitate classification (reduce the number of input features) and increase the accuracy, a number of techniques can be used to manipulate or transform the axes of the state space to a new space [55]. This new space is called *feature space*. The selection of the optimum number of the features is very important for the computation effort and accuracy. During the transformation some important information may be lost. A pattern is made up of measurements on this feature space. Feature extraction is optional, i.e. the multispectral image can be used directly, if desired.

In selecting or designing features, features that are simple to extract, invariant to irrelevant transformations, insensitive to noise, and useful for discriminating patterns in different categories might be preferrable [14].

Tso and Mather [55] mention that two methods can be used to reduce the number of input features without sacrificing accuracy. One is to project the original feature space on to a subspace (i.e. a space of smaller dimensionality). This can be done using either an orthogonal transformation including Tasseled Cap transform, principal component analysis, min/max autocorrelation factors, maximum noise fraction transformation or a self-organized feature map (SOM) neural network. The second method is to use separability measurements in the state space and then select the subfeature dimension in which separability is a maximum. The aim is to reduce the feature space dimension without prejudicing classification accuracy. Two separability indices, namely divergence index and B-distance are widely used. For more information refer to reference [55].

After determining the optimum feature space, the classification algorithms are used in that space. The points in that space which represents the patterns can be separated from each other by lines or curves called *decision boundary*. In higher dimensional space, these lines and curves become hyperplanes and hypersurfaces [24]. The classification algorithm assigns each pixel to a cluster of state space with respect to the decision boundary. This classification algorithm is named as a *decision rule*. The decision rule find the relationship between value of the pixel and its class. The function that partitions the feature space into subspaces according to the decision rule is called *discriminant function*. Thus, the image classification process involves the subdivision of feature space into homogenous regions separated by decision boundaries [24].

We assume that we have been given a set X of a finite number of points of d-dimensional space [3]

$$X = \left\{x^1, x^2, ..., x^n\right\}, \text{ where } x^i \in R^d (i = 1, 2, ..., n).$$

The subject of image classification is the partition of the set X into a given number q of overlapping or disjoint classes S_k with respect to predefined criteria

such that $X = \bigcup_{k=1}^{q} S_k$ [3].

Let $A = \{A_1, A_2, ..., A_n\}$ be a finite alphabet and the symbol A_k represents the land cover class S_k for example woodlands, water bodies, forest such that

$$a(i,j) = A_k \text{ , if } y(i,j) \in S_k.$$

In this study, $S_k(k = 1, 2, 3, 4, 5, 6)$ represents built-up land, agricultural land, forest land, water, barren land (soil) and barren land (rocky terrain).

Therefore, the classification problem is an *inverse problem* [**?**]. We can express this problem as:

$$\text{Given } y(i,j) = (y_1(i,j), y_2(i,j), ..., y_n(i,j)) \text{ determine } a(i,j),$$

where n is the number of features.

3.2 Classification Techniques

Classification techniques mainly vary according to the priori knowledge of the target area as the *supervised* and *unsupervised classification* (see Figure 3.2).

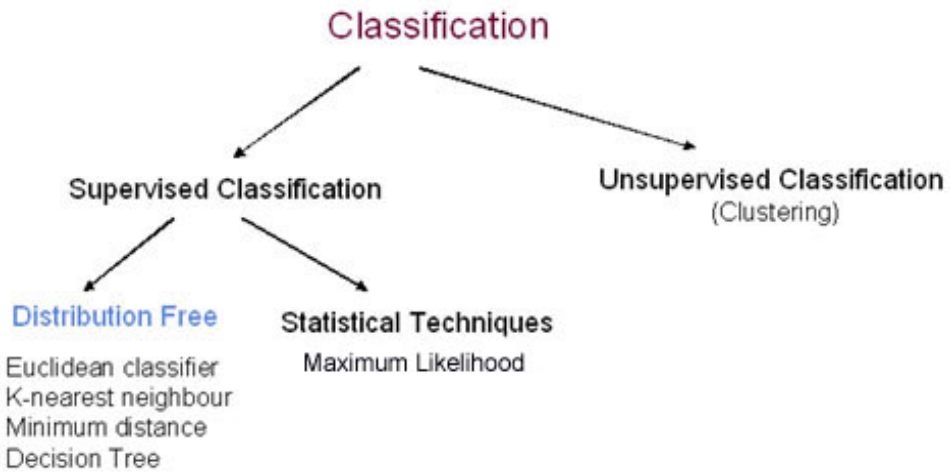

Figure 3.2: Classification Techniques.

3.3 Unsupervised Classification

Unsupervised techniques of classification are used when little or no more detailed information exists concerning the distribution of ground cover types. In low dimensional problems ($d \leq 3$), there are effective non-parametric rules to have high accuracy performance classification results. But in high dimensions, these methods fail [19]. In an unsupervised classification, the identities of the land cover types to be classified as classes within a scene are not generally known in advance because ground reference information is lacking or surface features within the scene are not well defined [26]. After classification procedure, the interpreter assigns the cluster's name.

The aim is to group pixels according to their similarities which is computed by a similarity measures like euclidean distance. To define a clustering algorithm a similarity measure, a distintiveness test and a stopping criteria rule are required [24]. The success of clustering techniques closely depend on the feature selection. Fundamental to all clustering techniques is the choice of similarity or dissimilarity measure between two objects [19].

For any feature vectors, $y^1 \in R^d$ and $y^2 \in R^d$ where d is the number of features, some of commonly used similarity measures are [24]:

Dot product: $\langle y^1, y^2 \rangle \triangleq (\ y^1)^T\ y^2 = \|y^1\|\,\|y^2\| \cos(y^1, y^2)$,

Similarity rule: $S(y^1, y^2) \triangleq \frac{\langle y^1, y^2 \rangle}{\langle y^1, y^1 \rangle + \langle y^2, y^2 \rangle\ - \langle y^1, y^2 \rangle}$,

Weighted Euclidean Distance: $d(y^1, y^2) \triangleq \sum_k \left[y^1(k) - y^2(k)\right]^2 w_k$,

Normalized Correlation: $\rho(y^1, y^2) \triangleq \frac{\langle y^1, y^2 \rangle}{\sqrt{\langle y^2, y^2 \rangle \langle y^1, y^1 \rangle}}$.

Important disadvantages of unsupervised techniques can be listed as: having limited control over classes and identities, getting no detailed information and low accuracy percentage compared with the supervised classification methods.

There are three kinds of clustering algorithms: *Combinatorial Algorithms, Mixture Modelling and Mode Seeking*. Mixture modelling and mode seekers use probability density functions. But, combinatorial algorithms use directly observed data. The most popular clustering algorithms directly assign each unknown data to a cluster without using any probability model describing the data [19].

In the next subsection one of the most popular combinatorial clustering algorithm, k-means, will be discussed deeply. This method was used to classify two different data, BILSAT-1 and Landsat ETM+ for the METU Settlement.

3.3.1 K-Means Classification Method

K-means algorithm is a nonparametric combinatorial algorithm which means that this method works directly on the observed data with no direct reference to an underlying probability model [19]. It is very fast and suitable for large data sets.

Let Y be a set of a finite number of pixels of d-dimensional space R^d where $Y = \{y_,^1 y^2, ..., y^n\}$ and $y^i \in R^d (i = 1, 2, ..., n)$.

Let q be the number of clusters S_k that is $Y = \bigcup_{k=1}^{q} S_k$.

If every element of the data belongs to only one cluster, then the clustering problem is a hard clustering problem. Here a hard unconstrained clustering problem is considered which means that

$$S_i \cap S_k = \emptyset, \forall i, k = 1, 2, ..., q, i \neq k$$

and no constraints are imposed on the clusters. In k-means clustering, each cluster S_k is characterized by its centroids which are the means of classified pixels value in that cluster.

Bagirov and Yearwood [3] define the clustering problem as below:

$$\text{minimize } \varphi(S, a) = \frac{1}{n} \sum_{i=1}^{q} \sum_{y \in S_i} \parallel a_i - y \parallel^2, \tag{3.3.1}$$

$$\text{subject to } \; S \in \overline{S}, a = (a_1, a_2, ..., a_q) \in \mathbb{R}^{d \times q},$$

where $\| \cdot \|$ denotes Euclidean norm, $\overline{S}$ is a set of all possible q-partions of the set Y, a_i is the center of the cluster S_i, $a_i = \frac{1}{|S_i|} \sum_{y \in S_i} y$ and $|S_i|$ is the cardinality of the set $S_i (i = 1, 2, ..., q)$.

Here, Equation (3.3.1) is an optimization problem [3] and function φ is the *discriminant function*. The k-means algorithm achieves a local minimum of this problem; in other words, it finds an optimal partitioning of the data distribution into the requested number of subdivision [3]. The final mean vectors resulting from the clustering will be at the centroids of each subdivision.

In k-means algorithm if the groups of points are not so-well seperated then the decision boundary between each cluster are not so clear cut and there may be some doubt about the class membership (label) of points that are close to the decision boundary [39]. This method does not consider class variability; thus, large differences in the variance of the classes often lead to misclassification [37].

A program *kmeansc.m* was written for the implementation of this method. Following the algorithm is pointed out.

K-Means Algorithm:

1. Determine the initial positions of means or in other words initial values of each dimension per mean in the feature space for each cluster.

2. Calculate the distance between each cluster mean and the unknown pixel itself using the Euclidean Distance.

3. Allocate the unknown pixel to the cluster which is the closest cluster than the others according Euclidean Distance criteria.

4. Do the steps 2 and 3 for all pixels (Decision boundaries are determined).

5. Calculate the new cluster mean location for each class.

6. Do these steps iteratively until relabelling the pixels does not cause any change in the positions of the means.

3.4 Supervised Classification

In the context of supervised classification methods, the analyst collect samples to train the classifier to determine discriminant functions in the feature space. These samples are named as the *training sets*. The decision boundaries determined by the discriminant functions are significantly affected by the properties and the size of the training sets [55]. The training set also identifies the class labels. The analyst should have sufficient knowledge of the type and the number of class labels before collecting the training samples [55]. For example, in the land cover classification, the identity and location of some of the land cover types, such as urban, agriculture, or wetland, are known a priori through a combination of fieldwork, analysis of aerial photography, maps, and personal experience [40].

Supervised classification can be distribution free or statistical. Statistical techniques are based on probability distribution model. Multivariate statistical parameters (means, standard deviations, covariance matrices, correlation matrices, etc.) are calculated for each training site. Every pixel in the target area is then assigned to the priori defined classes according to the highest likelihood of a being a member of any class. In case of the limited training data information, solutions of this method are not reliable because multivariate statistical parameters of each training site are not calculated accurately. Furthermore, assumed analytically tractable classes of probability distributions might not reflect the reality. Three statistical classifier generally used are parallelpiped method, minimum distance classifier and Gaussian maximum likelihood method. Maximum likelihood classifier is the most common method used in the applications of remote sensing as a parametric statistical method. In our study, that method was implemented as a representative for statistical methods and will be discussed deeply in the following section.

In contrast, distribution free methods do not require knowledge of any priori probability distribution functions [24]. Euclidean classifier, k-nearest neighbor, minimum distance, decision tree, neural networks are the distribution free methods. The mathematical description for the distribution free methods can be given as below [24]:

Suppose that there are k different pattern classes. It is defined such that k^{th}

discriminant function $g_k(y)$ takes the maximum value if y belongs to class k, that is, the decision rule

$$g_k(y) > g_t(y)\ t \neq k \Longleftrightarrow y \in S_k,$$

where y denote $d \times 1$ feature vector obtained from the observed image.

For a k class problem we need $k-1$ discriminant functions. These functions divide the d dimensional feature space into k different regions with a maximum $k(k-1)/2$ of hypersurfaces.

In remote sensing applications, popular methods among the distribution free methods are decision tree and neural neworks. Neural network models have an advantage of nonparametric method. Additional non-remotely-sensed data such as slope angle or soil type can more easily be incorporated into a classification using a non parametric model [39]. On the other hand, neural networks can be very complex computationally, need a lot of training samples to be applied successfully and their iterative training procedures usually are slow to converge [5]. The performance of the neural network models in classification is therefore more dependent on having representative training samples, whereas the statistical approaches need to have an appropriate model of each class [5].

To resolve interclass confusion beside artificial neural networks and decision trees, methods derived from fuzzy set theory, the incorporation of secondary information such as texture, context and terrain features, hybrid systems have been used as an alternative methods [55]. Fuzzy set classification logic, which takes into account the heterogeneous and imprecise nature of the real world, may be used in conjunction with supervised and unsupervised classification algorithm. Sometimes it is necessary to include nonspectral ancillary data when performing a supervised, unsupervised, and/or fuzzy classification to extract the desired information [26].

3.4.1 Gaussian Maximum Likelihood Classification Method

Gaussian maximum likelihood classification method is based on the assumption that frequency distribution of the class membership can be approximated by the multivariate normal distribution [39]. The reason for using the normal distribution can be given as below:

1. It provides a mathematically tractable, analytical solution to the decision boundaries [55].

2. Image samples selected for supervised training often exhibit normal like distribution [55].

To understand this method more easily, suppose two features are used to classify the image; in other words, the feature space has two dimensions. The geometrical shape of the projection of the bivariate (using two features) frequency distribution of this satellite image's q clusters to the feature space are a family of concentric ellipses centred on the bivariate mean of each class. These ellipses represent contours of probability of membership of the class. The probability of membership declines away from the mean centre which is the coordinates of the center points of each class. Therefore; the probability that a pixel shown by a point in two dimensional feature space belongs to class k $(k = 1, 2, ..., q)$ can be measured for each class in turn and that pixel is assigned to the class for which the probability of membership is highest [39]. Training data are used to estimate shapes of the distribution of the membership of each class and the location of the mean. This idea can be carried out more than two dimensions.

In Gaussian maximum likelihood method, the frequency distribution of the class membership is approximated by the multivariate normal distribution. This means that the probability $P_k(y)$ that a pixel vector y of d elements (features) is a member of class k is

$$P_k(y) = 2\pi^{-0.5d} \det(E_k)^{-0.5} \exp\left[-0.5((y - \widehat{y_k})^T E_k^{-1}(y - \widehat{y_k}))\right],$$

where E_k is the variance-covariance matrix of the sample data for class k, $\widehat{y_k}$ is the multivariate mean of class k. Here, $P_k(y)$ is the *discriminant function.*

Training data is used to determine the parameters of the probability function, variance-covariance matrix and mean. As it is mentioned before mean controls the location of the ellipse in the feature space and the variance-covariance matrix controls spread and orientation of the ellipse.

The probability function can be made more simpler for decreasing the computational cost. Since logarithmic function is strictly increasing, and hence, does not affect the order of the solutions that we are interested in, the evaluation of the exponential operator can be avoided by applying ln function both side of the expression:

$$g_k(y) = \ln(P_k(y)) = -0.5d\ln(2\pi) - 0.5\ln(\det(E_k)) - 0.5((y - \widehat{y_k})^T E_k^{-1}(y - \widehat{y_k})).$$

Therefore, $y(i,j)$ is assigned to class S_k of q classes if $g_k(y) > g_t(y)$ for all $t \neq k$ with $t, k = 1, 2, ..., q$.

MLC requires sufficient representative spectral training sample data for each class to accurately estimate the mean vector and covariance matrix needed by the classification algorithm [37]. If the training samples are not sufficient, the class mean vector and covariance matrix which are the representatives of the classes are estimated inaccurately cause the classification procedure being poor.

In this study a program was written to implement this method in *MATLAB*. Solutions are discussed in the following chapter.

Gaussian Maximum Likelihood Algorithm:

1. Selection of the training data for each class.
2. Calculation of statistical parameters (mean, covariance matrix) of normal distribution function from each training data.
3. Calculation the probability for each class per pixel.
4. Assignment each pixel to a class according to the maximum probability.

3.5 A Generalization of Distribution Free Classification

We have already discussed that classification is based on partitioning the feature space or a limited function space (if some neighbouring pixels are also involved to

increase the performance). For any partition of the feature space we can define a discriminant function:

$$f_k : S \rightarrow U,$$

where $U = T \cup F$ is the solution space, $S = C_1 \cup C_2 \cup ... \cup C_n$ is the state space, $C_i (i = 1, 2, ..., n)$ are the partitions belonging to the classes, and n is the number of classes, such that

$$\text{if } \; y(i,j) \in C_k \; , \quad f_k(y(i,j)) \in T$$

$$\text{else} \qquad\qquad , \quad f_k(y(i,j)) \in F$$

Development of various optimization and estimation methods let us consider a parametric discriminant function class and to find the optimum parameters partitioning the state space by using the training data. In fact, most of the well known distribution free classifier methods are effectively performing the same task. For example, neural networks optimize piecewise linear discriminants discriminants. K-nearest-neighbor method optimizes Euclidean distance, etc.. This is a very strong motivation to consider various parametric function classes rather than using preassumed discriminants. In this work, we developed a novel distribution free classifier based on threshold decomposition and Boolean discriminant functions as a particular example.

3.6 Threshold Decomposition and Boolean Discriminant Functions

As it is mentioned before, the point in the classification task is to partition the feature space into decision regions, each representing one category. In this part, we discuss the classification problem from the viewpoint of a distribution free classifier.

In the feature space, the decision region for the classes might be arbitrarily partitioned. Our purpose is to adopt to arbitrary shapes of these partitions. To find these partitions, firstly training data for each class which can be placed in different

regions of the feature space is selected. Then, the closest distance among training samples to the unknown pixel can be an alternative to adopt to a larger range of possible feature space partitioning. However, to use such a selection rule requires the comparision of each pixel with the full training set if we are working in the continuous variables domain. This is computationally expensive. Furthermore, it is not resistant to outliers in the training set; in other words, any incorrect training data selection can cause misclassification. The alternative is to find an appropriate discriminant function class, which can be inferred from the training data.

If we are able to divide the feature space into limited number of subspaces, there exists a Boolean function [32, 33, 47] which is uniquely separating each subspace from the others. The Boolean function in the variables $y_,^1 y^2, ..., y^n$ is a map $g : \{0,1\}^s \rightarrow \{0,1\}$ [47].

Thus, to determine a Boolean function as a discriminant, we suggest to use threshold decomposition originally developed for implementing order statistics estimators (e.g., stack filters) [11, 42]. Here, we consider to equip our classifier with the capability of adopting to arbitrary partitioning of state space at cost of radiometric resolution. Classification accuracy depends on the number of selected threshold levels. Moreover, more threshold levels mean more computation.

Suppose that Y is a set of a finite number of pixels of d-dimensional space R^d, where $Y = \{y_,^1 y^2, ..., y^n\}$ and $y^i \in R^d$ $(i = 1, 2, ..., n)$.

Let the number of the classes to be classified be q. We should determine a training data set each class. Let $M = \{x^1, x^2, ..., x^m\}$ be the training data set for class k $(k = 1, 2, ..., q)$. Here, $x^j \in R^d$ $(j = 1, 2, ..., m)$ such that $M \subset Y$. With the help of the whole training data set, we can find a Boolean classifier function which uniquely discriminates the dataset. To find the classifier as a Boolean function, first the training set is decomposed into binary digits according to the predefined threshold levels.

Suppose that $x^j \in R^d$ $(j = 1, 2, ..., m)$ is $(\alpha + 1)$-valued: $x^j \in \{0, 1, ..., \alpha\}^d$ (for a 8-bit image: $\alpha = 255$) and it may denote the patterns of training set for class k. *Threshold decomposing* of class k consists of elements x_p^j $(j = 1, 2, ..., m; p = 1, 2, ..., d)$ with respect to t^w $(w = 1, 2, ..., v) \in R^r$, being the threshold vector, where r is the number of predetermined thresholds, v is the number of threshold vectors

can be defined as:

$$T^k(x_p^j) = \begin{cases} 1, & \text{if } x_p^j \geq t_l^w;, \\ 0, & \text{otherwise} \end{cases} \quad (j = 1, 2, ..., m; p = 1, 2, ..., d; l = 1, 2, ..., r; w = 1, 2, ..., v). \tag{3.6.2}$$

where $T^k(x_p^j) = (T_1^k(x_p^j), T_2^k(x_p^j), ..., T_r^k(x_p^j))$. Here, $T : R^d \rightarrow \{0, 1\}^p$ is named as *the threshold decomposition function.*

Let us give an example to better understand threshold decompositon. Suppose that we have two training sets: V1 for $k = 1$ and V2 for $k = 2$, with two features per pixel to be classified. $V1 = \{x^1, x^2\} = \{(30, 40), (50, 60)\}$ and $V2 = \{x^3, x^4\} = \{(100, 120), (140, 160)\}$. Let the thresholds be the mean values of the same feature values of corresponding training data. For the first feature: $t^1 = (120, 40)$, and for the second one: $t^2 = (140, 50)$. The training data values after decomposition are

$$\begin{aligned}
&T^1(x_1^1) = (x_1^1 \geq t_1^1, x_1^1 \geq t_2^1) = (30 \geq 120, 30 \geq 40) = (0, 0), \\
&T^1(x_2^1) = (x_2^1 \geq t_1^2, x_2^1 \geq t_2^2) = (40 \geq 140, 40 \geq 50) = (0, 0), \\
&T^1(x_1^2) = (x_1^2 \geq t_1^1, x_1^2 \geq t_2^1) = (50 \geq 120, 50 \geq 40) = (0, 1), \\
&T^1(x_2^2) = (x_2^2 \geq t_1^2, x_2^2 \geq t_2^2) = (60 \geq 140, 60 \geq 50) = (0, 1), \\
&T^2(x_1^3) = (0, 1), \\
&T^2(x_2^3) = (0, 1), \\
&T^2(x_1^4) = (1, 1), \\
&T^2(x_2^4) = (1, 1).
\end{aligned}$$

As it is clear from the example, we use the same threshold levels for the same features. In this study, we use training data mean values arranged in a descending order as threshold levels. Also, minimum and maximum values of RGB features of each pixel are considered as threshold levels. The Boolean discriminant function for

the class k is:

$$BF_k(y^i) = F^k_{x^1}(y^i) \vee F^k_{x^2}(y^i) \vee ... \vee F^k_{x^m}(y^i) \ (i = 1, 2, ..., n; k = 1, ..., q) \quad (3.6.3)$$

$$F^k_{x^j}(y^i) = f^k_{x^j_1}(y^i) \ \wedge f^k_{x^j_2}(y^i) \ \wedge ... \wedge f^k_{x^j_d}(y^i) \ (j = 1, 2, ..., m), \quad (3.6.4)$$

$$f^k_{x^j_p}(y^i) = T^k_s(x^j_p)(y^i) \wedge \overline{T^k_{s+1}(x^j_p)(y^i)} \ (j = 1, 2, ..., m; p = 1, 2, ..., d). \quad (3.6.5)$$

where y is the image data sample (pixels to be classified), x denotes the training sample and $\{x^1, x^2, ..., x^m\}$ are the training samples for class k, n is the number of samples, q is the number of classes, m is the number of training samples in class k, d is the number of features. Moreover, $f : R^d \rightarrow \{0, 1\}$ is a Boolean function in *disjunctive normal form* [47] which uniquely identifies the subspaces of the p^{th} feature belonging to the training sample x^j_p according to s and $s + 1$. Here, T is the threshold decomposition function (see (3.6.2)) and s denotes the sequence number of $T^k(x^j_p)$ beginning from the end where $T^k(x^j_p)(s) = 1$ and $T^k(x^j_p)(s + 1) = 0$. Then, $T^k_s(x^j_p) \wedge \overline{T^k_{s+1}(x^j_p)} = 1 \wedge \overline{0} = 1 \wedge 1 = 1$. Furthermore, $F : R^d \rightarrow \{0, 1\}$ is a Boolean function in *disjunctive normal form* [47] that identifies the subspaces of all features belonging to the training sample. Finally, $BF_k : R^d \rightarrow \{0, 1\}$ is the Boolean discriminant function *conjunctive normal form* [47] which partitions the feature space into subspaces. Here, $\vee$ is the logical OR operation, $\wedge$ is the logical AND operation and $\overline{x}$ is the *complement* of a variable x in the Boolean expression.

The components of the vector $(T^k(x^j_p))$ $(j = 1, 2, ..., m; p = 1, 2, ..., d; k = 1, 2, ..., q)$ are 0 or 1 with a monotonously increasing order. This is the main advantage of building Boolean functions since the sequences of the transition from 0 to 1 uniquely determine Boolean discriminant function (see (3.6.5)).

For our complete image data set $Y = \left\{y^1_, y^2, ..., y^n\right\}$; it holds:

$$BF_k(y^i) = 1 \Longrightarrow y^i \in C_k \ (k = 1, 2, ..., q; i = 1, 2, .., n), \quad (3.6.6)$$

where C_k denotes the classes.

Therefore, the binary vectors $T^k(x^j_p)$, are used to obtain a Boolean discriminant function whose output is 1 if a pixel is lying within the same subspace with any of the training samples (see (3.6.6)). With these binary vectors, various Boolean

functions can be built.

According to (3.6.2) - (3.6.6), some subspaces might not include any training pixel and some might include training data from more than one class. The subspaces which do not include any training pixel are classified according to the minimum Hamming distance between unknown pixel and training data. *Hamming distance* is the sum of the unequal bits:

$$y^i \in C_k \text{ if } \min_{x \in ts}(H(T^k(y_p^j), T^k(x_p^j))) = \min_{x \in C_i}(H(T^k(y_p^j), T^k(x_p^j)))$$

$$H(T^k(y_p^j), T^k(x_p^j)) = \sum_{\alpha=1}^{p} T_\alpha^k(x_p^j) \oplus T_\alpha^k(y_p^j)$$

where α denotes the elements of binary vector, y is the data sample which is not assigned to a class, x denotes the training sample and ts is the training data set. Here, $T : R^d \rightarrow \{0,1\}^p$ is the threshold decomposition function and $\oplus$ denotes the logical EXNOR (exclusive OR) operator which is 1 if two binary variables are different and 0 else. Finally, $H : \{0,1\}^p \rightarrow \{0,1,...,p\}$ is the *Hamming distance*.

The subspaces including training data from more than one classes are assigned according to the Hamming distance using the threshold decomposition of mean values. For future study, dividing these subspaces by additional threshold levels is considered.

In this study, a program *booleanthresh.m* (see Appendix A) was written in MATLAB for the implementation of this method. The results are discussed in the next chapter.

Boolean Discriminant Classifier Algorithm:

1. Selection of the training data for each class.
2. Selection of threshold levels used for threshold decomposition.
3. Threshold decomposition of the input data according to the predefined threshold levels from Step 2.

4. Threshold decomposition of the training data set according to the same threshold levels.

5. Determination of the indicator to a Boolean classifier function which uniquely discriminates the dataset.

6. Assignment of the pixels on the image to one of the predefined classes with the indicators determined in Step 5.

7. Assignment of unclassified pixels from Step 6 according to the Hamming distance.

8. Assignment of pixels that belongs to more than one class according to the Hamming distance to the threshold decomposition of mean values.

Let us give an example with a multispectral image (A) to understand better how the program works. Let $A(k)$ ($k = 1, 2, 3$) be a matrix containing spectral reflectance values from a feature: red, green or blue. Thus, the state space is three dimensional space, each dimension represents red, green and blue feature values. Since the number of dimensions is not so high, there is no need to transform the state space to the feature space. State space is used directly for the classification. We have determined six classes to be classified: water, forest land, soil, rocky terrain, agriculture land and builtup. According to the classification problem, this three-dimensional state space should be divided to the six subspaces by the decision boundaries.

Step 1: Selection of the training data for each class.

Six training data are determined with the *trainselection.m* file. The user can select the training data from the image which appears on the screen with a mouse. Let us denote the training data for water by v^1, forest land by v^2, soil by v^3, rocky terrain by v^4, agriculture land by v^5, built-up by v^6. Here, v^j ($j = 1, 2, ..., 6$) is a matrix whose column represents the results from one feature where j denotes the class index. Since there are three features in this example, v^j matrix has three columns and the number of the rows are dependent on the number of the selected

training sample. So, v^j is a $(m \times 3)$ matrix where m denotes the number of the selected training sample corresponding to that class.

Suppose $y^i = (y_1^i, y_2^i, y_3^i)$ $(i = 1, 2, ..., m)$ represents a pixel where y_1^i is the first feature (red band) value, y_2^i is the second feature (green band) value and y_3^i is the third feature (green band) value of pattern (or pixel) y^i. Let m be the number of training samples for the corresponding class. $y_k^i, (i = 1, 2, ..., n; k = 1, 2, 3) \in \{0, 1, ..., 255\}$. For the first class training data $(j = 1)$, v^1 is obtained as follows:

$$v^1 = \begin{bmatrix} y_1^1 & y_2^1 & y_3^1 \\ y_1^2 & y_2^2 & y_3^2 \\ .. & .. & .. \\ .. & .. & .. \\ y_1^m & y_2^m & y_3^m \end{bmatrix}$$

Furthermore, r^j, g^j, b^j $(j = 1, 2, ..., 6)$ vectors are determined with *trainsort.m* (refer to Appendix!) where r^j is the first column of the matrix v^j, g^j is the second column of the matrix v^j and b^j is the third column of the matrix v^j. Here, j denotes the class index. The outputs from *trainsort.m* are r^j, g^j and b^j vectors with an ascending order and mean values $a^j = (a_1^j, a_2^j, a_3^j)$ $(j = 1, 2, ..., 6)$ of each training data v^j. Here, a^j is a three dimensional vector whose k^{th} $(k = 1, 2, 3)$ element represents the mean value of v^j matrix k^{th} $(k = 1, 2, 3)$ column. This means that a_1^j is the mean value of the first feature (red band) values of class j, a_2^j is the mean value of the second feature (green band) values of class j and a_3^j is the mean value of the third feature values of class j.

Step 2: Selection of threshold levels which are used for threshold decomposition.

First, mean values of the training data are arranged in a descending order. Classes (water, forest land, soil, rocky terrain, agriculture land and built-up) spectral reflectance is in an ascending order. This means that built-up spectral reflectance is close to 255, while water spectral reflectance is close to 0. The remaining data are arranged in order between built-up and water. Then, three threshold vectors

containing seven threshold levels are obtained from the mean values of each class training data. In this study, these threshold vectors are selected as follows:

$$\begin{aligned}
TR &= [0.5 \times (250 + a^6(1)), 0.5 \times (a^6(1) + a^5(1)), 0.5 \times (a^5(1) + a^4(1)), 0.5 \times (a^4(1) + a^3(1)), \\
&\quad 0.5 \times (a^3(1) + a^2(1)), 0.5 \times (a^2(1) + a^1(1)), 0.5 \times a^1(1)], \\
TG &= [0.5 \times (250 + a^6(2)), 0.5 \times (a^6(2) + a^5(2)), 0.5 \times (a^5(2) + a^4(2)), 0.5 \times (a^4(2) + a^3(2)), \\
&\quad 0.5 \times (a^3(2) + a^2(2)), 0.5 \times (a^2(2) + a^1(2)), 0.5 \times a^1(2)], \\
TB &= [0.5 \times (250 + a^6(3)), 0.5 \times (a^6(3) + a^5(3)), 0.5 \times (a^5(3) + a^4(3)), 0.5 \times (a^4(3) + a^3(3)), \\
&\quad 0.5 \times (a^3(3) + a^2(3)), 0.5 \times (a^2(3) + a^1(3)), 0.5 \times a^1(3)],
\end{aligned}$$

Step 3: Threshold Decomposition of the input data (A) according to the predefined threshold vectors TR, TG and TB.

As it is mentioned before, $A(k)$ $(k = 1, 2, 3)$ is a matrix represents the image which has only k^{th} feature values. Each matrix is seen on the screen in grayscale. The combination of these three matrices is seen in colour. If the matrices are ordered as red, green, blue, the image is seen in true colour format. File *thrdecom.m* decomposes the image A into Boolean vectors according to the threshold vectors TR, TG and TB. The outputs of this program are the vectors rbv, rcv, gbv, gcv and bbv whose elements are matrices of Boolean vectors. In this study;

$rbv = (rbv(1), rbv(2), ..., rbv(7))$, where $rbv(d)$ $(d = 1, 2, ..., 7)$ is a matrix with the same size of the image A. Using $TR(d)$ $(d = 1, 2, ..., 7)$, the d^{th} element of rbv is obtained by the threshold decomposition of $A(1)$ which is the image obtained from the first feature values of the target area. The entries of the matrix $rbv(d)$ $(d = 1, 2, ..., 7)$ are 0 or 1.Suppose that A image consists of four pixels. The different partitions of the matrix rbv are shown as follows:

$$
\begin{aligned}
A(1) &= \begin{bmatrix} A(1)_{11} & A(1)_{12} \\ A(1)_{21} & A(1)_{22} \end{bmatrix} \rightarrow rbv(1) = \begin{bmatrix} A(1)_{11} > TR(1) & A(1)_{12} > TR(1) \\ A(1)_{21} > TR(1) & A(1)_{22} > TR(1) \end{bmatrix} \\
A(1) &= \begin{bmatrix} A(1)_{11} & A(1)_{12} \\ A(1)_{21} & A(1)_{22} \end{bmatrix} \rightarrow rbv(2) = \begin{bmatrix} A(1)_{11} > TR(2) & A(1)_{12} > TR(2) \\ A(1)_{21} > TR(2) & A(1)_{22} > TR(2) \end{bmatrix} \\
& \cdots\cdots\cdots\cdots\cdots\cdots\cdots\cdots\cdots\cdots\cdots\cdots \\
A(1) &= \begin{bmatrix} A(1)_{11} & A(1)_{12} \\ A(1)_{21} & A(1)_{22} \end{bmatrix} \rightarrow rbv(7) = \begin{bmatrix} A(1)_{11} > TR(7) & A(1)_{12} > TR(7) \\ A(1)_{21} > TR(7) & A(1)_{22} > TR(7) \end{bmatrix}
\end{aligned}
$$

Furthermore, $rcv = (rcv(1), rcv(2))$, where $rcv(d)$ $(d = 1, 2)$ is a matrix with the same size of the image A. This matrix is obtained with threshold decomposition of $A(1)$ according to the minimum and maximum values of $A(2)$ and $A(3)$. The following matrix is an example of the rcv with A, consisting of four pixels:

$$
\begin{aligned}
rcv(1) &= \begin{bmatrix} A(1)_{11} > \min(A(2)_{11}, A(3)_{11}) & A(1)_{12} > \min(A(2)_{12}, A(3)_{12}) \\ A(1)_{21} > \min(A(2)_{21}, A(3)_{21}) & A(1)_{22} > \min(A(2)_{22}, A(3)_{22}) \end{bmatrix} \\
rcv(2) &= \begin{bmatrix} A(1)_{11} > \max(A(2)_{11}, A(3)_{11}) & A(1)_{12} > \max(A(2)_{12}, A(3)_{12}) \\ A(1)_{21} > \max(A(2)_{21}, A(3)_{21}) & A(1)_{22} > \max(A(2)_{22}, A(3)_{22}) \end{bmatrix}
\end{aligned}
$$

Moreover, $gbv = (gbv(1), gbv(2), ..., gbv(7))$ where $gbv(d)$ $(d = 1, 2, ..., 7)$ is a matrix with the same size of the image A. Using $TG(d)$ $(d = 1, 2, ..., 7)$, the d^{th} element of gbv is obtained by the threshold decomposition of $A(2)$ which is the image obtained from the second feature values of the target area.

We continue with $gcv = (gcv(1), gcv(2))$ where $gcv(d)$ $(d = 1, 2)$ is a matrix with the same size of the image A. This matrix is obtained with threshold decomposition of $A(2)$ according to the minimum and maximum values of $A(1)$ and $A(3)$.

Finally, $bbv = (bbv(1), bbv(2), ..., bbv(7))$ where $bbv(d)(d = 1, 2, ..., 7)$ is a matrix with the same size of the image A. Using $TB(d)$ $(d = 1, 2, ..., 7)$, the d^{th} matrix of bbv is obtained by the threshold decomposition of $A(3)$ which is the image obtained from the third feature values of the target area.

Step 4: Threshold Decomposition of the training data set according to TR, TG and TB.

File *fullthresdec.m* is used for the threshold decomposition of the training data set v^j $(j = 1, 2, ..., 6)$. The idea is the same as in the previous step, only the input data are different. The matrices $samplesrb, samplesrc, samplesgb, samplesgc, samplesbb$ are obtained as an output of this program. In this study, these matrices are determined as follows:

(i) $samplesrb^j$ $(j = 1, 2, ..., 6)$ is a matrix whose d^{th} $(d = 1, 2, ..., 7)$ column consists of the threshold decomposition of vector r^j $(j = 1, 2, ..., 6)$ according to $TR(d)$. Let us consider this matrix for the first class $(j = 1)$:

$$samplesrb^1 = \begin{bmatrix} r^1(1) > TR(1) & ... & r^1(1) > TR(7) \\ r^1(2) > TR(1) & ... & r^1(2) > TR(7) \\ ... & ... & ... \\ r^1(N) > TR(1) & ... & r^1(N) > TR(7) \end{bmatrix}$$

where N is the number of selected training samples for the first class and j is the class index.

(ii) $samplesrc^j$ $(j = 1, 2, ..., 6)$ is a matrix whose $d^{th}(d = 1, 2)$ column consists of the threshold decomposition of vector r^j $(j = 1, 2, ..., 6)$ according to the minimum and maximum of g^j $(j = 1, 2, ..., 6)$ and b^j $(j = 1, 2, ..., 6)$. Let us consider this matrix for the first class $(j = 1)$:

$$samplesrc^1 = \begin{bmatrix} r^1(1) > \min(b^1(1), g^1(1)) & r^1(1) > \max(b^1(1), g^1(1)) \\ r^1(2) > \min(b^1(2), g^1(2)) & r^1(2) > \max(b^1(2), g^1(2)) \\ ... & ... \\ r^1(N) > \min(b^1(N), g^1(N)) & r^1(N) > \max(b^1(N), g^1(N)) \end{bmatrix}$$

where N is the number of selected training sample for the first class and j is the class index.

(iii) $samplesgb^j$ $(j = 1, 2, ..., 6)$ is a matrix whose d^{th} $(d = 1, 2, ..., 7)$ column consists of the threshold decomposition of vector g^j $(j = 1, 2, ..., 6)$ according to the

$TG(d)$.

(iv) $samplesgc^j$ $(j = 1, 2, ..., 6)$ is a matrix whose d^{th} $(d = 1, 2)$ column consists of the threshold decomposition of vector g^j $(j = 1, 2, ..., 6)$ according to the minimum and maximum of r^j $(j = 1, 2, ..., 6)$ and b^j $(j = 1, 2, ..., 6)$.

(v) $samplesbb^j$ $(j = 1, 2, ..., 6)$ is a matrix whose d^{th} column vector $(d = 1, 2, ..., 7)$ consists of the threshold decomposition of vector b^j $(j = 1, 2, ..., 6)$ according to $TB(d)$.

Step 5: Determination of the indicator to a Boolean classifier function which uniquely discriminates the dataset.

Using the matrices that are obtained from the previous step, an indicator to a Boolean classifier function is found with the *infunfin.m* program. The output is the $indfunindcls^j$ $(j = 1, 2, ..., 6)$ matrix whose row is an indicator for each pixel from the training data. For the first class $indfunindcls^1$ matrix is obtained as follows:

$$indfunindcls^1 =$$

$$\begin{bmatrix} sum(samplesrb^1(1,:) & sum(samplesrc^1(1,:) & ... & sum(samplesbb^1(1,:) \\ sum(samplesrb^1(2,:) & sum(samplesrc^1(2,:) & ... & sum(samplesbb^1(2,:) \\ ... & ... & ... & ... \\ sum(samplesrb^1(M,:) & sum(samplesrc^1(M,:) & ... & sum(samplesbb^1(M,:) \end{bmatrix}$$

where M is the number of different indicators for the training sample corresponding to the first class. In this study, the remaining matrices are obtained with the same idea.

Step 6: Assignment of the pixels on the image to one of the predefined classes with the indicators.

Using the inputs rbv, rcv, gbv, gcv, bbv and $indfunindcls$, the *bccheck.m* file check which pixels on an image belong to the corresponding class. The output $bcindsson^j$ $(j = 1, 2, ..., 6)$ is a binary matrix with the same size of the original image A whose

elements is 1 if that pixel belongs to class j, 0 otherwise. Then,

$$sonmat = bcindsson^1 + bcindsson^2 + ... + bcindsson^6$$

is calculated. If an element of *sonmat* is equal to 1, then we find from which matrix $bcindsson^j, 1$ comes. Then, the pixel is assigned to that class j. If an element of *sonmat* is equal to 0, then we continue with Step 7. If an element of *sonmat* is greater than 1, we continue with Step 8.

Step 7: Assignment of unclassified pixels from step 6 according to Hamming distance.

In this step unclassified pixels are assigned to one of the predefined classess with the *Hamming distance criterion*. Firstly,

$$\begin{aligned} summ1 &= (rbv(1) + rbv(2) + ... + rbv(7)) \\ summ2 &= (rcv(1) + rcv(2)) \\ summ3 &= (gbv(1) + gbv(2) + ... + gbv(7)) \\ summ4 &= (gcv(1) + gcv(2)) \\ summ5 &= (bbv(1) + bbv(2) + ... + rbv(7)) \end{aligned}$$

matrices are calculated. The variables $summ1$ and $summ2$ include information about the first feature values of the image; $summ3$ and $summ4$ include information about the second feature values of the image and $summ5$ include information about the third feature of the image. To calculate the Hamming distance, $indfunindcls^j$ $(j = 1, 2, ..., 6)$ matrix is used as an indicator of each class. $indfunindcls^j(:, 1)$ and $indfunindcls^j(:, 2)$ are indicators for the first feature of j^{th} class, $indfunindcls^j(:, 3)$ and $indfunindcls^j(:, 4)$ are indicators for the second feature of j^{th} class. Lastly, $indfunindcls^j(:, 5)$ is an indicator for the third feature of j^{th} class. The Hamming distance is calculated between $summ1$ and $indfunindcls^j(:, 1)$, $summ2$ and $indfunindcls^j(:, 2)$, $summ3$ and $indfunindcls^j(:, 3)$, $summ4$ and $indfunindcls^j(:, 4)$, $summ5$ and $indfunindcls^j(:, 5)$. The distance is 0 if two binary variables are differ-

ent, and 1 else. For each class j, we sum up the distances. The pixels are assigned according to the maximum value of this sum.

Step 8: Assignment of pixels that belongs to more than one class according to the Hamming distance using the threshold decomposition of mean values.

There might be pixels that assigned more than one class. We use another criterion to assign that pixels. The Hamming distance is calculated between the vectors rbv, rcv, gbv, gcv and bbv of the pixels that assigned more than one class, and the vectors obtained from the threshold decomposition of training data mean values according to the same threshold levels that are used in this program. Again, the pixels are assigned according to the maximum value of this sum.

At the end of *booleanthresh.m* program, *bcindsson* matrix is obtained with the same size of the input image whose elements are valued from 1 to 6. Each number represents one class. When this numbers are coloured, the thematic image appears on the screen. According to the training data, the user assigns the class names to the colours.

3.7 Factors that Affect the Classification Performance

Some of the factors that influence the classification results are availability of remotely sensed data, landscape complexity, dimensionality of the feature space, the classification algorithm used, analyst's knowledge about the study area, and analyst's experience with the classifiers used [37].

Training Set: The most important issue in supervised classification is the adequacy of the training data in characterizing the properties of the chosen classes, because training set have a considerable influence on the accuracy of the resulting classification [7]. Previous studies showed that the training set size has a substantial effect on classification accuracy. There is not any constant number in that size, but it depends on the number of clusters to be classified, the classifier, dimensionality

of the feature space, homogeneity of the area. Acquiring such large training sets may be difficult and costly where a large number of classes is involved [45]. The classification results become worse as the geographical area of study increases [60].

Tso and Mather [55] realized that the important requirement for the maximum likelihood classifier is the number of pixels included in the training data set for each class which should be at least 10-30 times of the number of features. *Pal and Mather* [45] concluded that the ANN (Artifical Neural Network)-based classifier can perform successfully using training data sets that are smaller than those required to train statistical classifiers.

Dimensionality of the Feature Space: For statistical classifiers, *Hughes phenomenon* states that for a constant training data set size, when the number of features increase, the classifier performance decrease. Increasing the number of features provides more information to determine the decision boundaries, but at least this information is only useful if the number of trainig data increases proportionally [45].

When the dimensionality of the feature space is getting larger, it is expected that the classification accuracy becomes better [60].

Number of Clusters: From the literature, according to the various researches solution, it is concluded that the higher the number of classes used in a classification experiment, the more difficult and the less accurate the classification becomes [60].

Spatial Resolution: The classification accuracy is significantly affected by spatial resolution [60].

3.8 Classification Accuracy Assessment

A classification is not complete until the accuracy is assessed. The term *accuracy* is used to mean the quality of information derived from remotely sensed data [9, 16]. A classification error gives the information how the classified image represents the reality.

Fundamental steps in accuracy assessment are first designing the sample and collecting data for each sample. Then, building and testing the error matrix follow. The last step is analyzing the results [9].

There are four common accuracy measures used to determine whether the image has been classified adequately [34]. This accuracy measures are derived from the error matrix which is used for describing each pixel class allocation relative to the reference data [16]. Error matrices compare the relationship between known reference data (ground truth) and the corresponding results of an automated classification [34]. The four accuracy measures are:

Producer's accuracies (PA) are calculated by dividing the number of correctly classified pixels in each category by the number of training set pixels used for that category [34]. Producer's accuracy indicates how well training set pixels of the given cover type are classified.

$$PA = \frac{N_{ii}}{N_{i+}} \ (i = 1, 2, ..., q),$$

where N_{ii} represent the diagonal elements of error matrix, N_{i+} is the sum of i^{th} column elements and q is the number of classes.

User's accuracies (UA) are computed by dividing the number of correctly classified pixels in each category by the total number of pixels that were classified in that category [34]. User's accuracy indicates the probability that a pixel classified into a given category actually represents that category on the ground:

$$UA = \frac{N_{ii}}{N_{+i}} \ (i = 1, 2, ..., q),$$

where N_{ii} represent the diagonal elements of error matrix, N_{+i} is the sum of i^{th} row elements and q is the number of classes.

Overall Accuracy (OA) is computed by dividing the total number of correctly classified pixels by the total number of reference pixels [34].

$$OA = \frac{\sum_{i=1}^{q} N_{ii}}{N} \ (i = 1, 2, ..., q),$$

where N_{ii} represent the diagonal elements of error matrix, N is the sum of all row elements (total number of reference pixels) and q is the number of classes.

The (Kappa statistics is a measure of the difference between the actual agreement between reference data and a random classifier usually ranges between 0 to 1. For example, a value of 0.70 can be thought of as an indication that an observed classification is 70 percent better than one resulting from chance [34]. The Kappa statistics is computed as

$$\text{Kappa coefficient} = \frac{N \cdot \sum_{i=1}^{q} N_{ii} - \sum_{i=1}^{q} N_{i+} \cdot N_{+i}}{N^2 - \sum_{i=1}^{q} N_{i+} \cdot N_{+i}} \ (i = 1, 2, ..., q),$$

where N_{ii} represent the diagonal elements of error matrix, N_{+i} is the sum of i^{th} row elements, N_{i+} is the sum of i^{th} column elements, N is the sum of all row elements (total number of reference pixels) and q is the number of classes.

The main advantage to calculate *Kappa statistics* is to determine the statistical significance of any given error matrices which could be calculated from different dates of images or classification techniques [34].

CHAPTER 4

CLASSIFICATION RESULTS

The performance of three classifiers, k-means, Gaussian maximum likelihood and Boolean discriminant function classifier, pointed out in the previous chapter, were tested on multispectral imagery from BILSAT and Landsat-7 which have similar spatial and spectral resolution. Landsat image consists of 430×281 pixels and BILSAT image consists of 456×309 pixels. We performed the classification using Landsat and BILSAT images' various combinations of bands. In this study, we focused on four bands of Landsat images, namely: red (R), green (G), blue (B) and near infrared (nir) to keep the same band combinations with BILSAT imagery. In Landsat image, there is a cloud above the study area. We also performed the classification with cloud class, but in this study we focused on the solutions with skipping the cloud class. We did not choose the training and test data pixels from cloudy area.

Classification was performed first with six classes, water, forest land, agricultural land, built-up, soil and rocky terrain, which were described in the field study. Then, barren land subclasses, soil and rock terrain were merged in one class as a mixture barren land.

Two images' training data for each class were selected similarly by using *traindata.m* file which was written in MATLAB. Characteristics of training datas used for classification are shown in Figure 4.1 and Figure 4.2. The reflectance graphics are different for two images because images were acquired on various dates and radiometric properties of two imagery are different.

For testing the performance of the classifiers, test data for each class were selected similarly with the *testdata.m* file. Both training data and test data were selected with the help of field study, airphoto and IKONOS high resolution satellite image of the study area. At the end of the classification process to see how accurately the

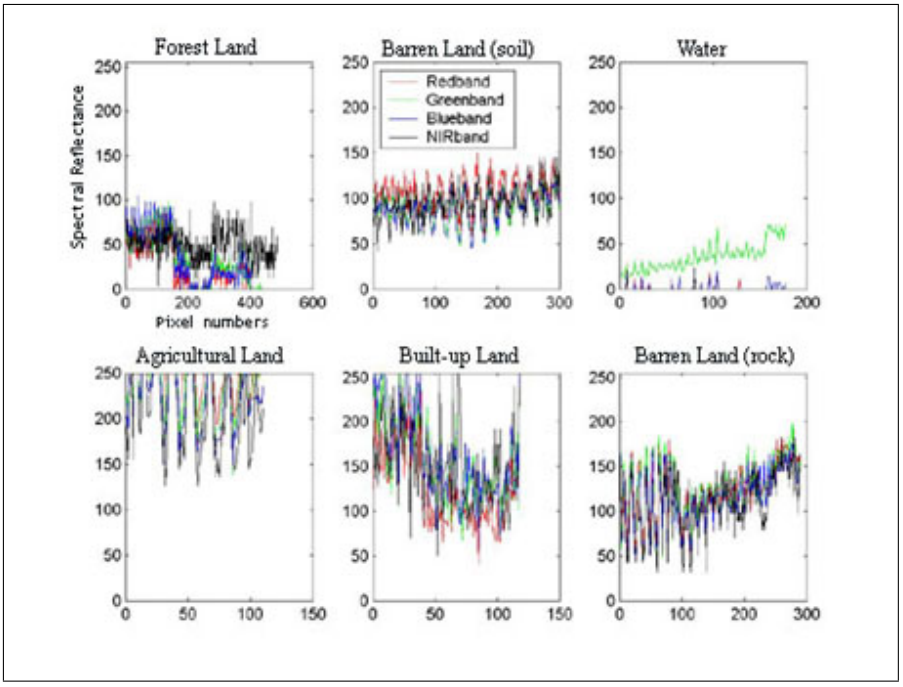

Figure 4.1: BILSAT training data characteristics of RGB and NIR band

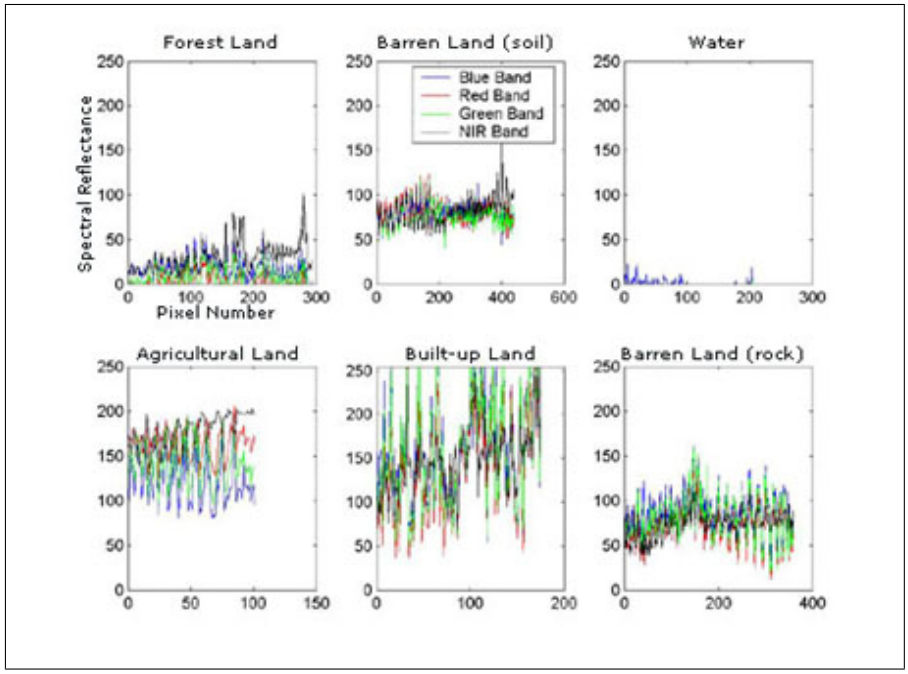

Figure 4.2: Landsat-7 training data characteristics of RGB and NIR bands

classification was performed, accuracy assessment was calculated for each classifier using *accuracy.m* file and Excel program. Accuracy.m file calculate the error matrix and according to this error matrix Excel program calculate the producer's accuracy, user's accuracy, overall accuracy and overall kappa statistics.

4.1 K-Means Classification

K-means clustering was considered under the context of unsupervised classification. We have assumed that we have no priori knowledge about the area. A program, *kmeansc.m*, was written with MATLAB to implement this method. In this algorithm, MATLAB's k-means algorithm was used as the basis. It has been assumed that the number of clusters of pixels were known in advance. Therefore, only initital class number value was given as an input. After the classification process we assigned to each colour a class name according to our field study and high resolution images. Classification results using Landsat-7 and BILSAT RGB combinations are shown in Figures 4.3-4.4 and RBnir band combinations are shown in Figures 4.5-4.6. The results after combining subclasses of barren land in one as a mixed barren land are shown in Figures 4.7-4.10.

Generally, it can be concluded from the results that the overall accuracy is low, as it is expected from this classifier. Due to the ecosytem in the lake causing close reflectance to the forest land in some places, k-means classifier could not manage to discriminate water from the forest land. Therefore, it is clear that there is a need to train the classifier by the training data to separate water and forest land. The results from other two supervised classification methods verified this idea. Changing the dimensions of feature space affected the classification performance.

Results from two images showed that although misclassification of lake, the shape of lake was detected better in Landsat solutions because of the better radiometric characteristics and correction of Landsat imagery. As it is expected, the accuracy is higher when rock terrain and soil are merged for each classification.

We tested the classifier with the initial class value bigger than six and then, combined the classes according to our prior knowledge about the area. It was seen that the classifier performance was getting better.

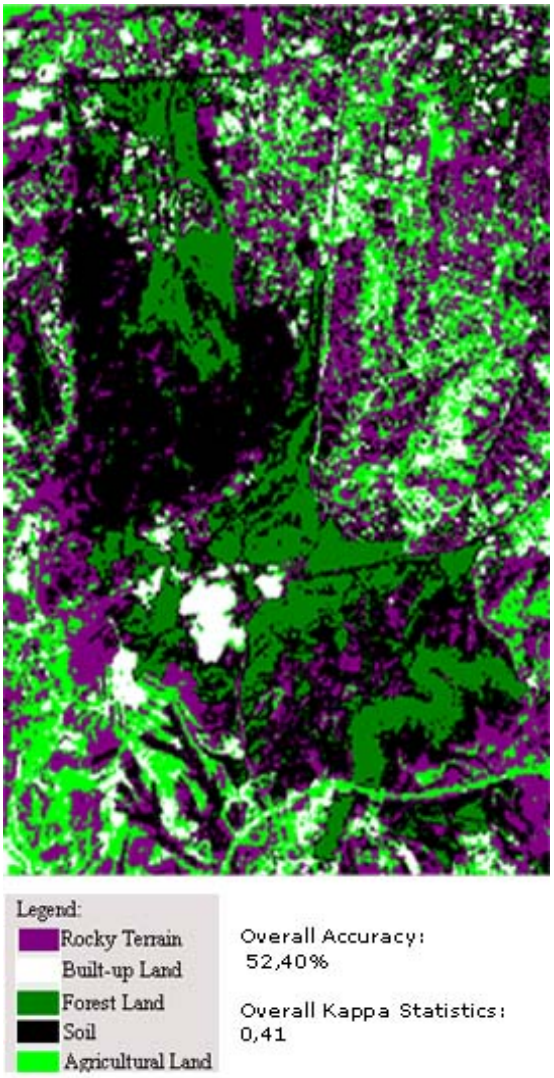

Figure 4.3: Classification of Landsat-7 RGB imagery using k-means classifier.

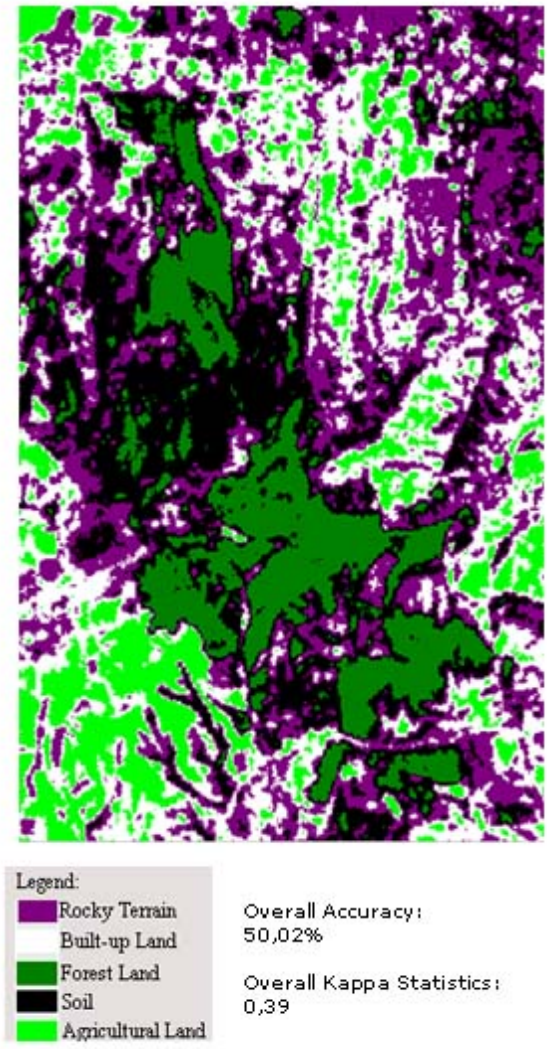

Figure 4.4: Classification of BILSAT RGB imagery using k-means classifier.

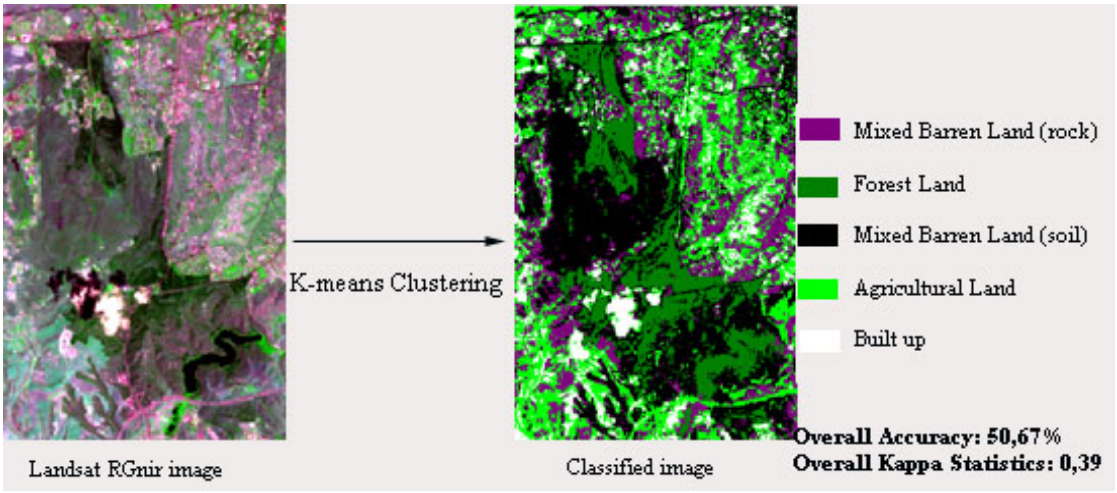

Figure 4.5: Classification of Landsat-7 RBnir imagery using k-means classifier

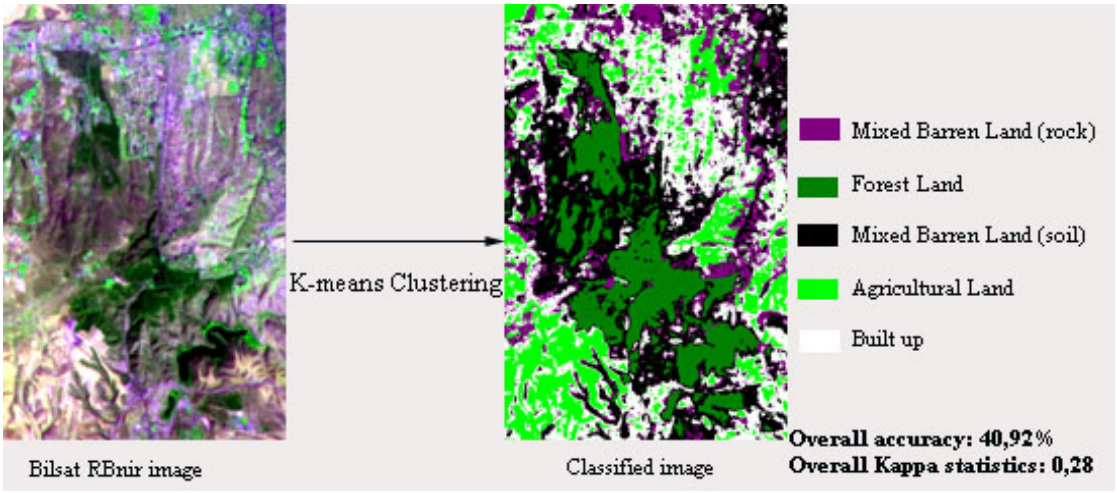

Figure 4.6: Classification of BILSAT RBnir imagery using k-means classifier

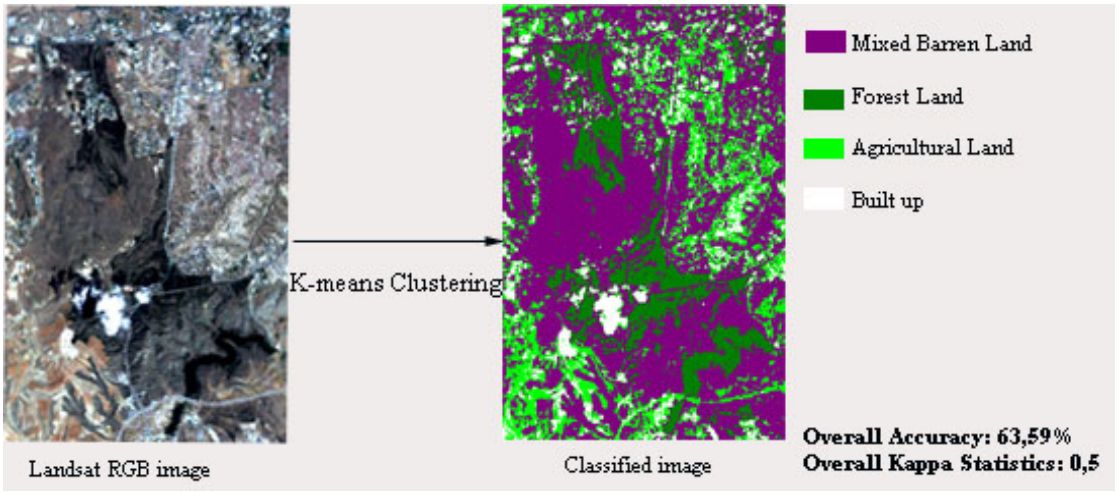

Figure 4.7: Classification of Landsat-7 RGB imagery using k-means classifier

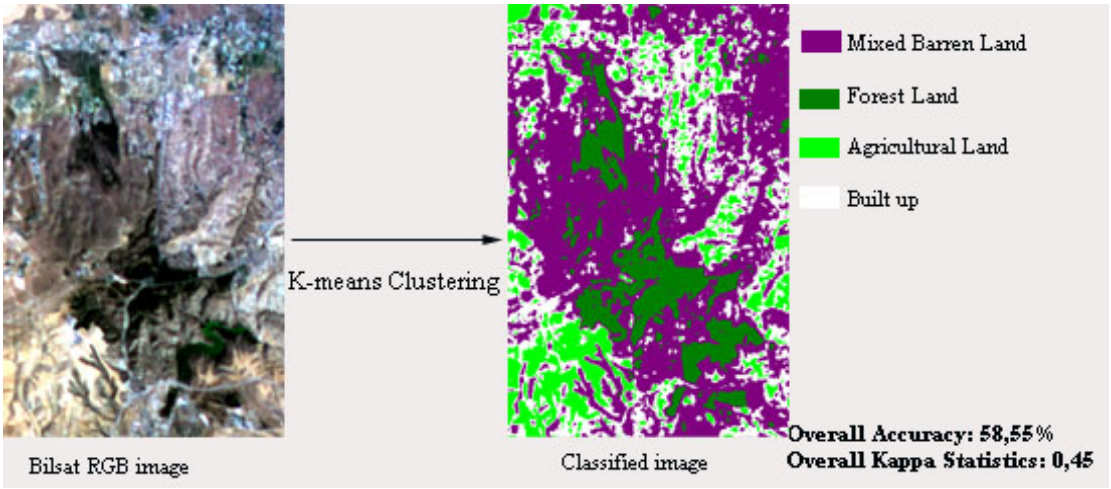

Figure 4.8: Classification of BILSAT RGB imagery using k-means classifier

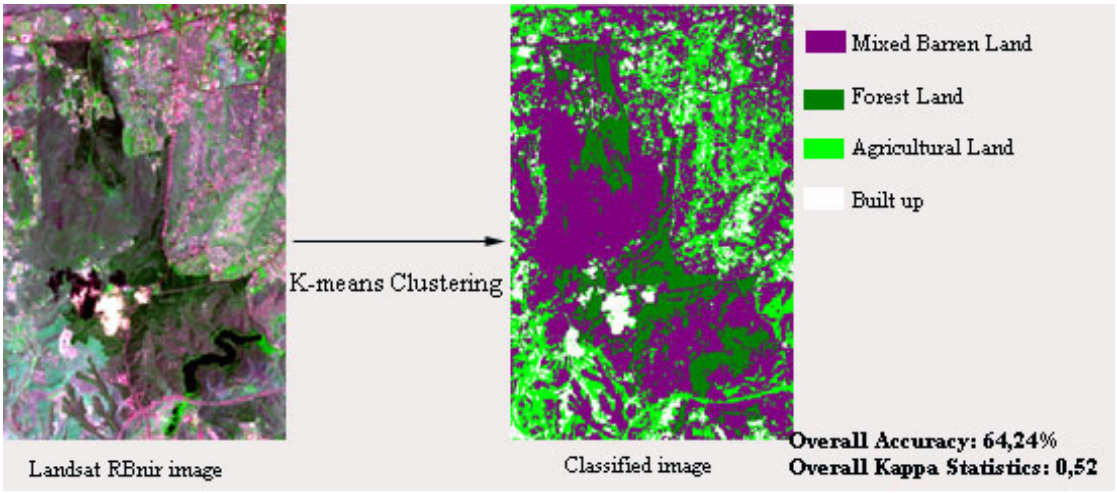

Figure 4.9: Classification of Landsat-7 RBnir imagery using k-means classifier

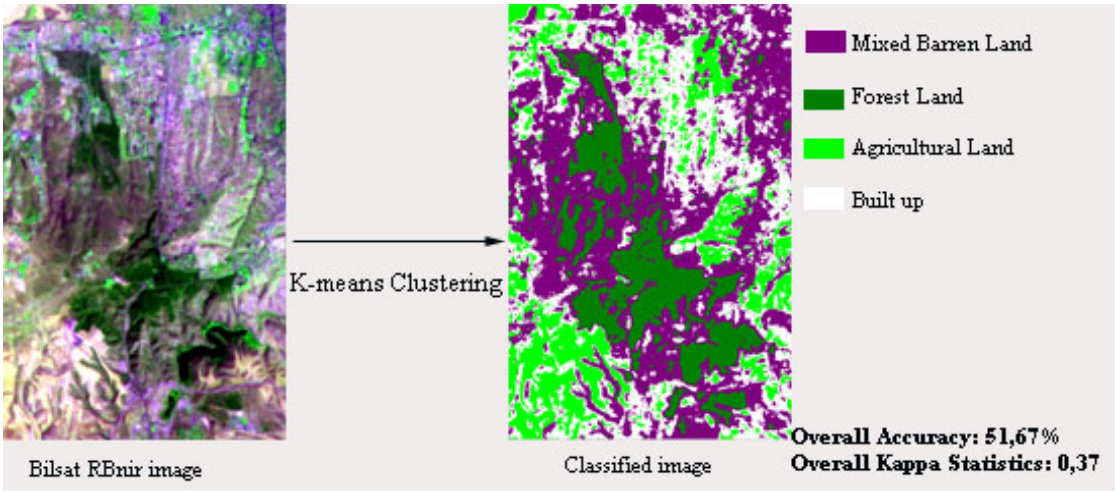

Figure 4.10: Classification of BILSAT RBnir imagery using k-means classifier

4.2 Gaussian Maximum Likelihood Classification

One of the algorithms implemented as a supervised classifier in this study is *Gaussian maximum likelihood classifier*. We determined six training classes. Classification was performed according to the assumption that each training class have a Gaussian distribution. Each training class mean and covariance matrix determined the Gaussian distribution function (see Figure 4.11-4.14).The program *glmc.m* was written in MATLAB for the implementation of this method.

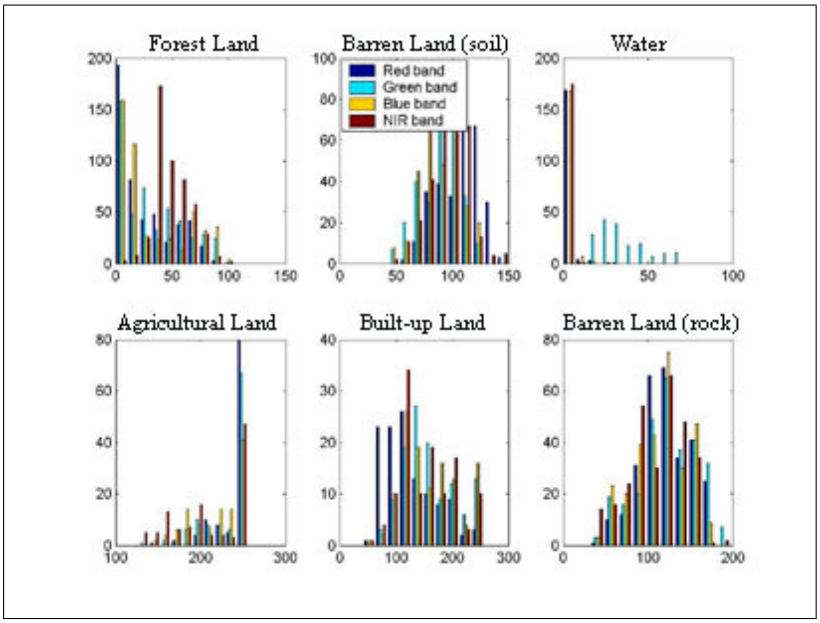

Figure 4.11: Histograms of each training class of BILSAT imagery

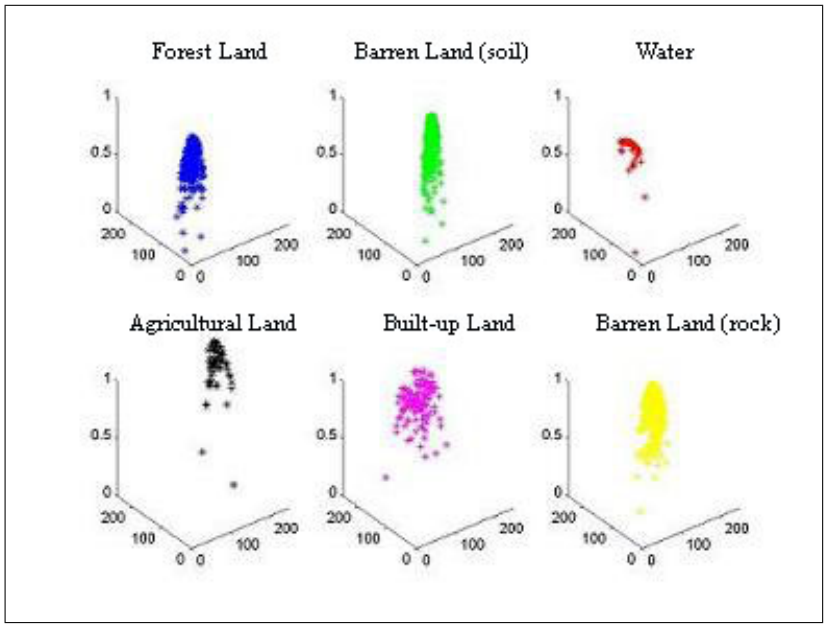

Figure 4.12: Probability density functions of each training class of BILSAT imagery of each training class

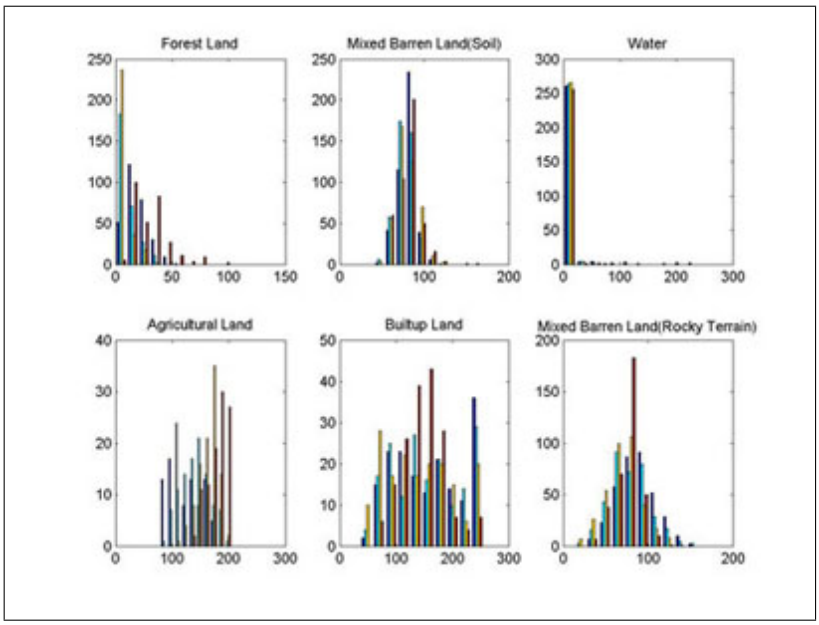

Figure 4.13: Histograms of each training class of Landsat imagery

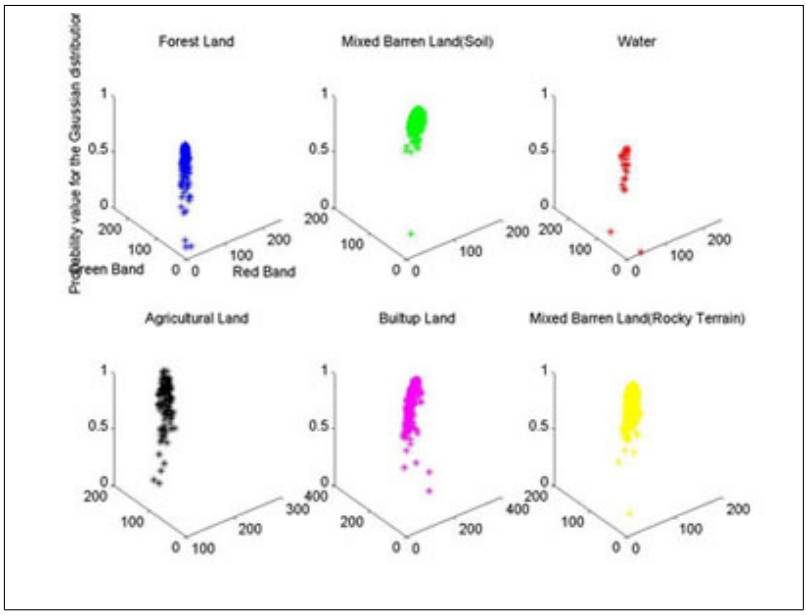

Figure 4.14: Probability density functions of each training class of Landsat imagery

For forest land and water classes, the distribution do not look like Gaussian (see Figure 4.11 and 4.13). This is one of the disadvantages of this method because the method assumes that all of the classes have the Gaussian distribution, whether it is correct or not. We tested this classifier with Landsat and BILSAT imagery's same band combinations which used for k-means classifier. The results with six classes are shown in Figures 4.15-4.18. The results after merging barren land subclasses, soil and rocky terrain, in one one class are shown in Figures 4.19-4.22.

Generally, the overall accuracy is *very high* with respect to the unsupervised classification as expected. Water and forest land were discriminated successfully with the help of training data. Accuracy was increased again when we merged the classes.

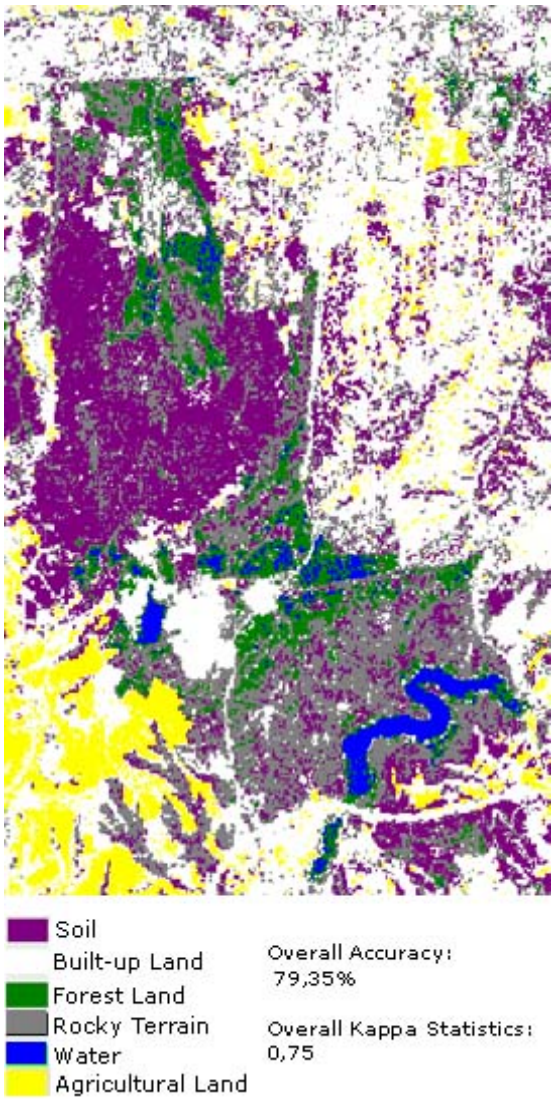

Figure 4.15: Classification of Landsat RGB imagery using Gaussian maximum likelihood classifier

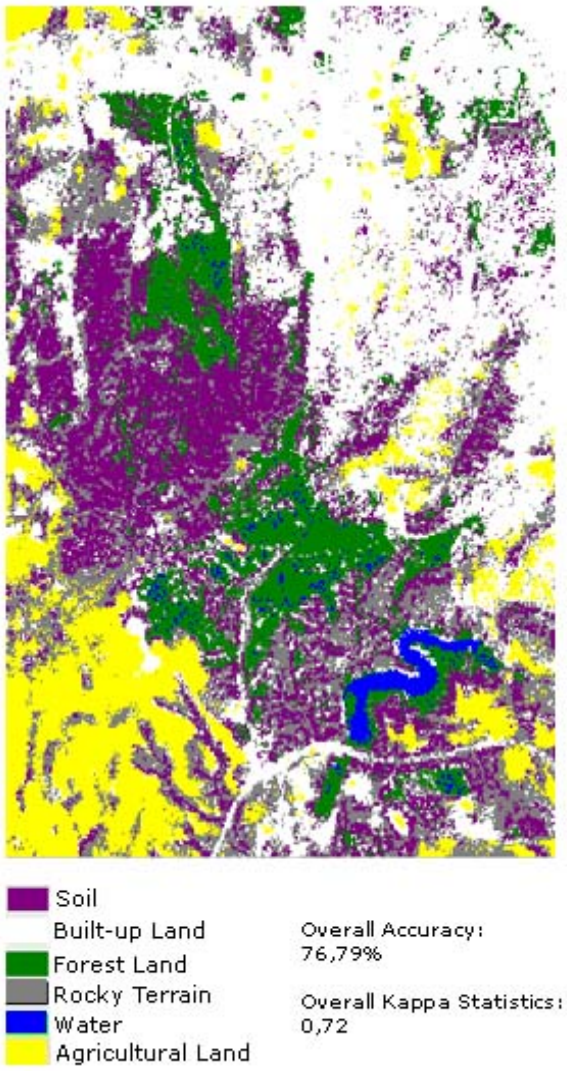

Figure 4.16: Classification of BILSAT RGB imagery using Gaussian maximum likelihood classifier

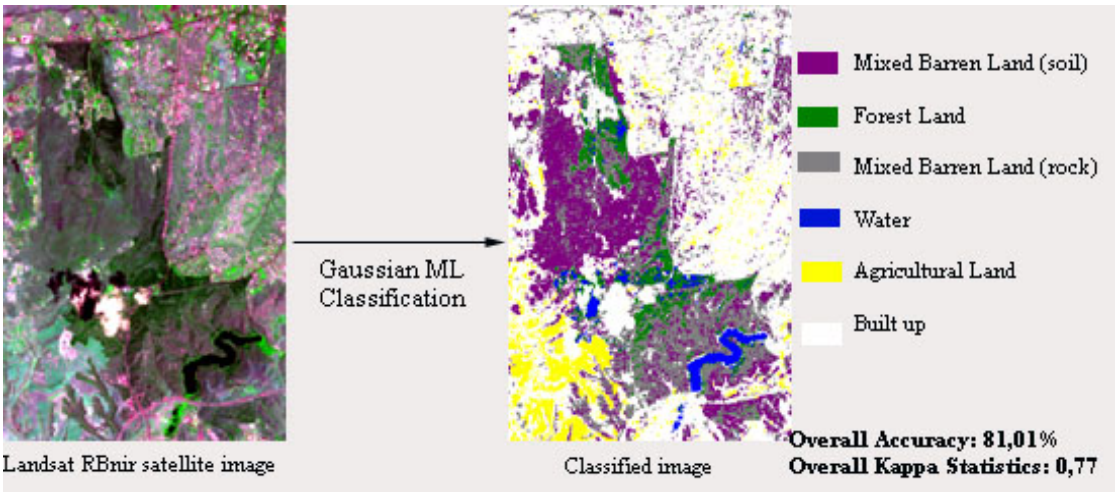

Figure 4.17: Classification of Landsat RBnir imagery using Gaussian maximum likelihood classifier

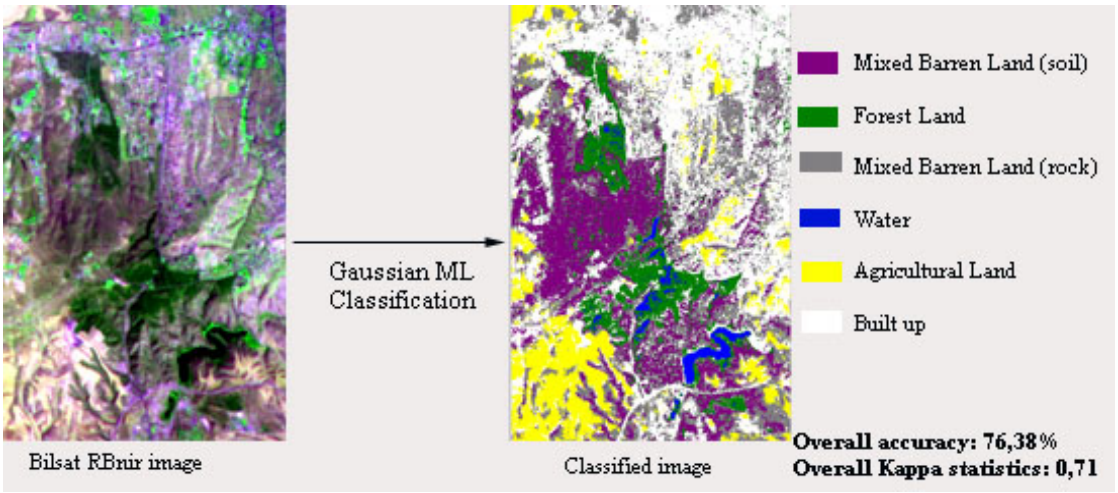

Figure 4.18: Classification of BILSAT RBnir imagery using Gaussian maximum likelihood classifier

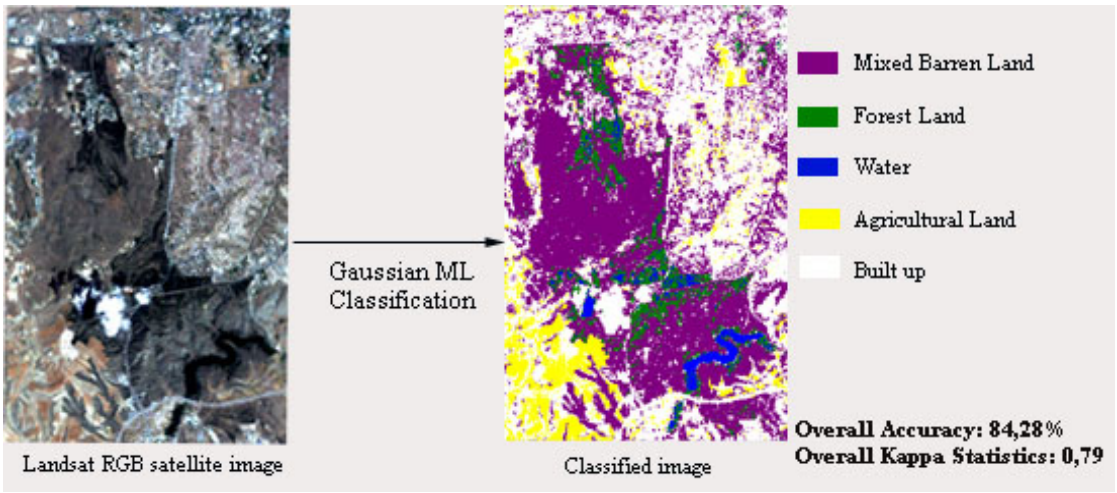

Figure 4.19: Classification of Landsat RGB imagery using Gaussian maximum likelihood classifier

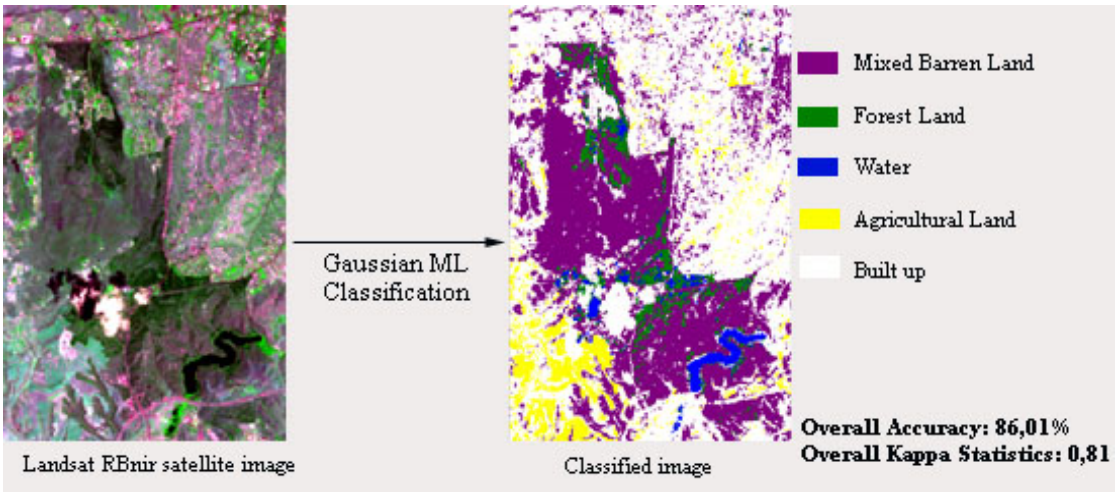

Figure 4.20: Classification of Landsat RBnir imagery using Gaussian maximum likelihood classifier

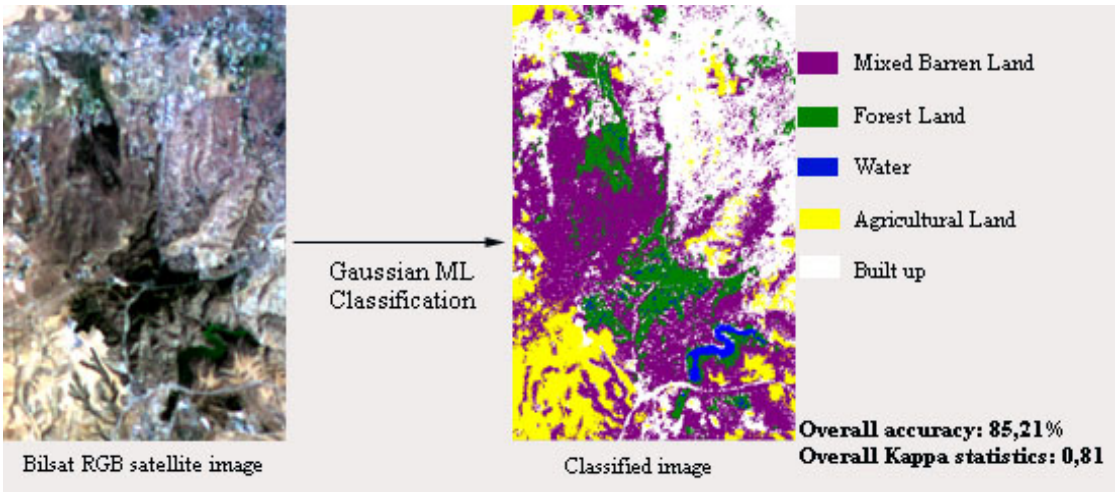

Figure 4.21: Classification of BILSAT RGB imagery using Gaussian maximum likelihood classifier

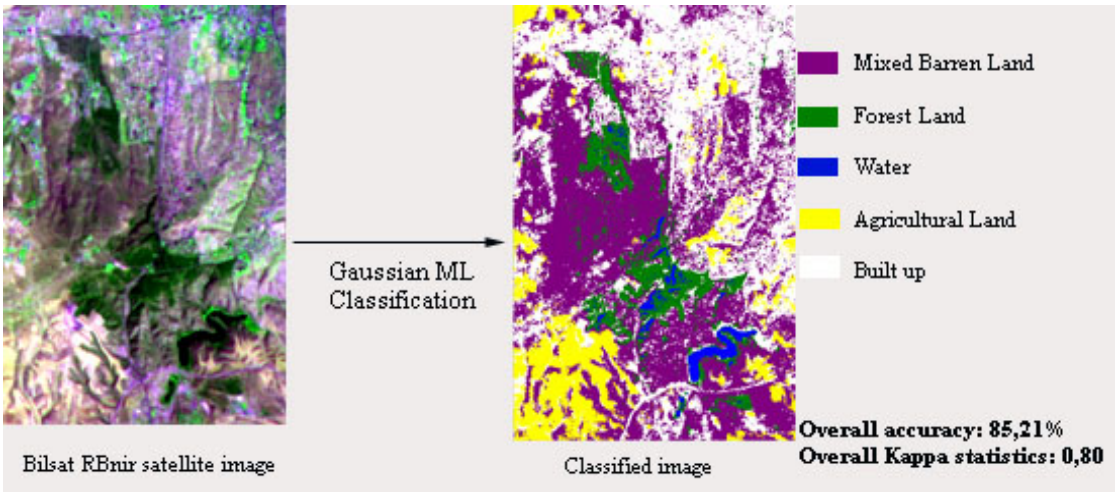

Figure 4.22: Classification of BILSAT RBnir imagery using Gaussian maximum likelihood classifier

4.3 Boolean Discriminant Function Classifier

In this study, a very simple implementation of Boolean discriminant function with seven threshold levels was considered and tested as a supervised classification. We used threshold levels and determined the Boolean functions according to these threshold levels which were acquired from the training data. The training data used for this classification method is the same with the Gaussian maximum likelihood classifier.

This method does not need a priori information or assumptions on the distributions of data. The classification results for six classes are shown in Figures 4.23 - 4.26, and for five classes, results are shown in Figures 4.27 - 4.30.

Seven threshold levels were selected for the pioneering work. Generally, solutions with seven threshold levels of this method are not as satisfactory as the Gaussian MLC. This method is open to the further developments. The results are sensitive to selection of thresholds and training data. Since the approach does not include too many priori assumptions, adaptive methods to select the parameters appropriately can be developed based on our pioneering contribution.

The number thresholds for each band determines the radiometric resolution of this method and it is highly distinctive on the performance. For an exaggerated number of threshold levels much better results are possible. In Figure 4.31, an almost perfect result for a limited region achieved by using approximately 100 threshold levels is shown. However, the computational costs of too many thresholds for a large image is not reasonable. The computation time when a very high number of thresholds are used is not only affected with the number of operations, but the data needed to be kept on RAM also increase and the computer starts to work with virtual memory which dramatically increases the unit time per operation. Therefore, some additional procedures to select the optimum threshold levels can improve the overall efficiency.

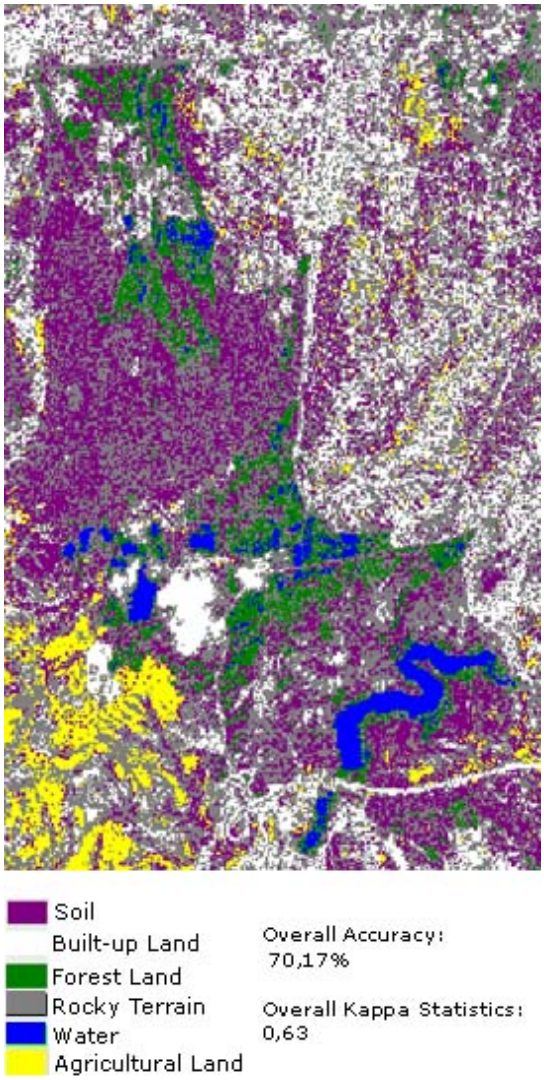

Figure 4.23: Classification of Landsat RGB imagery using Boolean discriminant function classifier

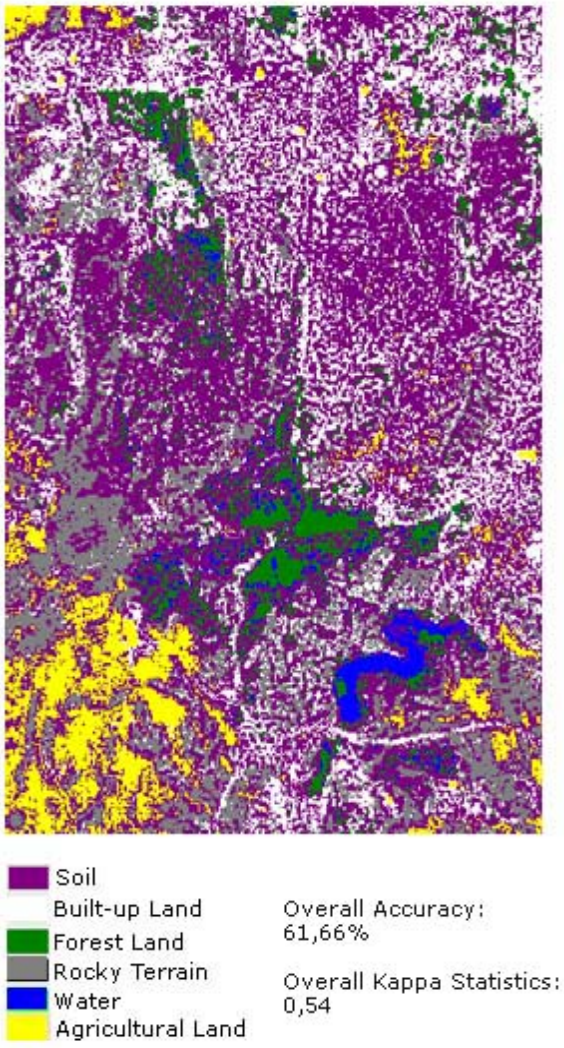

Figure 4.24: Classification of BILSAT RGB imagery using Boolean discriminant function classifier

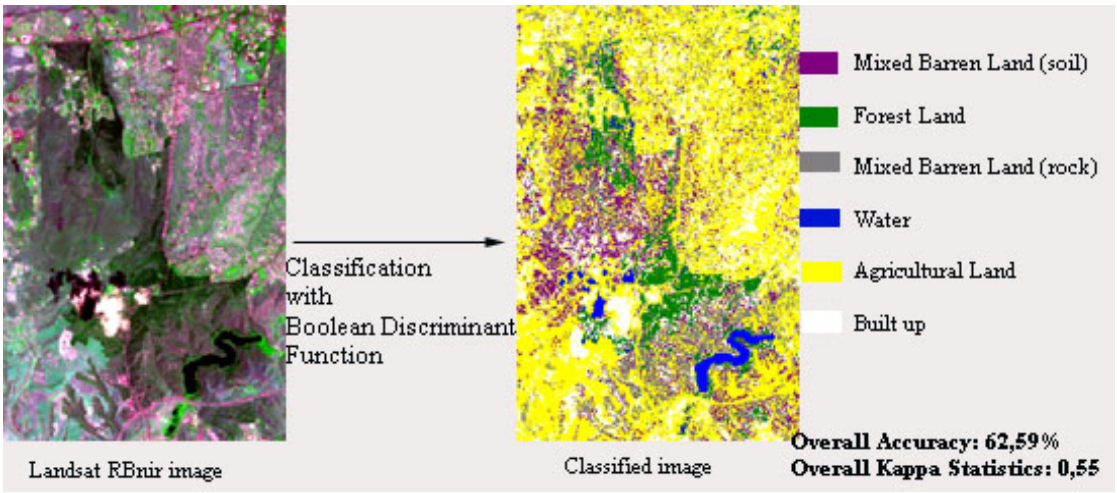

Figure 4.25: Classification of Landsat RBnir imagery using Boolean discriminant function classifier

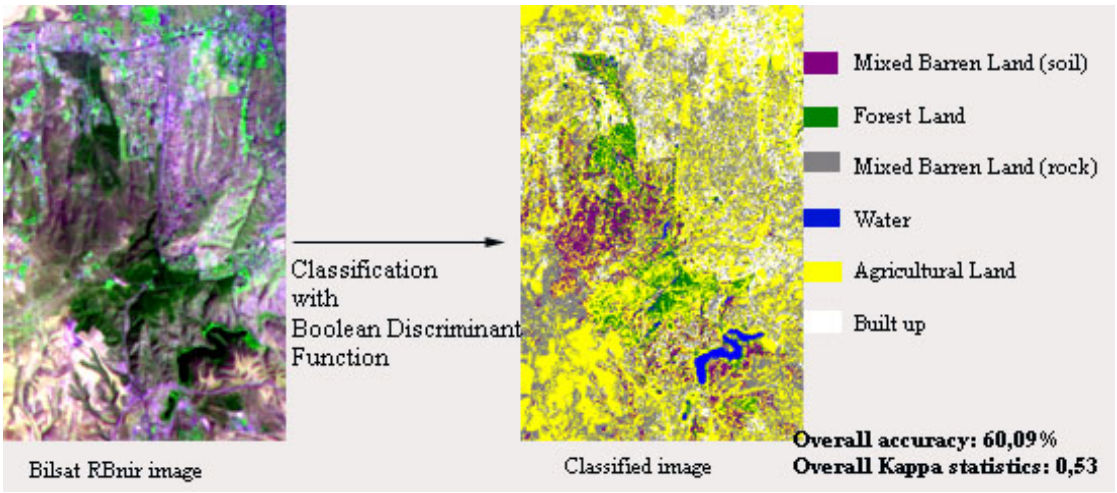

Figure 4.26: Classification of BILSAT RBnir imagery using Boolean discriminant function classifier

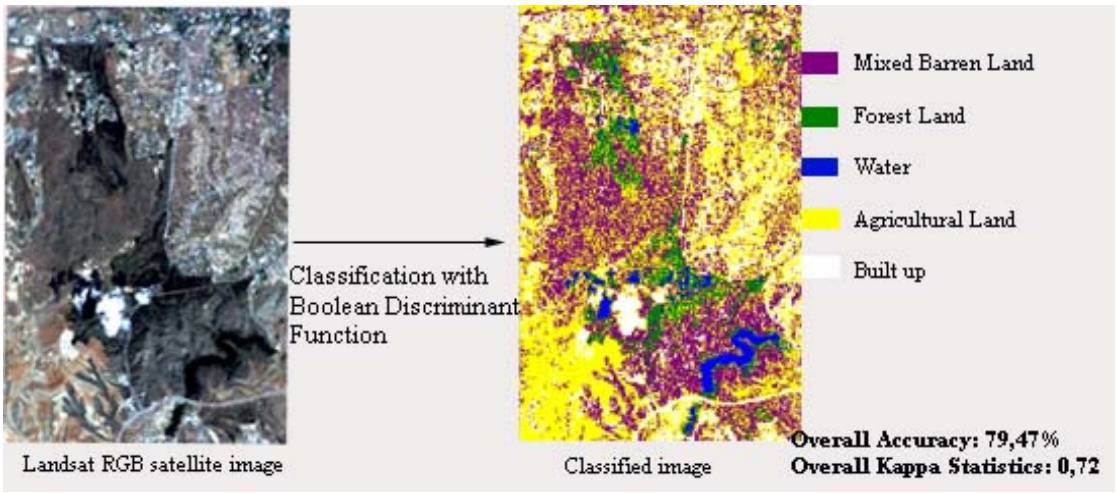

Figure 4.27: Classification of Landsat RGB imagery using Boolean discriminant function classifier

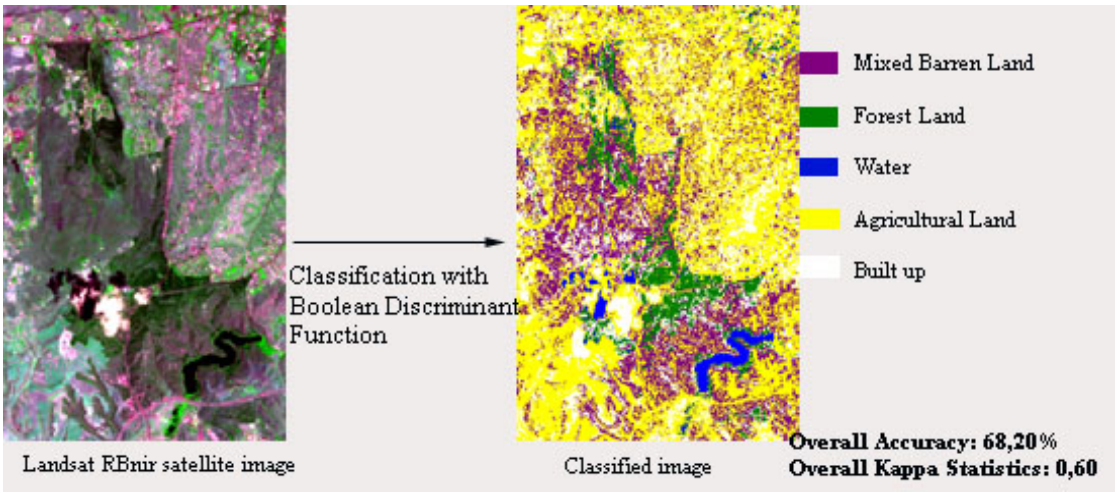

Figure 4.28: Classification of Landsat RBnir imagery using Boolean discriminant function classifier

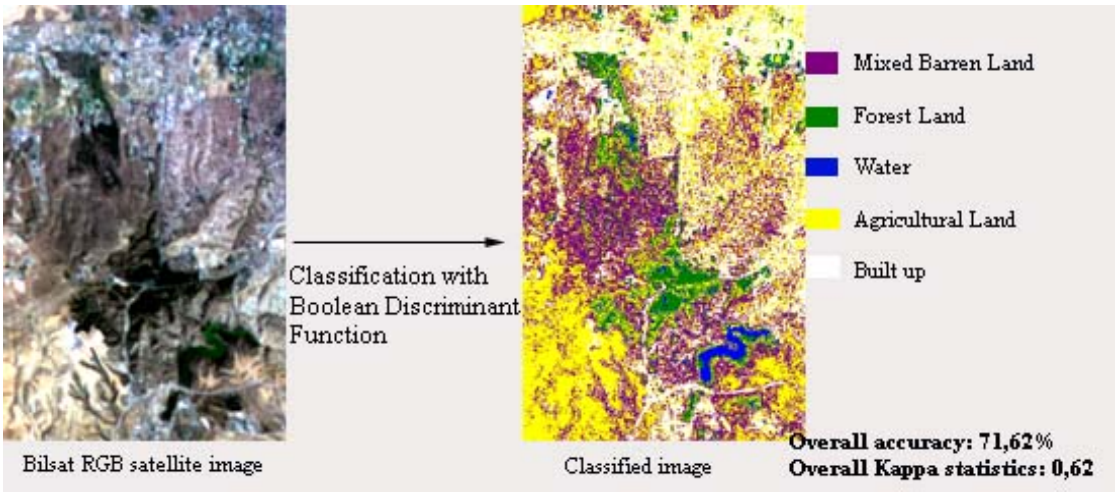

Figure 4.29: Classification of BILSAT RGB imagery using Boolean discriminant function classifier

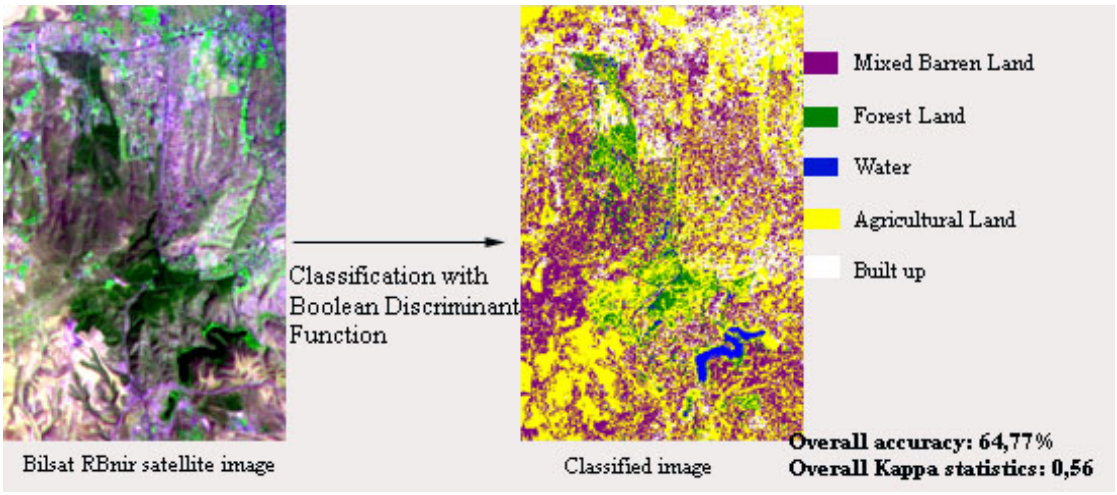

Figure 4.30: Classification of BILSAT RBnir imagery using Boolean discriminant function classifier

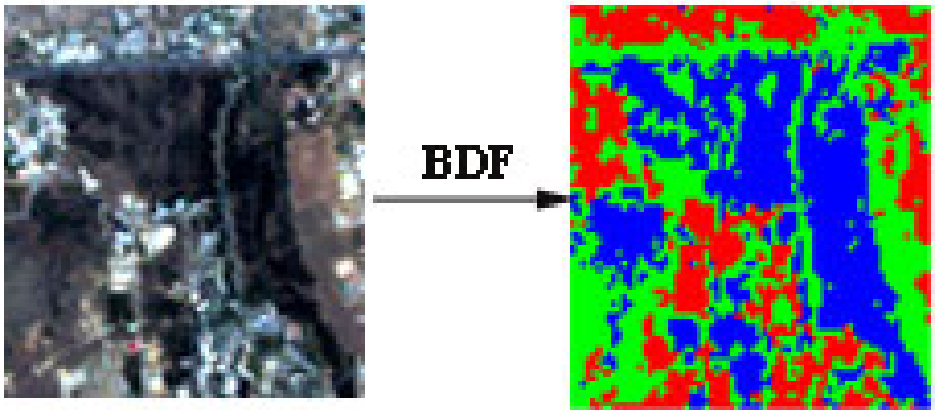

Figure 4.31: Classification with Boolean discriminant function using 100 threshold levels

4.4 Comparision of Methods

Table 4.1 and 4.2 show the CPU time for each classifer. K-means algorithm CPU time is affected from the initial mean values. 26sec is the average CPU time for k-means, but the program ended with 130sec for some initial values. During classification with Boolean discriminant function, the process for discriminating the pixels that are assigned more than one classes has much CPU time. Table 4.2 - 4.14 show the error matrices for each classifier. When comparing these three methods, several criteria were considered. The k-means algorithm was the fastest but had the lowest accuracy. In the case of limited information about the study area, k-means method can be used. This method works well also in large datasets. Maximum likelihood method had the highest accuracy. Boolean discriminant function results were sufficient for the beginning. Moreover, the accuracies of MLC and BDF classifications depend strongly on the accuracy and the consistency of the provided training sets [51].

Although BILSAT has higher spatial resolution than Landsat, its classification results were worse than Landsat because of the radiometric characteristics. Since in this study, only spectral reflectance was considered in the classification, here, the

results are directly related with the radiometric characteristics of each image.

Table 4.1: CPU time for each classifier using Landsat-7 RGB image.

Classifier	**CPU Time using Landsat image** (430×281 pixels)
K-means	26sec
Gaussian MLC	41sec
Boolean Classifier	40sec

Table 4.2: CPU time for each classifier using BILSAT RGB image.

Classifier	**CPU Time using BILSAT image**(456×309 pixels)
K-means	27sec
Gaussian MLC	47sec
Boolean Classifier	51sec

Table 4.3: Error matrix of classification results of Landsat RGB imagery with K-means classifier (six class).*

	RD							
CD	B	R	A	S	F	W	RT	UA
B	120	0	34	0	0	0	154	77,92%
R	3	113	155	24	0	0	295	38,31%
A	24	4	136	0	0	0	164	82,93%
S	1	267	2	413	65	5	753	54,85%
F	1	19	1	0	581	633	1235	47,04%
W	0	0	0	0	0	0	0	00,00%
CT	149	403	328	437	646	638	2601	
PA	80,54%	28,04%	41,46%	94,51%	89,94%	00,00%		
OA								52,40%
OK								0,41

Table 4.4: Error matrix of classification results of Landsat RGB imagery with K-means classifier (five class).*

	RD						
CD	B	A	MB	F	W	RT	UA
B	120	34	0	0	0	154	77,92%
A	24	136	4	0	0	164	82,93%
MB	4	157	817	65	5	1048	77,96%
F	1	1	19	581	633	1235	47,04%
W	0	0	0	0	0	0	00,00%
CT	149	328	840	646	638	2601	
PA	80,54%	41,46%	97,26%	89,94%	00,00%		
OA							63,59%
OK							0,51

*RD: Reference Data, CD: Classified Data, B: Built-up, R: Rocky terrain, A: Agriculture, S: Soil, F: Forest land, W: Water, RT: Row Total, CT: Column Total, PA: Producer's Accuracy, UA: User's Accuracy, OA: Overall classification Accuracy, OK: Overall Kappa Statistics).

Table 4.5: Error matrix of classification results of BILSAT RGB imagery with K-means classifier (six class).*

	RD							
CD	B	R	A	S	F	W	RT	UA
B	96	65	3	0	0	0	164	58,54%
R	75	236	0	10	1	0	322	73,29%
A	82	6	247	0	0	0	335	73,73%
S	38	218	0	314	132	0	702	44,73%
F	0	30	0	110	443	565	1148	38,59%
W	0	0	0	0	0	0	0	00,00%
CT	291	555	250	434	576	565	2671	
PA	32,99%	42,52%	98,80%	72,35%	76,91%	00,00%		
OA								50,02%
OK								0,39

Table 4.6: Error matrix of classification results of BILSAT RGB imagery with K-means classifier (five class).*

	RD						
CD	B	A	MB	F	W	RT	UA
B	96	3	65	0	0	164	58,54%
A	82	247	6	0	0	335	73,73%
MB	113	0	778	133	565	1024	75,98%
F	0	0	140	443	0	1148	38,59%
W	0	0	0	0	0	0	00,00%
CT	291	250	989	576	565	2671	
PA	32,99%	98,80%	78,67%	76,91%	00,00%		
OA							58,55%
OK							0,45

*RD: Reference Data, CD: Classified Data, B: Built-up, R: Rocky terrain, A: Agriculture, S: Soil, F: Forest land, W: Water, RT: Row Total, CT: Column Total, PA: Producer's Accuracy, UA: User's Accuracy, OA: Overall classification Accuracy, OK: Overall Kappa Statistics).

Table 4.7: Error matrix of classification results of Landsat RGB imagery with maximum likelihood classifier (six class).*

	RD							
CD	B	R	A	S	F	W	RT	UA
B	147	16	29	5	18	6	221	66,52%
R	0	313	1	54	124	8	500	62,60%
A	1	0	295	0	0	0	296	99,66%
S	0	74	3	378	19	1	475	79,58%
F	1	0	0	0	360	52	413	87,17%
W	0	0	0	0	125	571	696	82,04%
CT	149	403	328	437	646	638	2601	
PA	98,66%	77,67%	89,94%	86,50%	55,73%	89,50%		
OA								79,35%
OK								0,75

Table 4.8: Error matrix of classification results of Landsat RGB imagery with maximum likelihood classifier (five class).*

	RD						
CD	B	A	MB	F	W	RT	UA
B	147	29	21	18	6	221	66,52%
A	1	295	0	0	0	296	99,66%
MB	0	4	819	143	9	975	84,00%
F	1	0	0	360	52	413	87,17%
W	0	0	0	125	571	696	82,04%
CT	149	328	840	646	638	2601	
PA	98,66%	89,28%	97,50%	55,73%	89,50%		
OA							84,28%
OK							0,79

*RD: Reference Data, CD: Classified Data, B: Built-up, R: Rocky terrain, A: Agriculture, S: Soil, F: Forest land, W: Water, RT: Row Total, CT: Column Total, PA: Producer's Accuracy, UA: User's Accuracy, OA: Overall classification Accuracy, OK: Overall Kappa Statistics).

Table 4.9: Error matrix of classification results of BILSAT RGB imagery with maximum likelihood classifier (six class).*

	RD							
CD	B	R	A	S	F	W	RT	UA
B	236	79	1	1	12	5	334	70,66%
R	18	287	1	61	17	0	384	74,74%
A	27	1	248	0	0	0	276	89,86%
S	3	164	0	312	46	0	525	59,43%
F	7	24	0	60	485	77	653	74,27%
W	0	0	0	0	16	483	499	96,79%
CT	291	555	250	434	576	565	2671	
PA	81,10%	51,71%	99,20%	71,89%	84,20%	85,49%		
OA								76,79%
OK								0,72

Table 4.10: Error matrix of classification results of BILSAT RGB imagery with maximum likelihood classifier (five class).*

	RD						
CD	B	A	MB	F	W	RT	UA
B	236	1	80	12	5	334	70,66%
A	27	248	1	0	0	276	89,86%
MB	21	1	824	63	0	909	90,65%
F	7	0	84	485	77	653	74,27%
W	0	0	0	16	483	499	96,79%
CT	291	250	989	576	565	2671	
PA	81,10%	99,20%	83,32%	84,20%	85,49%		
OA							85,21%
OK							0,81

*RD: Reference Data, CD: Classified Data, B: Built-up, R: Rocky terrain, A: Agriculture, S: Soil, F: Forest land, W: Water, RT: Row Total, CT: Column Total, PA: Producer's Accuracy, UA: User's Accuracy, OA: Overall classification Accuracy, OK: Overall Kappa Statistics).

Table 4.11: Error matrix of classification results of Landsat RGB imagery with Boolean discriminant function (six class).*

	RD							
CD	B	R	A	S	F	W	RT	UA
B	117	50	1	0	0	0	168	69,64%
R	30	264	70	157	150	10	681	38,77%
A	1	0	250	0	0	0	251	99,60%
S	0	85	6	280	43	3	417	67,15%
F	0	4	1	0	312	23	340	91,76%
W	1	0	0	0	141	602	744	80,91%
CT	149	403	328	437	646	638	2601	
PA	78,52%	65,51%	76,22%	64,07%	48,30%	94,36%		
OA								70,17%
OK								0,63

Table 4.12: Error matrix of classification results of Landsat RGB imagery with Boolean Discriminant Function (five class).*

	RD						
CD	B	A	MB	F	W	RT	UA
B	117	1	50	0	0	168	69,64%
A	1	250	0	0	0	251	99,60%
MB	30	76	786	193	13	1098	71,58%
F	0	1	4	312	23	340	91,76%
W	1	0	0	141	602	744	80,91%
CT	149	328	840	646	638	2601	
PA	78,52%	76,22%	93,57%	48,30%	94,36%		
OA							79,47%
OK							0,72

*RD: Reference Data, CD: Classified Data, B: Built-up, R: Rocky terrain, A: Agriculture, S: Soil, F: Forest land, W: Water, RT: Row Total, CT: Column Total, PA: Producer's Accuracy, UA: User's Accuracy, OA: Overall classification Accuracy, OK: Overall Kappa Statistics).

Table 4.13: Error matrix of classification results of BILSAT RGB imagery with Boolean discriminant function (six class).*

	RD							
CD	B	R	A	S	F	W	RT	UA
B	160	138	3	42	29	0	372	43,01%
R	4	173	0	40	9	0	226	76,55%
A	4	0	211	0	0	0	215	98,14%
S	112	226	36	316	166	59	915	34,54%
F	11	18	0	33	333	52	447	74,50%
W	0	0	0	3	39	454	496	91,53%
CT	291	555	250	434	576	565	2671	
PA	54,98%	31,17%	84,40%	72,81%	57,81%	80,35%		
OA								61,66%
OK								0,54

Table 4.14: Error matrix of classification results of BILSAT RGB imagery with Boolean discriminant function (five class).*

	RD						
CD	B	A	MB	F	W	RT	UA
B	160	3	180	29	0	372	43,01%
A	4	211	0	0	0	215	98,14%
MB	116	36	755	175	59	1141	66,17%
F	11	0	51	333	52	447	74,50%
W	0	0	3	39	454	496	91,53%
CT	291	250	989	576	565	2671	
PA	54,98%	84,40%	76,34%	57,81%	80,35%		
OA							71,62%
OK							0,62

*RD: Reference Data, CD: Classified Data, B: Built-up, R: Rocky terrain, A: Agriculture, S: Soil, F: Forest land, W: Water, RT: Row Total, CT: Column Total, PA: Producer's Accuracy, UA: User's Accuracy, OA: Overall classification Accuracy, OK: Overall Kappa Statistics).

CHAPTER 5

CONCLUSION AND DISCUSSIONS

Remote sensing is a very complex system resulted in so many possible errors during transferring information from one subsystem to another. They might be originated from acquisition such as geometric aspects, sensor systems, platforms, ground control, scene considerations; data processing such as geometric rectification, radiometric rectification; data analysis such as quantitative analysis, classification system, data generalization, data conversion and error assessment. Most research work in remote sensing is aimed at minimizing these errors. In this study, efficiency of the classification process was the main concern.

The general *classification* problem was pointed out from the perspective of remote sensing. Three land cover classification techniques have been presented and implemented on Landsat-7 ETM+ imagery and BILSAT imagery: K-means algorithm and Gaussian maximum likelihood methods are well-known methods for unsupervised and supervised methods. The third one is the classification by using threshold decomposition and Boolean discriminant functions which is developed in this study. Implementation was performed with algorithms written in MATLAB.

BILSAT's images performance was tested and compared with Landsat-7. Although BILSAT has higher spatial resolution (27m), the classification results were better with the Landsat-7 imagery which has 30m spatial resolution. Here, the reason is BILSAT's images radiometric characteristics.

Six classes which are built-up, rocky terrain, soil, forest land, agriculture and water, were selected from METU settlement with the help of field study, high resolution satelite image from IKONOS and air photo. According to these classes, classification was performed and an error matrix was calculated with three meth-

ods. In general, k-means overall classification accuracy is 50%, maximum likelihood has 78% accuracy and Boolean discriminant function has 65% accuracy. When two kinds of barren land classes were combined in one class as a mixture barren land, the accuracies increased: k-means has 60% accuracy, maximum likelihood has 85% and boolean has 70% accuracy. From the results, maximum likelihood is the best one; but not open to further development, and it bases on an assumption which might not be real for another training set. On the other hand, Boolean classifier is open to improvements and some other features such as secondary measurements derived from the image to the feature space can be incorporated. It can be concluded that K-means is useful when there is not enough information about the study area.

CPU time for all classifiers was calculated. The fastest algorithm is k-means classifier. The time depends on the initial mean values. Choosing initial values far way from the exact cluster means resulted with high CPU time. Boolean classifier CPU time is better using Landsat image (430×281 pixels) than MLC. On the other hand, MLC is better than the Boolean classifier using BILSAT image(456×309 pixels). CPU time for all classifiers depends on the size of the image, number of clusters, number of features. For supervised classification methods, it is also strongly affected from the training data set.

The use of Boolean discriminant functions will be improved in future studies. This method might be promising, especially, when a class is formed by multiple classes. In the study we used closest distance between the training samples and unknown pixels. As a drawback, considering closest samples for classification is not robust to outliers (for example, a single training sample corrupted by noise could induce errors). However, the finiteness of the state space in this scheme can be utilized to solve such problems. We can assume that each partition should be connected within itself and eliminate the outliers (by morphological operations) by checking whether a subspace containing a training sample has neighbours belonging to the same class, and by checking the connectedness to the other parts of the corresponding partition. In this study, a classification has been performed with pixel considered for itself in this method. Due to the sensor characteristics, each pixel's information appears also in its neighborhood. Therefore, considering the neighborhood of each pixel will increase the classification accuracy. Another possible

improvement to this method can come from the region growing method. Starting from training samples, looking at neighborhood of each pixel and decision function, each pixel can be added to one of the classes.

Now, most of the studies in classification use additional information, e.g. terrain elevation, slope, aspect, texture and other sources of image such as radar, laser data to increase the classification accuracy. To add one of the dominant discerning features also can result in a better solutions for this study.

Our investigation uses threshold decomposition and Boolean discriminant function as a particular examples of the chosen approach. Many different parametric function classes can be optimized as discriminants and new optimization methods, e.g. non-smooth optimization [3] will future serve for further progress, together with an extension of this pioneering contribution.

Considering the literature and this study, we conclude that selection of training data is very important clue for classification. Training data should be determined very carefully and various sources of information should also be incorporated if it is possible. Furthermore, the selection of the categories has also a direct impact on the perceived accuracy of the classification methods.

REFERENCES

[1] Anderson, James R., Hardy, Erneste E., Roach, J.T. and Witmera, R. E., *Land use and land cover classification system for use with remote sensor data,* A revision of the land use classification system as presented in U.S. Geological Survey Circular 671, Geological Survey Professional Paper 964.

[2] Arbel D., Cohen E., Citroen M., Blumberg D.G. and Kopeika N.S., *Landsat TM Satellite Image Restoration Using Kalman Filters*, Photogrammetric Engineering & Remote Sensing, 70, 1, (2004) 91-100.

[3] Bagirov, A. M., and Yearwood, J., *A new nonsmooth optimization algorithm for minimum sum-of-squares clustering problems*, preprint, Centre for Informatics and Applied Optimization, University of Ballarat, Australia, 2003.

[4] Beklioğlu, Meryem, Burnak, S. Levent , and İnce, Özlem, *Benthi-planktivorous fish-induced low water quality of lake Eymir before biomanipulation,* Turk J. Zool., 24, (2000) 315-326.

[5] Benediktsson, Jon A., Swain, P.H., and Ersoy O. K., *Neural network approaches versus statistical methods in classification of multisource remote sensing data,* IEEE Transactions on Geoscience and Remote Sensing, 28, 4, (1990) 540-552.

[6] Bischof, H., Schneider, W., and Pinz, A. J., *Multispectral classification of landsat-images using neural networks*, IEEE Transactions Geoscience Remote Sensing, 30, (1992) 482-490.

[7] Campbell, J. , *Introduction to Remote Sensing*, the Guilford Press, 1996.

[8] CEOS, *Earth Observation Handbook,* ESA, 2002.

[9] Congalton, Russell G., and Green Kass, *Assessing the Accuracy of Remotely Sensed Data : Principles and Practices*, Lewis Publications, 1999.

[10] Cooke, Tristrom, *A lower bound on the performance of the quadratic discriminant function*, Journal of Multivariate Analysis, (2003) 371-383.

[11] Coyle, Edward J., Lin, Jean-Hsang, and Gabbouj, Moncef, *Optimal stack filtering and the estimation and structural approaches to image processing*, IEEE Transactions on Acoustics, Speech and Signal Processing, 37, 12, (1989) 2037-2066.

[12] Cracknell, A.P., *A Review Article, Synergy in Remote Sensing-What is in a pixel?*, International Journal of Remote Sensing, 19, 11,(1998) 2025-2047.

[13] Ediriwickrema, J., and Khorram, Siamak, *Hierarchical maximum-likelihood classifiation for improved accuracies*, IEEE Transactions on Geoscience and Remote Sensing, 35, 4, (1997) 810-816.

[14] Erdem, Nilüfer, and Diri, Banu, *Classification tool, senior project,* report, Computer Engineering Department, Yıldız Techncal University, 2005.

[15] Finnerty, Scott, and Sen, Sandip, *Simulated annealing based classification*, IEEE, (1994) 824-827.

[16] Foody, Giles M., *Status of land cover classification accuracy assessment,* Remote Sensing of Environment, (2002) 185-201.

[17] Gabbouj, Moncef, *Digital Image Processing Lecture Notes,* Tampere University of Technology, 2004.

[18] Gao, Jay, Chen, Huifen, Zhang, Ying, and Zha Yong, *Knowledge-based approaches to accurate mapping of mangroves from satellite data,* Photogrammetric Engineering&Remote Sensing, 70, 11, (2004) 1241-1248.

[19] Hastie, T., Tibshirani, R., and Friedman, Jerome, *The Elements of Statistical Learning, Data Mining, Inference and Prediction,* Springer, 2001.

[20] Heermann, P. D., and Khazenie, N., *Classification of multispectral remote sensing data using a back-propagation neural network*, IEEE Transactions on Geoscience and Remote Sensing, 30, (1992) 81-88.

[21] Houston, A., and Rycroft, M., *Keys to Space, An Interdisciplinary Approach to Space Studies,* International Space University Publication, 2003.

[22] IKONOS Product Imagery Products and Product Guide, IKONOS Space Imaging, 2004.

[23] Jackson, Qiong, and Langrebe, D.A., *An adaptive method for combined covariance estimation and classification*, IEEE Transactions on Geoscience and Remote Sensing, 40, 5, (2002) 1082-1087.

[24] Jain, A.K., *Fundamentals of Digital Image Processing*, University of California, Prentice Hall Information and System Sciences Series, 1989.

[25] Jain, A.K., Murty, M. N., and Flynn, P.J., *Data clustering: a review,* ACM Computing Surveys, 31, 3, (1999) 277-323.

[26] Jensen, J., *Introductory Digital Image Processing, A Remote Sensing Perspective,* Prentice Hall Series in Geographic Information Science, 1996.

[27] Kartikeyan, B., Majumder, K. L., and Dasgupta, A.R., *An expert system for land cover classification,* IEEE Transactions on Geoscience and Remote Sensing, 33, 1, (1995), 58-66.

[28] Kartikeyan, B., Sarkar, A., Majumder, K L., *A segmentation approach to classification of remote sensing imagery*, International Journal of Remote Sensing, 19, 9, (1998) 1695-1709.

[29] Kelly, Maggi, Shaari, David, Guo, Qinghua, and Liu, Desheng, *A comparision of standard and hybrid classifier methods for mapping hardwood mortality in areas affected by "sudden oak death"*, Photogrammetric Engineering&Remote Sensing, 70, 11, (2004) 1229-1239.

[30] Khorram, S., *Digital Image Processing,* International Space University Summer Session Program Lecture Notes, 2003.

[31] Körümdük, Cumali, and Peştemalcı, Vedat, *Determination of Forest Covered Areas in the Northern of Adana City by Using Satellite Data,* MSc. Thesis, Çukurova University, 2002.

[32] Lai, Pak-Cheung, and Zeng, Bing, *Fast sub-optimal design of extended threshold Boolean filters,* IEEE, (1999) 438-441.

[33] Lee, Ki Dong, and Lee, Yong Hoon, *Threshold Boolen filters*, IEEE Transactions on Signal Processing, 42, 8, (1994) 2022-2036.

[34] Lillesand, T. M., and Kiefer, R. W., *Remote Sensing and Image Interpretation*, University of Wisconsin, John Wiley&Sons, 2000.

[35] Liu, Weiguo, Gopal, Sucharita, and Woodcock, Curtis E., *Uncertainty and confidence in land cover classification using a hybrid classifier approach,* Photogrammetric Engineering&Remote Sensing, 70, 8, (2004) 963-971.

[36] Liu, Z. K., and Xiao, J. Y., *Classification of remotely-sensed image data using artificial neural networks*, International Journal of Remote Sensing, 12, 11, (1991) 2433-2438.

[37] Lu, Dengsheng, Musel, Paul, Batistella, Mteus, and Moran, Emilio, *Comparision of land cover classification methods in the Brazilian Amazon basin*, Photogrammetric Engineering&Remote Sensing, 70, 6, (2004) 723-731.

[38] Lu, Dengsheng, and Weng, Qihao, *Spectral mixture analysis of the urban landscape in Indianapolis with Landsat ETM+ imagery,* Photogrammetric Engineering&Remote Sensing, 70, 9, (2004) 1053-1062.

[39] Mather, P.M., *Computer Processing of Remotely Sensed Images, An Introduction,* School of Geography, the University of Nottingham, UK, Wiley, 1999.

[40] Mausel, P.W., Kamber, W.J., and Lee, J.K., *Optimum band selection for supervised classification of multispectral data,* Photogrammetric Engineering and Remote Sensing, (1990).

[41] McCauley, James Darrell, and Engel, Bernard A., *Communications,* IEEE Transactions on Geoscience and Remote Sensing, 33, 6, (1995) 1103-1109.

[42] Muneyasu, Mitsuji, Yasui, Yoshihiro, and Hinamoto, Takao, *A design of adaptive stack filters using pattern classification,* IEEE, (1999) 534-538.

[43] Myint, Soe Win, Lam, Nina S.-N., and Tyler, J.M., *Wavelets for urban spatial feature discrimination: comparisions with fractal, spatial autocorrelation, and spatial co-occurrence approaches*, Photogrammetric Engineering&Remote Sensing, 70, 7, (2004) 1313-1316.

[44] Orun, Ahmet B., *Automated İdentification of Man-made textural features on satellite imagery by Bayesian networks,* Photogrammetric Engineering&Remote Sensing, 70, 2, (2004) 211-216.

[45] Pal, Mahesh, and Mather, Paul M., *An assessment of the effectiveness of decision tree methods for land cover classification,* Remote Sensing of Environment 86, (2003) 554-565.

[46] Paola, Justin D., and Schowengerdt, Robert A., *A detailed of back propagation neural network and maximum likelihood classifiers for urban land use classification,* IEEE Transactions on Geoscience and Remote Sensing, 33, 4, (1995) 981-996.

[47] Peter, Clote, and Kranakis, Evangelos, *Boolean Functions and Computation Models*, Springer, 2001.

[48] Platt, R.V., and Goetz, A.F.H., *A comparision of AVIRIS and Landsat ETM+ land use classification at the urban area,* Photogrammetric Engineering&Remote Sensing, 70, 7, (2004) 813-819.

[49] Porter, Reid, Harvey, Neal, Perkins, Simon, Theiler, James, Brumby, Steven, Bloch, Jeff, and Gokhale, Maya Szymanski, *Optimizing Digital Harware Perceptrons for Multi-Spectral Image Classification.*

[50] Punch, W.F., Goodman, E.D., Pei, Min, Chia-Sun, Lai, Hovland, P., and Enbody, R., *Further Research on Feature selection and classification using genetic algorithms,* ICGA93, (1993) 557-594, Champaign 3.

[51] Salu, Yehuda, and Tilton, James, *Classification of multispectral image data by the binary diamond neural network and by nonparametric, pixel by pixel methods,* IEEE Transactions on Geoscience and Remote Sensing, 31, 3, (1993) 606-617.

[52] Schackelford, Aaron K., and Davis, Curt H., *A fuzzy classification approach for high-resolution multispectral data over urban areas*, IEEE, (2002) 1621-1623.

[53] Schowengerdt, R.A., *Remote Sensing, Models and Methods for Image Processing,* University of Arizona, Academic Press, 1997.

[54] Smiths, Paul C., *Multiple classifier systems for supervised remote sensing image classification based on dynamic classifier selection,* IEEE Transactions on Geoscience and Remote Sensing, 40, 4, (2002) 801-813.

[55] Tso, B., and Mather, P.M., *Classification Methods for Remotely Sensed Data*, Taylor and Francis, London and New York, 2001.

[56] Usul, Nurünnisa, and Doganoglu, Veysel, *METU Land and Campus in GIS,* METU project supported by DPT.

[57] *Visual Interpretation of Images with the Help of Colour Composites: Getting to Know the Study Area*, ISU Lecture Notes, 2003.

[58] Walter, Volker, *Object based classification of remote sensing data for change detection,* ISPRS Journal of Photogrammetry and Remote Sensing, 58, (2004) 225-238.

[59] Wang, Ywqiao, and Zhang, Xinsheng, *A SPLIT model for extraction of subpixel impervious surface information,* Photogrammetric Engineering&Remote Sensing, 70, 7, (2004) 821-828.

[60] Wilkinson, Graeme G., *Results and implications of a study of fifteen years of satellite image classifications experiments,* IEEE Transactions on Geoscience and Remote Sensing, 43, 3, (2005) 433-440.

[61] Yang, Limin, Huang, Chengquan, Homer, Collin H., Wylie, B.K., and Coan, Micheal J., *An approach for mapping large-area impervious surfaces: synergistic use of Landsat 7 ETM+ and high spatial resolution imagery,* manuscript submitted to Canadian Journal of Remote Sensing (research paper), (2002) USGS.

[62] Yoshida, Tomoji, and Sigeru, Omatu, *Neural network approcah to land cover mapping,* IEEE Transactions on Geoscience and Remote Sensing, 32, 5, (1994) 1103-1109.

[63] Yüksel, Gökhan et al., *BILSAT-1: first year in orbit-operations and lessons learned*, the 18th Annual AIAA/USU Conference on Small Satellites, (2004).

[64] Zavaljevski, Aleksandar, *Classification and Detection in Multispectral Images,* PhD thesis in Electrical Engineering, University of Cincinnati, 1996.

[65] Zhu, Changqing, and Yang, Xiaomei, *Study of remote sensing image texture analysis and classification using wavelet*, International Journal of Remote Sensing, 19, 16, (1998) 3197-3203.

[66] Airborne Remote Sensing Basics
http://hydrolab.arsusda.gov/rsbasics/noise.php (accessed 06 Sep. 2005).

[67] Electromagnetic spectrum From Wikipedia, the free encyclopedia.
http://en.wikipedia.org/wiki/Electromagnetic-spectrum (accessed 06 Sep. 2005).

[68] Fundamentals of Remote Sensing, Remote Sensing Tutorial, Canada Centre for Remote Sensing, Natural Resources, Canada
http://www.ccrs.nrcan.gc.ca/ccrs/homepg.pl?e (accessed 06 Sep. 2005).

[69] Google Earth
http://earth.google.com/ (accessed 06 Sep. 2005).

[70] Hyperspectral Remote Sensing Systems and Analysis Glenn J. Fitzgerald, Ph.D. USDA-ARS, Shafter, CA
http://webpages.acs.ttu.edu/smaas/asa2000/fitzgerald.htm (accessed 06 Sep. 2005).

[71] Landsat-7 Science Data User's Handbook
http://ltpwww.gsfc.nasa.gov/IAS/handbook/handbook_toc.html (accessed 06 Sep. 2005).

[72] Middle East Technical University homepage
www.metu.edu.tr (accessed 06 Sep. 2005).

APPENDIX A

FILE *booleanthresh.m*

% (C) Selime Gürol (September, 2005)

function $bcindsson = booleanthresh(A, n, v1, v2, v3, v4, v5, v6)$

% A is the input matrix.

% n is the number of classes

% *bcindsson* matrix is the output whose elements valued from 1 to 6. If the user

% represents the numbers with colours, thematic map is appeared on the screen.

% $v1, v2, v3, v4, v5, v6$ are the training data for each class. These training data

% are selected with trainselection.m file.

% $v1$ represents training data for water

% $v2$ represents training data for forest

% $v4$ represents training data for rock

% $v5$ represents training data for agriculture

% $v6$ represents training data for builtup

tic;

% Determination of RGB and mean values for each training data set with an

% order.

$[r1, g1, b1, a] = trainsort(v1);$

$[r2, g2, b2, b] = trainsort(v2);$

$[r3, g3, b3, c] = trainsort(v3);$

$[r4, g4, b4, d] = trainsort(v4);$

$[r5, g5, b5, e] = trainsort(v5);$

$[r6, g6, b6, f] = trainsort(v6);$

% Selection of threshold levels to be used for threshold decomposition

$TR = [0.5*(f(1)+250) \;\; 0.5*(f(1)+e(1)) \;\; 0.5*(e(1)+d(1)) \;\; 0.5*(d(1)+c(1))$
$0.5*(c(1)+b(1)) \;\; 0.5*(b(1)+a(1)) \;\; 0.5*a(1)]$

$TG = [0.5*(f(2)+250) \;\; 0.5*(f(2)+e(2)) \;\; 0.5*(e(2)+d(2)) \;\; 0.5*(d(2)+c(2))$
$0.5*(c(2)+b(2)) \;\; 0.5*(b(2)+a(2)) \;\; 0.5*a(2)]$

$TB = [0.5*(f(3)+250) \;\; 0.5*(f(3)+e(3)) \;\; 0.5*(e(3)+d(3)) \;\; 0.5*(d(3)+c(3))$
$0.5*(c(3)+b(3)) \;\; 0.5*(b(3)+a(3)) \;\; 0.5*a(3)]$

% Threshold Decomposition of the input image according to the TR, TG and
% TB threshold vectors and remaining feature values

$[rbv, rcv, gbv, gcv, bbv] = thrdecom(A, TR, TG, TB);$

% Assignment of each pixel to the classes

$[bcinds1, nonind1] = solution(v1, r1, g1, b1, TR, TG, TB, rbv, rcv, gbv, gcv, bbv);$
$[bcinds2, nonind2] = solution(v2, r2, g2, b2, TR, TG, TB, rbv, rcv, gbv, gcv, bbv);$
$[bcinds3, nonind3] = solution(v3, r3, g3, b3, TR, TG, TB, rbv, rcv, gbv, gcv, bbv);$
$[bcinds4, nonind4] = solution(v4, r4, g4, b4, TR, TG, TB, rbv, rcv, gbv, gcv, bbv);$
$[bcinds5, nonind5] = solution(v5, r5, g5, b5, TR, TG, TB, rbv, rcv, gbv, gcv, bbv);$
$[bcinds6, nonind6] = solution(v6, r6, g6, b6, TR, TG, TB, rbv, rcv, gbv, gcv, bbv);$
$bcinds(:,:,1) = bcinds1;$
$bcinds(:,:,2) = bcinds2;$
$bcinds(:,:,3) = bcinds3;$
$bcinds(:,:,4) = bcinds4;$
$bcinds(:,:,5) = bcinds5;$
$bcinds(:,:,6) = bcinds6;$
$[x, y] = size(A(:,:,1));$
$son\_mat = bcinds1 + bcinds2 + bcinds3 + bcinds4 + bcinds5 + bcinds6;$
t1=toc
tic
for $i = 1 : x$

for $j = 1 : y$

$son = son\_mat(i, j)$;

if $son == 1$;

$bcindsson(i, j) = find(bcinds(i, j, :) == 1)$;

% Assignment of pixels that are assigned more than one classes

elseif $son > 1$

$K(1, :) = rbv(i, j, :)$;

$K(2, :) = gbv(i, j, :)$;

$K(3, :) = bbv(i, j, :)$;

$KK(1, :) = rcv(i, j, 1)$;

$KK(2, :) = rcv(i, j, 2)$;

$KK(3, :) = gcv(i, j, 1)$;

$KK(4, :) = gcv(i, j, 2)$;

indis=find$(bcinds(i, j, :) == 1)$;

comp= $[a; b; c; d; e; f]$;

for $k = 1 : length(indis)$

$meant = comp(indis(k), :)$;

$L(1, :, k) = meant(1) > TR$;

$L(2, :, k) = meant(2) > TG$;

$L(3, :, k) = meant(3) > TB$;

$LL(1, :, k) = meant(1) > min(A(i, j, 2), A(i, j, 3))$;

$LL(2, :, k) = meant(1) > max(A(i, j, 2), A(i, j, 3))$;

$LL(3, :, k) = meant(2) > min(A(i, j, 1), A(i, j, 3))$;

$LL(4, :, k) = meant(2) > max(A(i, j, 1), A(i, j, 3))$;

$SUM1(k) = sum(sum(K == L(:, :, k)))$;

$SUM2(k) = sum(sum(KK == LL(:, :, k)))$;

$SUM(k) = SUM1(k) + SUM2(k)$;

end

$location = find(SUM == max(SUM))$;

$bcindsson(i, j) = indis(location(1))$;

clear $location$

clear SUM

```
% Assignment of unclassified pixels
    else
        D = [nonind1, nonind2, nonind3, nonind4, nonind5, nonind6];
        DDD = find(D == max(D));
        bcindsson(i, j) = DDD(1);
    end
    clear LLL
end
end
t2=toc

%%%%%%%%%%%%%%SUBFUNCTIONS%%%%%%%%%%%
function [rout, gout, bout, meantrain] = trainsort(vin)
% vin is the training data set
% The outputs rout, gout, bout are red band, green band and
% blue band values with an order for the corresponding training set
% meantrain is a 3D vector whose elements are the mean values of RGB
% bands of corresponding training data set
vpro = sort(vin);
vpro = vpro(2 : length(vpro) - 1, :);
meantrain = mean(vpro);
rout = vpro(:, 1);
gout = vpro(:, 2);
bout = vpro(:, 3);

%%%%%%%%%%%%%%%%%%%%%%%%%%%%%%%%%%%%%%%%%%%
function [rbv, rcv, gbv, gcv, bbv] = thrdecom(A, TR, TG, TB);
% inputs are an image 3D-matrice and 3 vectors of thresholds for each band
% outputs are 3D matrices of Boolean vectors
sizeimg = size(A);
sizered = length(TR);
sizegreen = length(TG);
```

$sizeblue = length(TB);$

$rbv = zeros(sizeimg(1), sizeimg(2), sizered);$

$rcv = zeros(sizeimg(1), sizeimg(2), 2);$

$gbv = zeros(sizeimg(1), sizeimg(2), sizegreen);$

$gcv = zeros(sizeimg(1), sizeimg(2), 2);$

$bbv = zeros(sizeimg(1), sizeimg(2), sizeblue);$

for $i = 1 : sizered$

$\quad rbv(:, :, i) = A(:, :, 1) > TR(i);$

end

$rcv(:, :, 1) = A(:, :, 1) > min(A(:, :, 2), A(:, :, 3));$

$rcv(:, :, 2) = A(:, :, 1) > max(A(:, :, 2), A(:, :, 3));$

for $i = 1 : sizegreen,$

$\quad gbv(:, :, i) = A(:, :, 2) > TG(i);$

end

$gcv(:, :, 1) = A(:, :, 2) > min(A(:, :, 1), A(:, :, 3));$

$gcv(:, :, 2) = A(:, :, 2) > max(A(:, :, 1), A(:, :, 3));$

for $i = 1 : sizeblue,$

$\quad bbv(:, :, i) = A(:, :, 3) > TB(i);$

end

%%

function $[bcindsout, nonindout] = solution(vin, rin, gin, bin, TR, TG, TB, rbv, rcv, gbv, gcv, bbv)$

% *solution.m* is a function that assigns the pixels to the classes.

% Threshold Decomposition of the training data set according to the TR,
% TG and TB threshold vectors and remaining feature min, max values.

$[samplesrb, samplesrc, samplesgb, samplesgc, samplesbb] =$
$fullthresdec(vin, rin, gin, bin, TR, TG, TB);$

% Determination of the indicator to a Boolean classifier function which uniquely
% discriminates the dataset

$indfunindcls = infunfin(samplesrb, samplesrc, samplesgb, samplesgc, samplesbb);$
$[bcinds, nonind] = bccheck(rbv, rcv, gbv, gcv, bbv, indfunindcls);$
$bcindsout = bcinds;$
$nonindout = nonind;$

%%%%%%%%%%%%%%%%%%%%%%%%%%%%%%%%%%%%
function $[samplesrb, samplesrc, samplesgb, samplesgc, samplesbb] =$
$fullthresdec(vin, rband, gband, bband, TR, TG, TB)$

% Threshold Decomposition of $rband$
$[samplesrb, samplesrc] = thresdec(vin, rband, gband, bband, TR);$

% Threshold Decomposition of $gband$
$[samplesgb, samplesgc] = thresdec(vin, gband, rband, bband, TG);$

% Threshold Decomposition of bband according to the TB threshold vector
for $i = 1 : length(vin) - 2$
for $k = 1 : length(TR)$
    $samplesbb(i, k) = bband(i) > TB(k);$
end
end

%%%%%%%%%%%%%%%%%%%%%%%%%%%%%%%%%%%%
function$[samplesband1, samplesband1comp] = thresdec(vin, band1, band2,$
$band3, TIN)$
% $samplesband1$ is a matrix that its ith column is a Boolean vector obtained
% from threshold decomposition of band1 according to the $TIN(i)$ threshold
% level $(i = 1, 2, ..., length(TIN))$
% $sampleband1comp$ columns are the Boolean vectors obtained from the
% threshold decomposition according to the min, max values of $band2$ and $band3$.

for $i = 1 : length(vin) - 2$

```
for k = 1 : length(TIN)
      samplesband1(i, k) = band1(i) > TIN(k);
   end
end
for i = 1 : length(vin) − 2
   samplesband1comp(i, length(TIN)+1) = band1(i) > min(band2(i), band3(i));
   samplesband1comp(i, length(TIN)+2) = band1(i) > max(band2(i), band3(i));
end
%%%%%%%%%%%%%%%%%%%%%%%%%%%%%%%%%%%%%%
function indfunindcls =
infunfin(samplesrb, samplesrc, samplesgb, samplesgc, samplesbb);
% input is the samples known to belong to the same class (training samples of
%a class)
% it is a set of matrices of boolean vectors
% output is an indicator to a Boolean classifier function which uniquely
% discriminates the dataset
sizzr = size(samplesrb);
sizzg = size(samplesgb);
sizzb = size(samplesbb);
nofsamples = sizzr(1);
indfunindcls = [sum(samplesrb(1, :)), sum(samplesrc(1, :)),
sum(samplesgb(1, :)), sum(samplesgc(1, :)), sum(samplesbb(1, :))];
k = 1;
for i = 2 : nofsamples
indfunindclse = [sum(samplesrb(i, :)), sum(samplesrc(i, :)),
sum(samplesgb(i, :)), sum(samplesgc(i, :)), sum(samplesbb(i, :))];
    lll = sum(indfunindcls(1, :) == indfunindclse);
   for j = 1 : k,
         lll = max(lll, sum(indfunindcls(k, :) == indfunindclse));
   end
   if lll < 5
      indfunindcls = [indfunindcls; indfunindclse];
```

```
        k = k + 1;
    end
end
%%%%%%%%%%%%%%%%%%%%%%%%%%%%%%%%
function [bcinds, nonind] = bccheck(rbv, rcv, gbv, gcv, bbv, indfunindcls);
% checks which pixels on an image belong to the corresponding class
% inputs are the threshold decompositon vectors
% output is a binary matrix
sizind = size(indfunindcls);
nofors = sizind(1);
summ1 = sum(rbv, 3);
summ2 = sum(rcv, 3);
summ3 = sum(gbv, 3);
summ4 = sum(gcv, 3);
summ5 = sum(bbv, 3);
indic = zeros(size(summ1));
unclassifiedtotal = 0;
unclassifiedtotal1 = 0;
unclassifiedtotal2 = 0;
unclassifiedtotal3 = 0;
unclassifiedtotal4 = 0;
unclassifiedtotal5 = 0;
for  i = 1 : nofors
    ind1 = (summ1 == indfunindcls(i, 1));
    ind2 = (summ2 == indfunindcls(i, 2));
    ind3 = (summ3 == indfunindcls(i, 3));
    ind4 = (summ4 == indfunindcls(i, 4));
    ind5 = (summ5 == indfunindcls(i, 5));
    indik = ind1. * ind2. * ind3. * ind4. * ind5;
    indic = indic + indik;
end
nonind = sum(sum(ind1)) + sum(sum(ind2)) + sum(sum(ind3))+
```

$$sum(sum(ind4)) + sum(sum(ind5));$$
$$bcinds = indic > 0.1;$$

APPENDIX B

BILSAT IMAGE OF METU SETTLEMENT

APPENDIX C

LANDSAT IMAGE OF METU SETTLEMENT